Høgskulen på Vestlandet

Master Thesis

ING5002

Predefinert informasjon

Startdato:	24-05-2018 10:33	**Termin:**	2018 VÅR
Sluttdato:	01-06-2018 14:00	**Vurderingsform:**	Norsk 6-trinns skala (A-F)
Eksamensform:	Masteroppgave		
SIS-kode:	203 ING5002 1 MOPPG 2018 VÅR		
Intern sensor:	(Anonymisert)		

Deltaker

|	
Navn:	Svein Arne Bjørkheim
Kandidatnr.:	5
HVL-id:	135348@hvl.no

Informasjon fra deltaker

Tittel *: Kjøleeffektivitet av vanndråper som blir påført til en varm overflate av rustfritt stål

Engelsk tittel *: Cooling efficiency of water droplets impinging on a hot stainless steel surface

Tro- og loverklæring *: Ja

Inneholder besvarelsen konfidensiell materiale?: Nei

Jeg bekrefter at jeg har registrert oppgavetittelen på norsk og engelsk i StudentWeb og vet at denne vil stå på vitnemålet mitt *: Ja

Jeg godkjenner avtalen om publisering av masteroppgaven min *

Ja

Cooling efficiency of water droplets impinging on a hot stainless steel surface
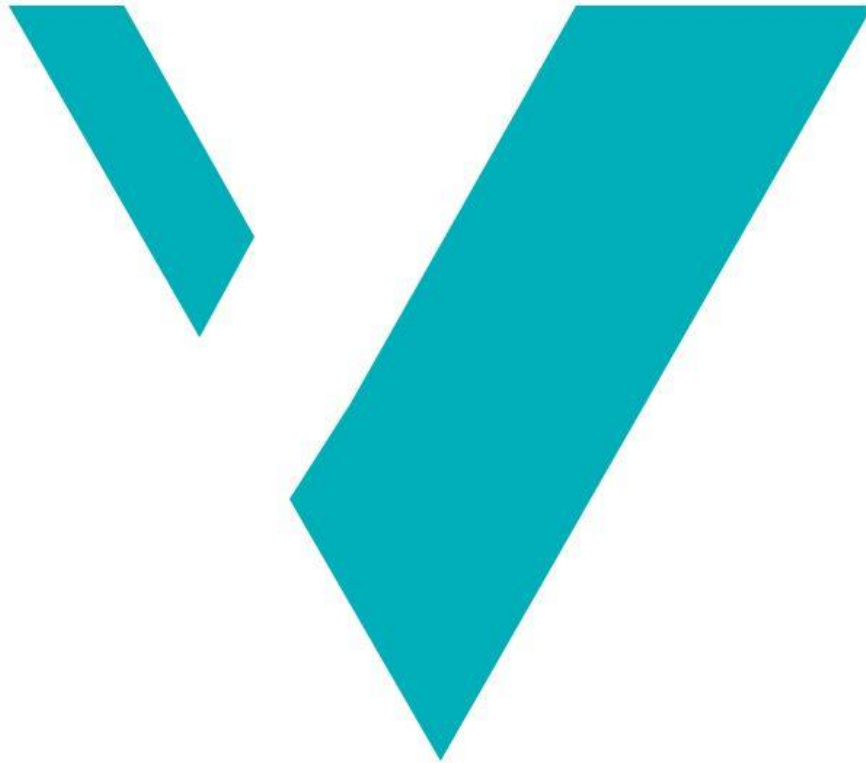
Svein Arne Bjørkheim

WESTERN NORWAY UNIVERSITY OF APPLIED SCIENCES

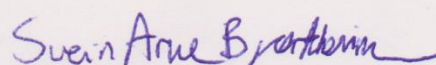Master Thesis in Fire Safety Engineering

Haugesund
June 2018

Q RÅDGIVNING

Western Norway University of Applied Sciences

Cooling efficiency of water droplets impinging on a hot stainless steel surface

Master Thesis in Fire Safety Engineering

Author: Svein Arne Bjørkheim	_Svein Arne Bjørkheim_ Author sign.
Thesis extracted: Fall 2017	Open assignment

Main Tutor: Monika Metallinou Log

External Tutor: Joachim S. Bjørge

| Keywords:

Droplet impinging, firewater, deluge, stainless steel, inclination, droplet cooling efficiency, cooling effect, impact velocity, boiling regimes, boiling crisis, critical heat flux | Number of pages: 61
+
Attachments: 16
= 77

Haugesund, 1st of June 2018 |

This thesis is a part of the master's program in Fire Safety engineering at Western Norway University of Applied Sciences. The author is responsible for the methods used, the results that are presented, the conclusion and the assessments done in the thesis.

Preface

This thesis ends my 2 years of education within Master of Fire Safety at Western Norway University of Applied Sciences (HVL), and in total of 5 years of higher education.

It is important to mention that the general idea of the issue, Excel sheet and experimental setup of this master thesis was developed by Professor Torgrim Log and Joachim Bjørge. The Excel sheet, the experimental setup and the issue was further developed by the author, Joachim Bjørge and Associate Professor Monika Metallinou to be more suited for my master thesis.

Acknowledgments

I want to execute my gratitude to all the people who supported and helped me along the way, both morally and academically. I want to thank Joachim Bjørge, Associate Prof. Monika Metallinou and Prof. Torgrim Log for all the professional help and support. I will also give a special thanks to Joachim Bjørge and Q Rådgivning for the mission regarding my master thesis. I want to thank all my teachers, lecturers and fellow students from the college/university who helped and supported me to get the necessary knowledge.

I want to give a special thanks to my parents, Kjell Bjørkheim and Siv Bjørkheim for all the support regarding my entire schooling. I want to thank my girlfriend, Maria Ghurayeb, for the massive moral support regarding my master's degree. I want to thank my ex-tutor from middle school, Tove Berg, for helping me through a rough time, academically, and pushed me to my utter limits, in addition to believing in me when few other teachers did.

Aksdal, May 31, 2018

Svein Arne Bjørkheim

Abstract

The behavior of water droplets applied to hot metal surfaces depends strongly on the metal surface temperature. Four distinct boiling regimes, film evaporation, nuclear boiling, transition boiling and film boiling are observed, with large differences in heat exchange between surface and the droplet. The purpose of the present work was to study water droplet cooling efficiency as a function of temperature for stainless steel in these boiling regimes. Stainless steel (AISI 316) discs (50 mm diameter and 10 mm thickness) were preheated to 430°C and cooled to 80°C by water droplets. Droplet of 2,5 mm, 3,2 mm and 3,7 mm diameter were released from 25 cm, 50 cm and 100 cm height, respectively resulting in impingement speeds of 2,2 m/s, 3,1m/s and 4,4 m/s. The hot metal surface was aligned in 3 positions, i.e. horizontal, 30° or 60° inclination. These combinations resulted in 27 experimental data series, each consisting of five droplet tests cooling the disc and sandwiched between two reference tests without releasing water droplets. The water flow was carefully tuned to 0,023 g/s for all the droplet experiments to compare cooling efficiency based on the same water application rate.

Four thermocouples were used for recording temperature versus time within the stainless steel disc. Based on the differences in cooling rate with and without droplets cooling the metal disk, disk mass and heat capacity, the absolute cooling rate of the droplets were obtained. Comparing this cooling rate to the heat flow required to completely evaporate the droplets gave the dimensionless cooling efficiency.

Evenly across the results, smallest droplets were observed to have a higher cooling efficiency in a wider temperature range, while the largest droplets demonstrated a higher peak efficiency (i.e. higher boiling crisis), which was recorded to be between approximately 64% and 85% respectively for the different configurations. Based on most of the results, the droplet cooling efficiency increased with increasing impact velocity, due to higher momentum impact and a larger contact area. However, regarding the horizontal stainless steel disc setup – middle-sized and smallest droplets, the effect of bouncing was less prominent, and droplets had a higher ability to be attached to the surface (i.e. lower Weber number). The droplet cooling efficiency decreased with increased inclination for the lowest impact velocity (2,2 m/s), due to a lower amount of possible directions for reflecting disintegrated droplets. For higher droplet velocities, the droplets resulted in higher cooling efficiency for 30° inclination.

Similar to the results published by other workers, a maximum in heat transfer was observed at about 160 – 220°C. Above this temperature, the cooling efficiency was reduced to about 10 % for temperatures in the film boiling region (i.e. temperatures above 290 - 300°C). This indicates that firewater must be applied before the metal becomes too hot, else the water spray cooling will be very limited.

It is recommended to study this topic further, either on a larger scale or by altering several parameters,

i.e. droplet sizes, surface roughness and impact velocity.

Sammendrag

Oppførselen til vanndråper på varme metalloverflater avhenger sterkt av overflatetemperaturen på metall. Fire forskjellige boiling-regimer, film evaporation, nucleate boiling, transition boiling og film boiling kunne observeres, med store forskjeller i varmeveksling mellom overflaten og dråpen. Hensikten med nåværende arbeid var å studere vanndråpe-kjøleeffektivitet som en funksjon av temperatur for rustfritt stål i disse kokende regimer. En skive av rustfritt stål (AISI 316) (50 mm diameter og 10 mm tykkelse) ble forvarmet til 430 ° C og avkjølt til 80 ° C med vanndråper. Dråpe på 2,5 mm, 3,2 mm og 3,7 mm diameter ble frigjort fra henholdsvis 25 cm, 50 cm og 100 cm høyde, hvilket resulterte i slaghastigheter på henholdsvis 2,2 m / s, 3,1 m / s og 4,4 m / s. Den varme metalloverflaten var justert i 3 stillinger, dvs. horisontal, 30 ° eller 60 ° helning. Disse kombinasjonene resulterte i 27 eksperimentelle dataserier, hver bestående av fem dråpetester som kjølte platen i mellom to referansetester uten å slippe vanndråper. Vannstrømmen ble nøye innstilt til 0,023 g / s for alle dråpeforsøkene for å sammenligne kjøleeffektivitet basert på samme vannpåføringshastighet.

Fire termoelementer ble brukt til å registrere temperatur versus tid i skiven. Basert på forskjellene i kjølehastighet med og uten dråper kjøler metallskiven, diskmasse og varmekapasitet, ble dråpenes absolutte kjølehastighet oppnådd. Sammenligning av denne kjølehastigheten til varmestrømmen som kreves for å fordampe dråpene helt, ga den dimensjonsløse kjøleeffektiviteten.

I film boiling- området (dvs. temperaturer over ca. 290-300 ℃), kan 10 % dråpeeffektivitet være forventet, som følgende betyr at risikoreduserende handlinger ved bruk av brannvann bør bli ansett så tidlig som mulig, for å utøve sin primæreffekt.

Jevnt over resultatene, er de minste dråpene observert å ha en høyere sammenhengende effektivitet i et bredere temperaturområde, samtidig som de største dråpene demonstrerte en høyere topp-effektivitet (dvs. høyere toppunkt), som vil være på henholdsvis ca. 64 % og 85 %. Basert på de fleste resultatene, vil dråpeeffektivitet øke med høyere slaghastighet, på grunn av høyere påvirkning fra dråpen, samt et større kontaktareal. Likevel, i henhold til horisontalt oppsett – medium og minste dråper, der effekten av «spretting» var mindre innlysende, og dråpene hadde en større evne til å feste seg til overflaten (dvs. mindre Weber tall), som igjen ga en høyere dråpeeffektivitet. Dråpeeffektiviteten økte med avtagende helning, angående den laveste slaghastigheten (2,2 m/s), på grunn av et mer begrenset utvalg av muligheter angående de reflekterte oppløste dråpene. Likevel, dersom slaghastigheten økte, demonstrerte dråpene en høyere dråpeeffektivitet ved 30 ° helning.

I likhet med resultatene som ble publisert av annen forskning, ble det observert maksimalt i varmeoverføring ved ca. 160-220 ° C. Over denne temperaturen ble kjøleeffektiviteten redusert til ca.

10% for temperaturer i film boiling området (dvs. temperaturer over 290-300 ° C). Dette indikerer at brannvann må påføres før metallet blir for varmt, ellers vil kjøling av vann være svært begrenset.

Det vil være anbefalt å forske på dette ytterligere, på større skala eller å forandre parametere, dvs. dråpestørrelser, overflate ruhet, og slaghastighet.

Table of Content

Figures and tables

Terminology and abbreviations

Some of the terminology and abbreviations used in this report is listed below.

Active fire protection	Technical fire protection with a function activated after fire is detected, auto fire alarm is triggered, or fire is noticed (KBT).
Boiling crisis/critical heat flux	Local maximum in droplet cooling effect (Liang og Mudawar 2016).
Consequence	Possible outcome by an undesired event (KBT).
Deluge	Sprinkler installation, either an independent installation or an affiliated sub-assembly, equipped with open sprinkler heads or spray nozzles associated with the deluge valve or a multi-function control arrangement, which causes all heads to deliver water when the plant is triggered (KBT).
Depressurization	Ventilation from enclosed spaces via holes, openings or abrasive surfaces (KBT).
Disintegrated droplets	A droplet breaks up into many smaller droplets because of impact onto a solid surface. These smaller droplets are referred to as *disintegrated droplets*.
Droplet cooling efficiency	Dimensionless number between 0 to 1 which can describe the percentage of the total water droplet cooling effect.
Effect	Energy per unit of time [W = J/s] (KBT).
Fire	Unwanted or uncontrolled combustion process characterized by heat dissipation accompanied by smoke, flame or glow (KBT).
Fire safety measure	Measures for preventing fire or reducing the consequence of fire (KBT).
Global heat load	Heat exposing whole pipes, vessels or segments, which is used for pressure profile calculation (The Norwegian Oil Industry Association (OLF) 2008).
Heat flux	Heat transferred per unit area [W/m^2] (Drysdale 2011).
Impact velocity	Velocity governed by gravitational acceleration *g* and height.
Jet fire	Ignited leakage by pressurized flammable liquid or gas (KBT).
Leidenfrost	Local minimum in droplet cooling effect (Bernardin og Mudawar 1999).
Local peak heat load	Heat load exposing only a small area of pipes, vessels or segments, which is used for rupture calculation (The Norwegian Oil Industry Association (OLF) 2008).

Passive fire protection	Surface treatment, cladding or stand-alone systems like fire will provide thermal protection that reduces the rate of heat transfer to the protected object or area (KBT).
Risk	Expression of the combination of probability and consequence of an undesired event (KBT).
Risk analysis	Systematic procedure for describing or calculating risk. The risk analysis is performed by mapping undesired incidents, and the causes and consequences of these (KBT).
AISI	American Iron and Steel Institute
ALARP	As Low As Reasonable Practicable
CFD	Computational Fluid Dynamics
DAL	Dimensioning Accidental load
ISO	International Organization for Standardization
FW	Firewater
NORSOK	Norsk Sokkels Konkurranseposisjon

Chapter 1

1. Introduction

This chapter will give a description of the background, scope, and the limitations of the thesis.

1.1. Background

Firewater is often used for active fire protection in offshore and onshore industries, where the risk of fire escalation is severe compared to other businesses. Large tank vessels and the metal pipes in Oil and Gas facilities need to be protected from heat exposure, to avoid ruptures in the structures. *NORSOK S-001 Technical safety* covers safety principles and requirements for offshore petroleum installations (The Norwegian Oil Industry Association (OLF) 2008), while some onshore facilities, such as Statoil Kårstø, have their own safety principles. It is previously shown in major accidents that fires involving large tank vessels are difficult to suppress. Therefore, it will require a massive amount of water or foam to extinguish, which may lead to a *boilover.* In this case, the total fire area will increase. (Casal 2017)

Metallic objects have a unique ability to equalize heat within the object, due to high thermal conductivity (Drysdale 2011). Stainless steel has moderate thermal conductivity (around 16 W/mK), and hot spots can occur in parts of the equipment not in contact with liquids, if affected by an external fire. Since steel loses half of its strength at approximately 500 ℃ (Standard norge Revidert 2015). It is therefore crucial to cool down the material by firewater as early as possible to avoid loss of containment, and major escalations.

In order to reduce the risk of rupture, firewater must perform its intended function. Above a certain temperature point, called *critical heat flux temperature*, water droplets tend to lose contact with the metal surface, which consequently will reduce the heat transfer rate from surface to droplet. After that point, the heat transfer rate will be reduced until it has reached its local minimum point, called *Leidenfrost* temperature. (Kazemi 2005).

According to the Major Accident Regulation (2016), it is required to conduct a risk assessment to reduce either consequence or probability for major accidents (i.e. risk reduction), called a *risk-based performance analysis* (Storulykkeforskriften 2016). When performing a risk reduction, the ALARP principle (As low as reasonable Practicable) must be regarded to obtain the best short- and long termed results, provided that the costs are not significantly disproportionate to the risk reduction accomplished (Petroleumstilsynet 2016). The oil and gas industry are in a phase where major cost cut has been implemented, which makes the ALARP principle an extremely important tool for developing safety measures. The goal is to obtain the highest degree of risk reduction possible, by using the means

the facility have at disposal. Technical and operational regulation (2016) indicates that the effect of active fire protection become disregarded when developing a passive fire protection, and vice versa (Petroleumstilsynet 2016). This will mean that developing safety measures is on a conservative level and can consequently lead to a higher cost than necessary.

1.2. Scope

This thesis focuses on cooling efficiency of water droplets impinging on a heated stainless steel surface. Through small-scale experiments, the influence of droplet mass, droplet velocity and surface inclination to the efficiency of heat transfer between droplets and heated solid surface was studied, for a temperature range of 80 – 400 ℃. Various droplet sizes (3 different diameters) impinging from 3 different heights (which results to 3 different velocities) on a hot metal surface with three different inclinations, results to 27 series of experimental data. From each of the experimental data, the droplet cooling efficiency as a function of disc temperature will be examined. Hopefully, the results will give a better understanding of the optimized impinging velocity, droplets sizes and inclinations, and how these parameters will influence the surface temperature.

Baseline experiments, to examine the effect of mere natural air-cooling, were regularly conducted and variations were examined. These were used as reference experiments, in order to analyze the cooling efficiency of water droplets, when both phenomena are present. The cooling effect of water droplets is obtained by subtracting the baseline (heat transfer-cooling alone) from the total cooling effect (heat transfer-cooling and water droplets act simultaneously) (Bjørge, et al. 2018). This report will also give a literature review of the most relevant parameters which is affected during the experiments, in addition to some research on this topic, including some requirements given in NORSOK standard. Lastly, there will be a discussion which will be reflecting and analyzing all experimental data, by including practical approach, literature and previous research.

1.3. Limitations

Numerous of metallic objects and metallic pairings exists, but the thesis will be limited to only use stainless steel during the experiments. The test object will be a stainless steel disc cylinder with thickness 10 mm and diameter 50 mm, the small-scale experiments will also be limited to a cage made of wood and fine mesh screen, which is size 1,1 m x 0,55 m x 1,55 m height. The water supply will be a water bag connected to a small water tube and is then linked to various outlet nozzles (injection needle) to decide the different droplet sizes. Each of the experiment series will consists of a total of five droplet experiments and two baseline experiments. The stainless steel disc will also be limited to three different inclinations; horizontal, 30º and 60º. This thesis will analyze the mere cooling effect, so the report will mainly exclude the effect of fires.

Chapter 2

2. Literature review

This chapter will provide the necessary theory behind the experiments of the master thesis. This includes the various modes of heat transfer, water droplet theory based on previous research, and a short review of *NORSOK S-001 Technical Safety*, which regulates the safety requirements of offshore petroleum facilities.

2.1. Heat transfer mechanism

Before the droplet theory can be touched, it is important to have a managerial knowledge of the roles of heat transfer mechanism, and how they can affect the experiments. The various modes of heat transfer can be listed as convection, conduction and radiation. It will also be a review of thermal inertia and thermal diffusivity.

2.1.1. Convection

Convection is characterized as the motion of a transmitting medium. Convection transports enormous amount of energy during a fire to the surrounding environment by the motion of hot gases (Drysdale 2011). In this report, it will mainly focus on natural convection, which is described as a natural buoyant fluid motion of heat without any external forces (i.e. fan or mechanical ventilation). If the surface temperature of a solid medium is different from the surrounding air temperature, convection heat transfer will occur, and can be expressed as Eq. 2.1 (Drysdale 2011)

$$\dot{q}_h^{''} = h(T_s - T_\infty) \tag{2.1}$$

where:

h	Heat transfer coefficient	[W/m^{2}K]
$\dot{q}_h^{''}$	Convective heat flux	[W/m^2]
T_s	Surface temperature	[K]
T_∞	Surrounding air temperature	[K]

The formula describes that if the surrounding air temperature stays constant, while the surface is being cooled down to a lower temperature, the effect of cooling by mere natural convection will decrease. This phenomenon will be further analyzed in the baseline experiments in later sections.

2.1.2. Thermal conduction

Conduction is described as the heat that diffuses through a medium, typically solid materials, such as steel, wood, PVC and so forth. Thermal conduction will mainly be governed by thermal conductivity,

expressed as k, which is each of the materials specific ability to conduct heat. Phrased more mathematically, thermal conductivity is the proportionality between the conductive heat transfer and spatial derivate of temperature and can be expressed as Eq. 2.2. (Drysdale 2011)

$$\dot{q_k}'' = k\left(\frac{dT}{dx}\right)$$
(2.2)

where:

k	Thermal conductivity	[W/mK]
$\dot{q_k}''$	Conductive heat flux	[W/m²]
$\dfrac{dT}{dx}$	Temperature gradient	[K/m]

Thermal conductivity of materials is temperature dependent and for several materials (for example crystalline) also dependent on orientation. This means that k is not a mere constant throughout a fire scenario (Drysdale 2011). Steel's thermal conductivity will normally vary from 15,6– 46,7 W/m℃ depending on temperature range and different qualities (Kodur og Harmathy 2016), which subsequently means that steel is a better conductor of heat compare to i.e. wood (Drysdale 2011). The thermal conductivity of stainless steel will lay around 16 W/m℃, which is in the lower layer of steel's ability to conduct heat (Engineers edge, LCC 2017).

2.1.3. Thermal radiation

Thermal radiation involves heat transfer by electromagnetic waves, highly governed by the temperature of the emitting surface. Since absolute temperature is raised in fourth power (Eq. 2.3), radiation becomes more important as temperature increases. The total radiation emitted by unit area of a grey surface can be expressed as Stefan- Boltzmann equation (Drysdale 2011)

$$\dot{q_r}'' = \varepsilon \sigma T^4$$
(2.3)

where:

$\dot{q_r}''$	Radiative heat flux	[W/m²]
ε	Emissivity of the surface	[-]
σ	Stefan- Boltzmann constant ($5{,}67 \times 10^{-8}$ W/m²K⁴)	[W/m²K⁴]
T	Temperature of the emitted surface	[K]

Thermal radiation will exist mostly at the beginning of the experiments (temperature around 400 ℃), since radiation becomes increasingly dominant at temperatures above 400 ℃. The material and its

color will affect emissivity (ε_λ). Emissivity is the ratio between the emissive power of a real surface (E_λ) and the total amount of energy emitted by a black body ($E_{b,\lambda}$), and can be expressed as (Eq. 2.4) (Drysdale 2011):

$$\varepsilon_\lambda = \frac{E_\lambda}{E_{b,\lambda}} \tag{2.4}$$

Emissivity for a particular metal will vary with temperature and surface roughness. Heavily oxidized stainless steel will have an emissivity of approximately 0,7-0,8 on temperatures in a range of 200 - 500 ℃, while lightly oxidized stainless steel will have an emissivity in a range of approximately 0,1-0,4 dependent on temperatures of 30 - 400 ℃. (Lautenberger, et al. 2016)

2.1.4. Thermal inertia and heat capacity

Thermal inertia is the product of thermal conductivity, density and specific heat capacity ($k\rho c$) (Drysdale 2011). The higher the thermal inertia, the longer the time to heat up the entire body to the surrounding temperature. All properties except the density will vary considerably with temperature (Drysdale 2011). Density of the stainless steel disc is 7839 kg/m^3 and was determined by knowing mass and volume of the disc.

According to literature, thermal conductivity of stainless steel will be around 16 W/mK and specific heat will be around 502 J/kgK (Engineers edge, LCC 2017). However, specific heat capacity of stainless steel (AISI 316) will depend on temperature accordingly to Figure 2.1. The 3rd degree function was determined by knowing the heat capacity of several temperatures (British Stainless Steel Association). The correlation was also used to determine the heat capacity during the experiments (see Appendix A.4).
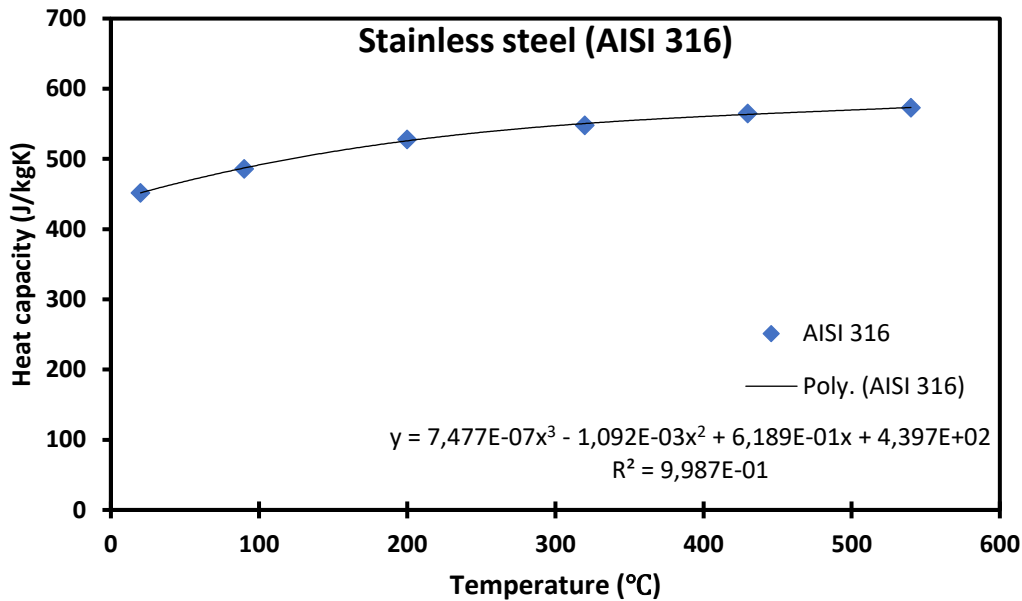
Figure 2.1 Heat capacity vs. temperature for a stainless steel (AISI 316) disc. Figure adapted based on information gathered from *(British Stainless Steel Association)*.

2.1.5. Thermal diffusivity

Thermal diffusivity is the materials ability to equalize heat and is a measure of heat transfer in an object, directly related to thermal conductivity. The formula for diffusivity can be expressed as Eq. 2.5 (Drysdale 2011)

$$\alpha = \frac{k}{\rho c} \tag{2.5}$$

where:

α	Thermal diffusivity	[m^2/s]
k	Thermal conductivity	[W/mK]
ρ	Density	[kg/m^3]
c	Heat capacity	[J/kgK]

2.2. Water droplet physics

Several researchers have studied cooling of solid surfaces by water droplets and the effect of firewater. Kazemi (2005) studied droplet impaction on solid surfaces exposed to jet fires, by investigatinged *hot spots* in steel components exposed to fires, including finding a method to prevent or mitigate hot spots by water droplets interaction. Drange (2011) studied selected problems related to accidental process

fires. This includes full-scale experimenting on propane jet fires and examined the heat attenuation in water spray in a full-scale offshore flare situation.

Liang and Mudawar (2016), provides a review of drop impact on heated walls from several publications, describing the four boiling regimes; *film evaporation, nucleate boiling, transition boiling* and *film boiling.* Misyura (2017) studied the effect of Weber number, droplet sizes and wall roughness on water droplets` boiling crisis (i.e. the phenomenon when energy transfer between droplet and solid surface is at the maximum). Fukuda et al. (2014) studied the behavior of small droplet impinging on a hot surface. They experimented the effect of various surface roughness's (*Ra* 0,04, *Ra* 0,2, *Ra* 3 and *Ra* 10), various droplet diameters (300-700 μm) and several droplets impinging velocities (1,0-4,0 *m/s*).

It is important to understand the various parameters which directly influence the droplet cooling efficiency, or the cooling effect of the droplets. This section will explain the parameters affecting the droplet experiments, including a short review of the various boiling regimes.

2.2.1. Boiling regimes

There are four types of boiling regimes; *film evaporation, nucleate boiling, transition boiling* and *film boiling*. The various boiling regimes are summarized in Figure 2.2 below.
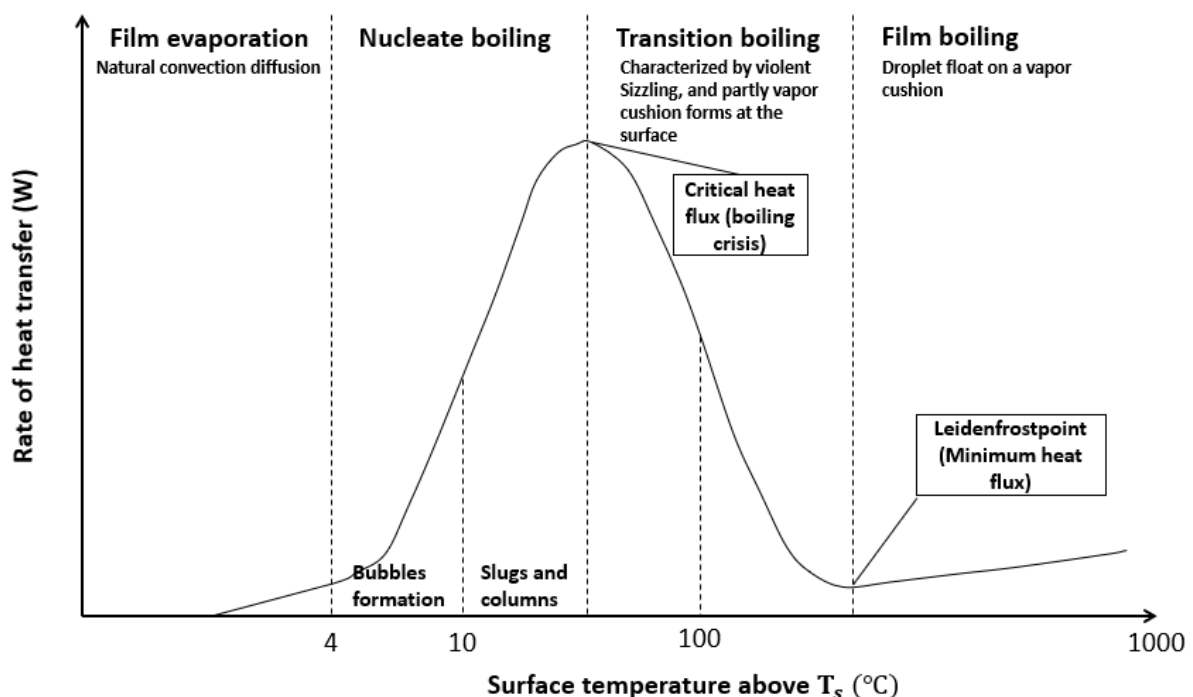
Figure 2.2 Representation of the various boiling regimes at ambient atmospheric pressure. There are four different regimes; film evaporation, nucleate boiling, transition boiling and film boiling. Figure adapted from *(Faghri, Zhang and Howell 2010), (Bernardin og Mudawar 1999)* and *(Liang og Mudawar 2016).*

Film evaporation occurs both beneath and slightly above saturation (T_s) (around 1-4 ℃ above saturation) and is characterized by natural convection diffusion (Log 2016). Natural convection, as explained in previous subsections, is the heat transferred due to temperature difference between the heated surface and the surrounding air. In this regime, the impinging droplet will spread at on the solid surface in three different stages: initial, fundamental and final. (Liang og Mudawar 2016).

Nucleate boiling starts approximately 4 ℃ above saturation temperature (T_s) and is characterized by the start of bubble formation within the saturated liquid, which is slowly boiling. Figure 2.3 Presents photos of droplets impinging on heated metal surface (aluminum) in the nucleate boiling regime 145 ℃. Various impingement velocities have been studied (Liang og Mudawar 2016)

v_{drop} = 1.65 m/s v_{drop} = 2.55 m/s v_{drop} = 3.48 m/s
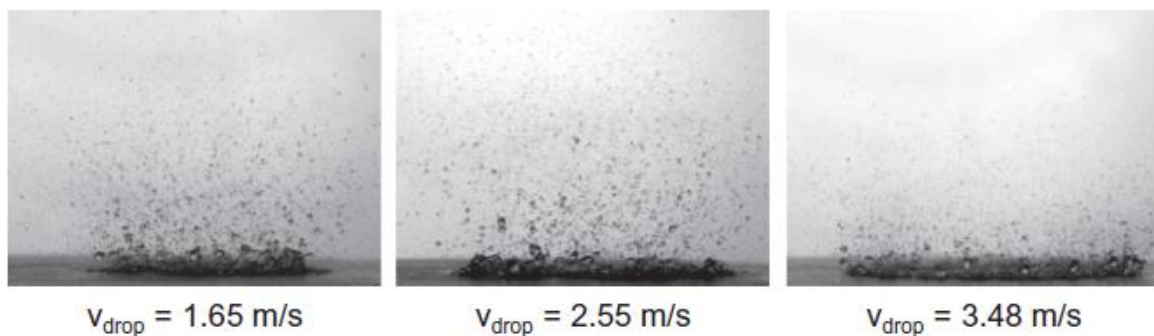
Figure 2.3 Secondary droplet break-ups at various velocities, at an aluminum surface with surface temperature of 145 ℃. *(Liang og Mudawar 2016)*

By further increasing the surface temperature, the rate of heat transfer will increase until *critical heat flux*, which will mark the transition to the *transition boiling regime*. (Liang og Mudawar 2016).

Increasing the temperature above the temperature associated with the critical heat flux, leads to reduced contact between surface and droplets, as vapor cushions partly form and collapse below the droplets. The phenomenon is accompanied by violent sizzling. The heat flux will therefore be reduced which consequently reduces the droplet cooling efficiency. This regime is called transition boiling, and according to Liang and Mudawar (2016), this regime is not yet accurately determined by researchers. However, it is currently known that this regime will be the transition between the two extrema's, hence the name. By further increasing the surface temperature, a local minimum point in heat flux will be revealed, called *Leidenfrost temperature*. (Liang og Mudawar 2016) In this point, there will be a stable vapor film below the droplet (Gottfried, Lee og Bell 1966).

The mentioned Leidenfrost temperature will mark the transition to the film boiling regime, where droplets floats on a vapor cushion. Figure 2.4 represents the difference between droplet impinging in film evaporation regime and film boiling regime.
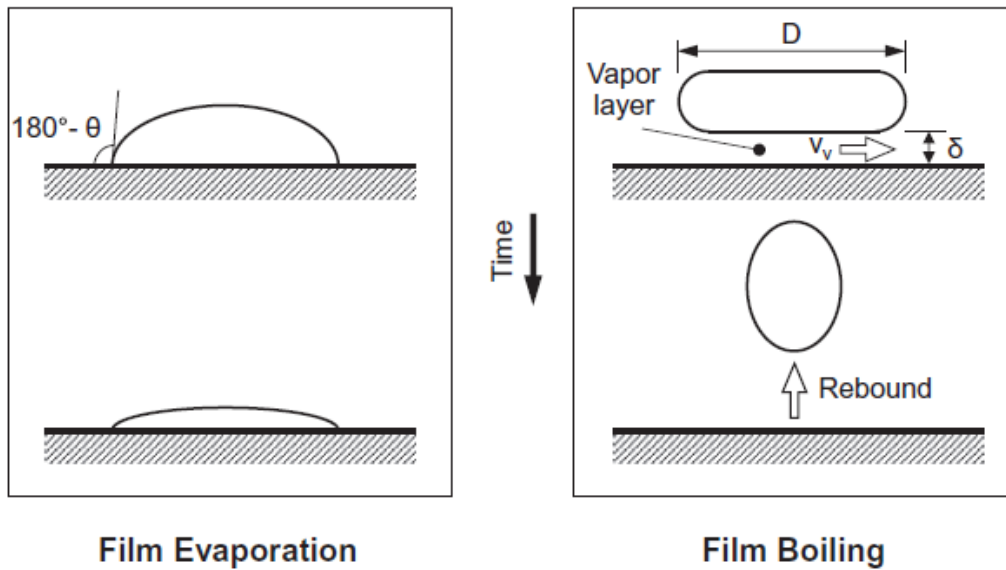
Figure 2.4 Graphic representation of droplet impinging on a heated surface, in both film evaporation and film boiling regime. *(Liang og Mudawar 2016)*.

By further increasing the surface temperature, heat flux will (marginally) increase due to the increasing temperature differences above the vapor layer (Liang og Mudawar 2016).

2.2.2. Leidenfrost temperature

As previously explained, The Leidenfrost temperature is the local minimum point in heat flux, which consequently means the surface temperature at which the droplet evaporation time is highest. For water, this temperature will vary from 150 ℃ to 210 ℃ above saturation temperature, dependent on material surface and the droplet impinging. As mentioned previously, there will be a vapor film stabilized below the droplet, as demonstrated in figure 2.5. (Gottfried, Lee og Bell 1966)
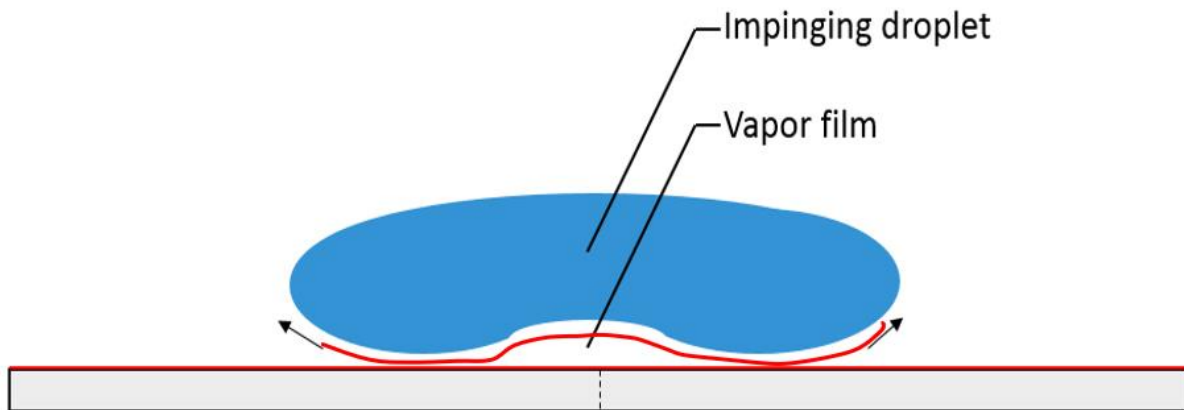
Figure 2.5 Droplet on a hot surface at Leidenfrost temperature. It demonstrates that the water droplet is not in contact with the surface, but floats on a stable vapor film (There will be a stable vapor film below the droplet). Figure adapted based on information provided from *(Gottfried, Lee og Bell 1966)*.

2.2.3. Weber number

Weber number (*We*) is a dimensionless parameter describing the kinetic forces divided by the surface tension, which is useful to analyze the interface between two different fluids (Frohn og Roth 2000). In this case, the interface between the droplet and surface. The formula for Weber number can be expressed as Eq. 2.6 (Frohn og Roth 2000).

$$We = \frac{\rho_f v_{drop}^2 l_{drop}}{\sigma} \tag{2.6}$$

where:

We	Weber number	[-]
ρ_f	Density of the fluid, typically 1000 kg/m³ for water	[kg/m³]
v_{drop}	Velocity of droplet	[m/s]
l_{drop}	Droplet diameter	[m]
σ	Surface tension	[N/m]

Based on the various parameters in the formula, Weber number is a parameter which could give valid information regarding droplet break-up prior to impact. It is also shown that for higher Weber numbers, when velocity and droplet diameter is dominant, the droplets tend to disintegrate into smaller droplets (Frohn og Roth 2000).

2.2.4. Effect of surface roughness and droplet contact angle

Contact angles of droplet on various metal surfaces will vary on the surface roughness (Kandlikar og Steinke 2002). In this master thesis, stainless steel with surface roughness Ra 3,0 μm was used.

To better understand the concept of droplet contact angle, this is illustrated in Figure 2.6. The contact angle can be divided into two phases; a*dvancing contact angle* and *receding contact angle.* The advancing contact angle refers to the state when the droplet is impinging onto the surface and expanding, while the receding contact angle refers to the state when the droplet *already* has hit the surface and will be sliding along the surface, reducing its contact area (Kandlikar og Steinke 2002).
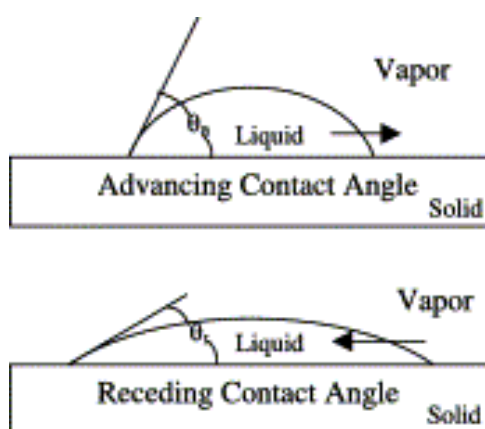
Figure 2.6 Illustration of the two phases of droplet contact angles; advanced contact angle and receding contact angle. Figure obtained from *(Kandlikar og Steinke 2002).*

These two conditions will naturally depend on the surface roughness of the material. Kandlikar and Steinke (2002) did some research on contact angles at copper and stainless steel as a function of surface roughness. They discovered that the contact angle will decrease at first with increasing surface roughness till it reaches approx. $R_a = 0,25$ μm. By further increasing the roughness, the droplet contact angle tends to increase.

Figure 2.7 summarizes their test results of contact angles as a function of surface roughness. It is notable to mention that these results apply for copper and stainless steel, as well as in ambient conditions ($T = 22$ ℃). (Kandlikar og Steinke 2002)
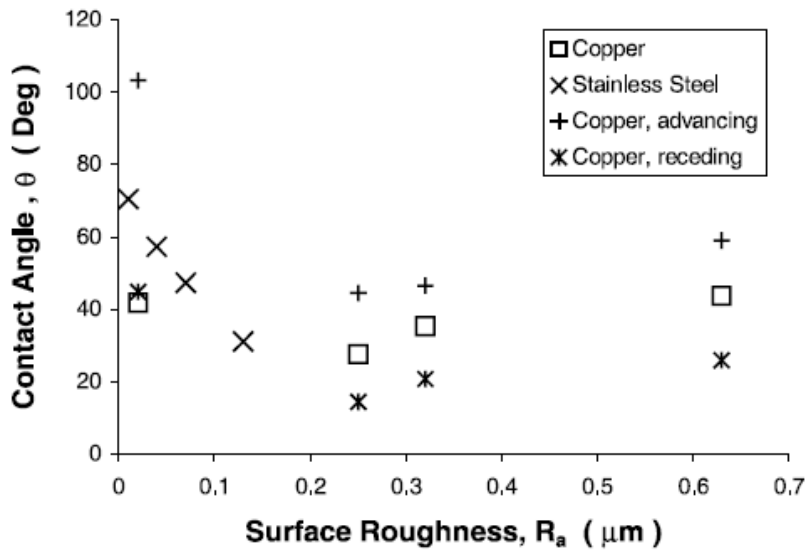
Figure 2.7 Demonstration of various contact angles as a function of surface roughness. The results for surface roughness for stainless steel up to approx. $R_a = 0,12 \, \mu m$, and various angles for copper at different roughness'. *(Kandlikar og Steinke 2002)*

2.2.5. Impact velocity

From the equations of motion, the impact velocity of droplet falling from a given height h_0 can be calculated by Eq. 2.7 (Hewitt 2014). The letter g is known as gravitational acceleration and will be considered a constant of 9,81 m/s^2 during the calculations. Since the gravitational acceleration is pointed downwards (negative y-direction), it will be indicated with a negative sign (Hewitt 2014). By applying these considerations into the motion formula, Equation 2.7 is derived.

$$v^2 = v_0^2 - 2g(h - h_0) \tag{2.7}$$

where:

v	Droplet impact velocity	[m/s]
v_0	Initial velocity of droplet	[m/s]
g	Gravitational acceleration	[m/s^2]
h	Height of stainless steel disc, which in this case is $h = 0$	[m]
h_0	Initial height of droplet	[m]

The initial velocity of droplet, as well as height of stainless steel disc is considered zero during the experiments, which rearranges the equation:

$$v = \sqrt{2gh_0} \qquad (2.7)$$

Figure 2.8 illustrates a conceptual sketch of the droplet impinging on the surface and showcases each of the parameters from Equation 2.7. The figure is divided into two parts; first part *(a)* for the initial state, and the second part *(b)* for the end state, when the droplet is impinging the surface.
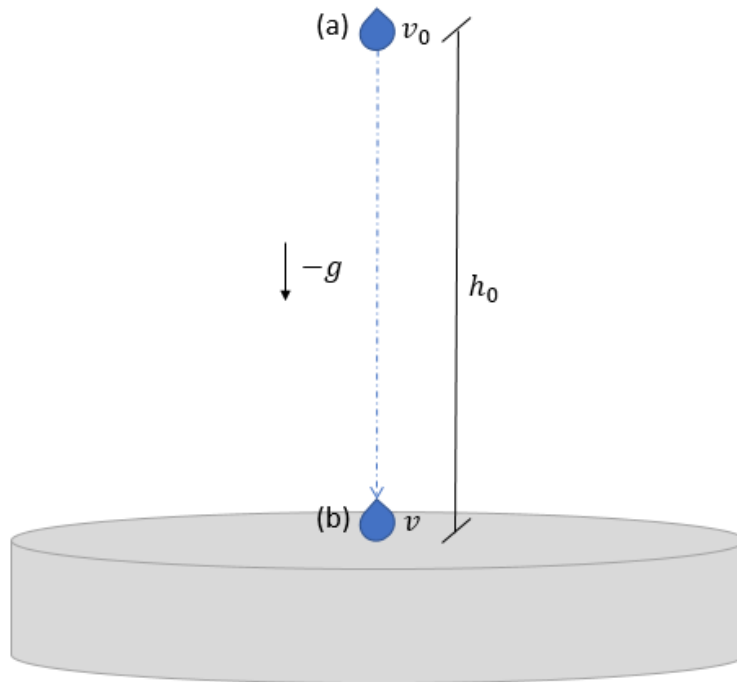
Figure 2.8 Sketch that illustrates droplet in two stages of motion energy; (a) the initial state, when the droplet is only affected by potential energy ($v = 0$, and height is equal to h_0). (b) the end state, when the droplet is impinging the surface ($v \neq 0$, and height is equal to zero). In-between those stages, the magnitude of the velocity is governed by the gravitational acceleration g. Figure adapted from *(Hewitt 2014)*

After a certain height, the droplet will obtain constant velocity, consequently meaning that the acceleration will be equal to zero. This velocity is called terminal velocity, where the drag forces (F_d) upwards and gravitational forces (F_g) downwards will equalize each other (Hall 2015). Figure 2.9 will give a graphic representation of how terminal velocity will operate.

Figure 2.9 Graphic representation of the terminal velocity principle, where drag forces is equal to gravitational forces. Figure adapted from *(Hall 2015)*.

2.2.6. Droplet cooling efficiency

One of the main issue of this master thesis is to address the droplet cooling efficiency. The methodology for calculating the droplet cooling efficiency in Excel will be described in Appendix A.4. In this master thesis, the heating process of the droplets from room temperature to boiling temperature, will be disregarded. It will merely focus on the interaction between the droplets and the surface, noted droplet cooling efficiency. The droplet cooling efficiency is based on the relation between *the actual heat transfer by the droplets* and *the rate of heat required to completely evaporate the droplets* (Equation 2.8)*. (Drysdale 2011).*

$$\chi_{drop} = \frac{\dot{Q}_{drops}}{\dot{Q}_{evap}} \tag{2.8}$$

where:

χ_{drop}	Droplets cooling efficiency	[-]
$\dot{Q}_{drops}$	Rate of heat transfer by droplet	[W]
$\dot{Q}_{evap}$	Rate of heat required to evaporate the droplet	[W]

The rate of heat transfer by the droplets will be addressed by a calculative procedure conducted in Excel and described in Appendix A.4. The difference between the total heat flow removed from the stainless steel disc and the heat lost by convection and radiation, will equal the heat flow by the droplets. The rate of heat required to evaporate the droplets will be addressed by knowing the mass rate ($\dot{m}_{rate}$) and the evaporation energy per gram of water (ΔH_{evap}) (Eq. 2.9). (Drysdale 2011).

$$\dot{Q}_{evap} = \dot{m}_{rate} \cdot \Delta H_{evap} \qquad (2.9)$$

where:

$\dot{m}_{rate}$	Mass rate of the droplets	[g/s]
ΔH_{evap}	Evaporation energy	[J/g]

2.3. NORSOK S-001

NORSOK S-001 defines the principles and requirements the safety design of offshore installations for production of oil and gas. This NORSOK standard will also, in some cases be applied for mobile offshore drilling units. (The Norwegian Oil Industry Association (OLF) 2008)

For each of the Safety critical elements (SCE) pointed out in S-001, there must be established a performance standard (PS), which include reliability and availability, interaction to other SCE and survivability. The performance standard will be based on requirements and recommendations provided in NORSOK standard, with associated standards and guidelines. (The Norwegian Oil Industry Association (OLF) 2008)

2.3.1. Firewater

The purpose of a firefighting system is to provide a quick and consistent means for extinguishing or control fires and mitigate explosion effects. The firefighting systems` performance will typically depend upon:

- Diesel system
- Emergency power system
- Instrument air system
- Hydraulic system

This NORSOK standard will also provide functional requirements, such as firewater supply system, firewater pump arrangement and will then give more specific requirements related to the selected firefighting system. The standard refers to NFPA 13, NFPA 15 and NFPA 16 for design guidelines. (The Norwegian Oil Industry Association (OLF) 2008)

There are specified some requirements regarding firewater pump capacity, amount of water per area and more. These specifications will naturally satisfy the performance requirements given in regulations. Some of these specifications will be summarized in Table 2.1 below.

Table 2.1 Some specifications from NORSOK s-001 regarding firewater. Information obtained from *(The Norwegian Oil Industry Association (OLF) 2008)*. *Converted from (l/min)/m^2 to (g/s)/m^2 **Multiplied with the relevant area of the experiments. The purpose is to link the specifications to this specific master thesis. The area will be a value of approximately 0,002 m^2, see section 3.1 regarding the test object.

Issue	Specification			
Firewater supply	Shall cover the largest Firewater demand, and the neighbor fire area with largest demand, plus supply to two hydrants			
Firewater pump	4 x 50 % of the largest area with respect to capacity and availability. Alternatively, it is accepted with a 3 x 100 % pump system configuration.			
Firewater flow	**Type of area**	**Flow [(l/min)/m^2]**	**Flow [(g/s)/m^2] ***	**Flow [g/s] ***
	Process areas	10 (l/min)/m^2	166,7 (g/s)/m^2	0,33 g/s
	Equipment surfaces	10 (l/min)/m^2	166,7 (g/s)/m^2	0,33 g/s
	Wellhead, including riser balconies and manifolds located on FPSO turrets.	20 (l/min)/m^2	333,3 (g/s)/m^2	0,66 g/s
	Other areas	In accordance with ISO 13702	-	-
Deluge nozzles	Deluge nozzles for area coverage on fully open process and drilling areas should be of the high velocity types			

2.3.2. Heat load

Table 2.2 represents dimensioning heat loads. It should be noted that the effect of area deluge is not accounted for in Table 2.2. The effect of deluge may be considered for process piping/equipment provided proper documentation is available on the effect of deluge as well as on the reliability of the Firewater supply system. (The Norwegian Oil Industry Association (OLF) 2008)

Table 2.2 Heat flux values *(The Norwegian Oil Industry Association (OLF) 2008)*

	Jet fire		Pool fire
	For leak rates	**For leak rates**	

	m > 2 kg/s kW/m^2	0,1 kg/s < m < 2 kg/s kW/m^2	kW/m^2
Local peak heat load	350	250	150
Global average heat load	100	0	100

The global average heat load demonstrates the average heat load that expose a significant part of the segment or structure. Consequently, provides a major part of the heat input to the entire process segment and, thus, affects the pressure in the segment. The local peak heat load, on the other hand, exposes a small local area of the process segment or of the structure to the peak heat flux. Consequently, determining the rupture temperature of different equipment and piping within the process segment. (The Norwegian Oil Industry Association (OLF) 2008)

Chapter 3

3. Experimental setup

This chapter will give an accurate overview of the experiment setup. The chapter will also give an overview of the experiment procedure, and the most crucial parameters.

3.1. Droplet impinging experiment

Figure 3.1 demonstrates the experimental setup of the small-scale droplet experiment. The experiment procedures for conducting the experiment will be explained in section 3.1.1. Bjørge et.al (2018) developed and constructed the basic idea of the experimental setup and was further developed by the author (in cooperation with Bjørge et.al).
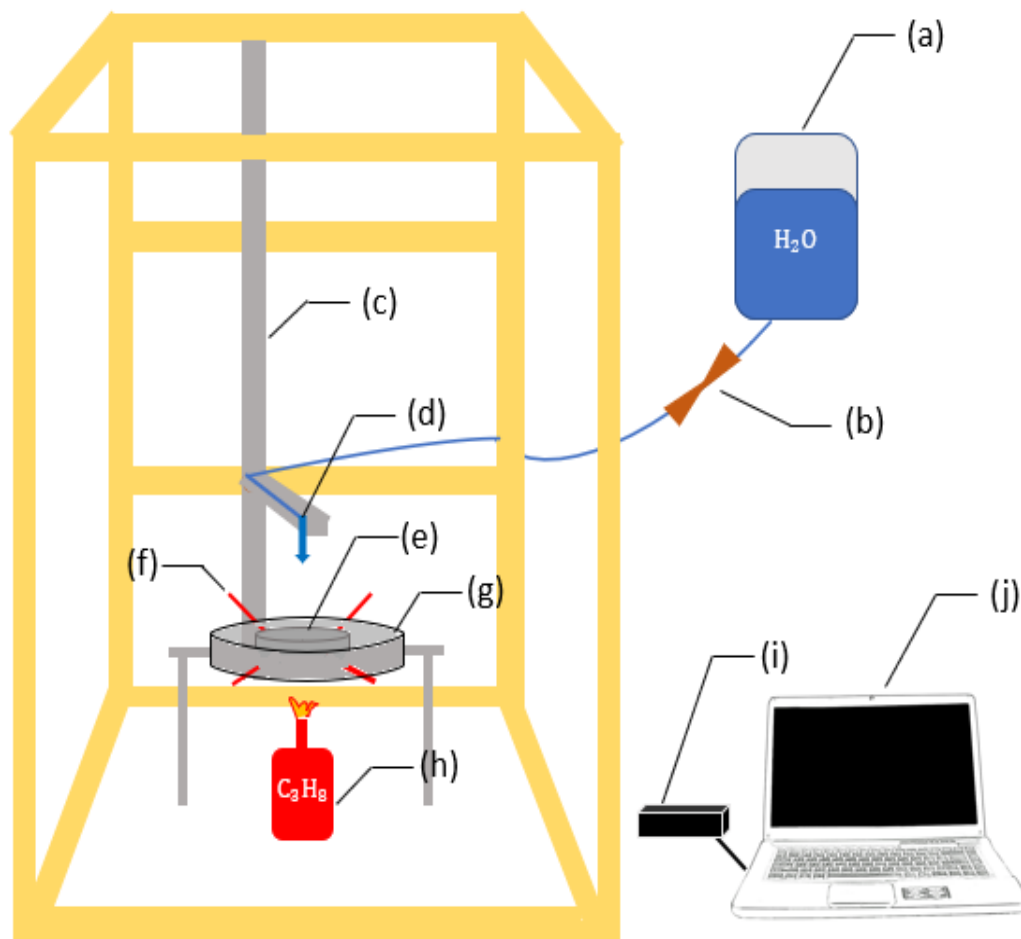
Figure 3.1 Three-dimensional sketch of the wood framed test cage and the experimental setup. (The figure is not in scale)

(a) Bag of water

The water bag works as a water supply throughout the experiments. The bag contains fresh deionized water (changed at least once a week). A thin, plastic tube attached to the bag, leads the water further, to an injection needle.

(b) Valve

The valve was used to adjust the droplet interval during the droplet experiments. Trials conducted before the experiments, revealed that the most appropriate fixed mass rate was set to around 0,023 g/s. The valve was shut (i.e. no water supply) during the baseline experiments.

(c) Pole and beam

The pole is a rack steel-rod and allowed for adjusting the needle at various heights. This will consequently allow for different impinging velocities, as discussed in Section 2.2.5. Investigated heights and corresponding theoretical impingement velocities are shown in Table 3.1. By using Equation 2.8 for the various heights, the theoretical impinging velocities as function of height can also be presented in the table. Due to the sensitivities by determining the real impinging velocity, the calculations are simplified by assuming that the theoretical velocities and the real velocities are the same. Consequently, means that drag forces is disregarded. This assumption is justified, as droplets impinging from 1 m agrees closely to the velocity calculated by the effect of gravity, with $\pm$ 0,01 m/s accuracy (Pasandideh-Fard, et al. 2001). The heights are measured from the surface of the disc to the sharp end of the needle.

Table 3.1 Various theoretical impinging velocities as a function of height.

Height (h_0)	Impact velocity (v)
0,25 m	2,21 m/s
0,50 m	3,13 m/s
1,00 m	4,43 m/s

The beam, the injection needle and the water tube will be shielded by a small aluminum foil, illustrated in Figure 3.2.
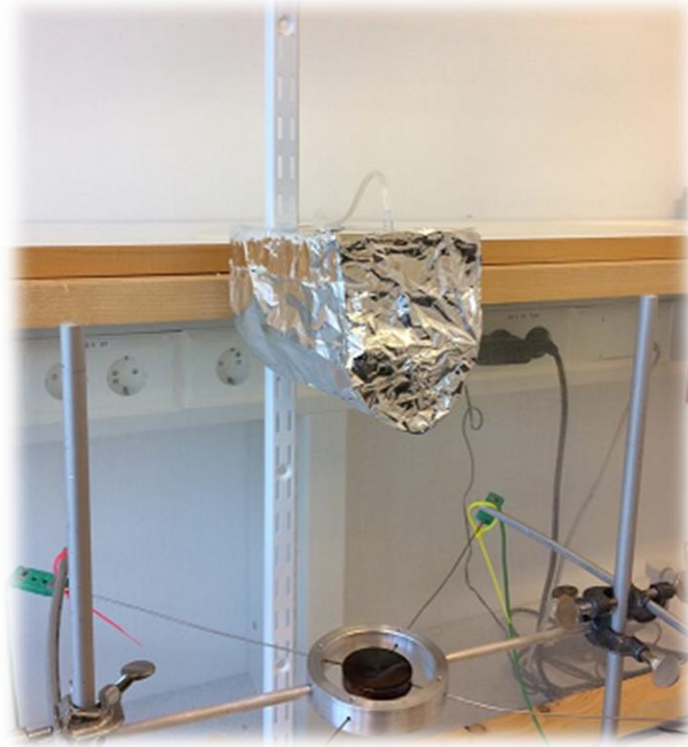
Figure 3.2 Photograph of the aluminum foil shielding the steel beam and injection needle.

(d) Injection needle

The injection needle, attached to the small water tube, was used to produce the droplets impinging onto the test object (stainless steel disc). The injection needles used to vary the droplet sizes are presented in Table 3.2.

Table 3.2 Various types of injection needles, and their sizes

Color	Producer	Needle dimension	Needle diameter
Orange	Terumo	25Gx1" 0,5x25 mm	0,5 mm
Yellow	B. Braun	19Gx1 ½" 1,10x40 mm	1,1 mm
White	Kruuse	16Gx 1" 1,60x25 mm	1,6 mm

Before and after each experiment involving impinging droplets, 20 droplets were collected and weighted. It was assumed that the droplets radius during the experiment is the averaged radius calculated from the weighted droplets before and after the experiment. By using following relation between mass and volume, and by assuming a spherical shape of the droplets, the droplet diameter can be addressed (Eq. 3.1):

$$\rho = \frac{m}{V}$$ (3.1)

Where:

ρ	Density of water (Typically 1000 kg/m³)	[kg/m³]
m	Mass of droplet	[kg]
V	Volume of the droplet (spherical)	[m³]

By using volume of a sphere, the equation can be rearranged to:

$$D = 2 \cdot \sqrt[3]{\frac{3m}{4\pi\rho}} \tag{3.1}$$

(e) Stainless steel disc

The stainless steel disc was placed approximately 0,3 m above the laboratory bench. The design of the disc, as well as mass, and horizontal area are shown below (Table 3.3 and Figure 3.3).

Table 3.3 Area and mass of the stainless steel disc.

Material	Mass	Area
Stainless steel (AISI 316)	0,1539 kg	1963,5 mm²

A sketch of the disc indicated with the disc's dimensions and the location of the thermocouples, is presented in Figure 3.3.
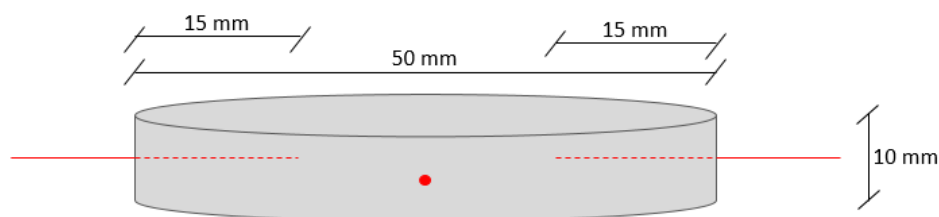
Figure 3.3 Sketch of the stainless steel disc, including location of four thermocouples (red lines).

(f) Thermocouples

In order to record the disc temperature, four thermocouples were placed in placed in the disc as shown in Fig. 3.3 and Fig. 3.5. at a depth of 15 mm inside the stainless steel disc. Two other thermocouples measured the ambient temperature. All six thermocouples were standard 1,6 mm diameter type K (cromel alumel) mantel thermocouples, delivered by Pentronic (Pentronic T/C type K model 8102000).

(g) Ring-holder

The ring-holder is a cylinder-based ring with two additional circular beams, threaded to the ring from each side. The ring-holder consists of aluminum and was used to adjust the stainless steel disc to various inclinations. The various angles tested were horizontal (0°), 30°, and 60° (Figure 3.4).
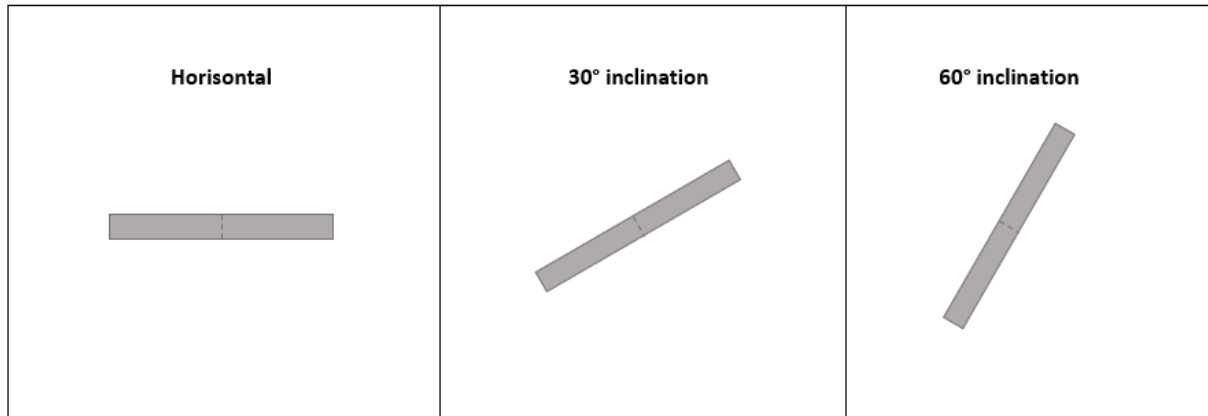
Figure 3.4 Illustrative side-view of the stainless steel disc, with three different inclinations.

Figure 3.5 shows a concept sketch of the ring-holder, and each of the parts indicated on the figure ((i)-(iii)) will be explained down below.
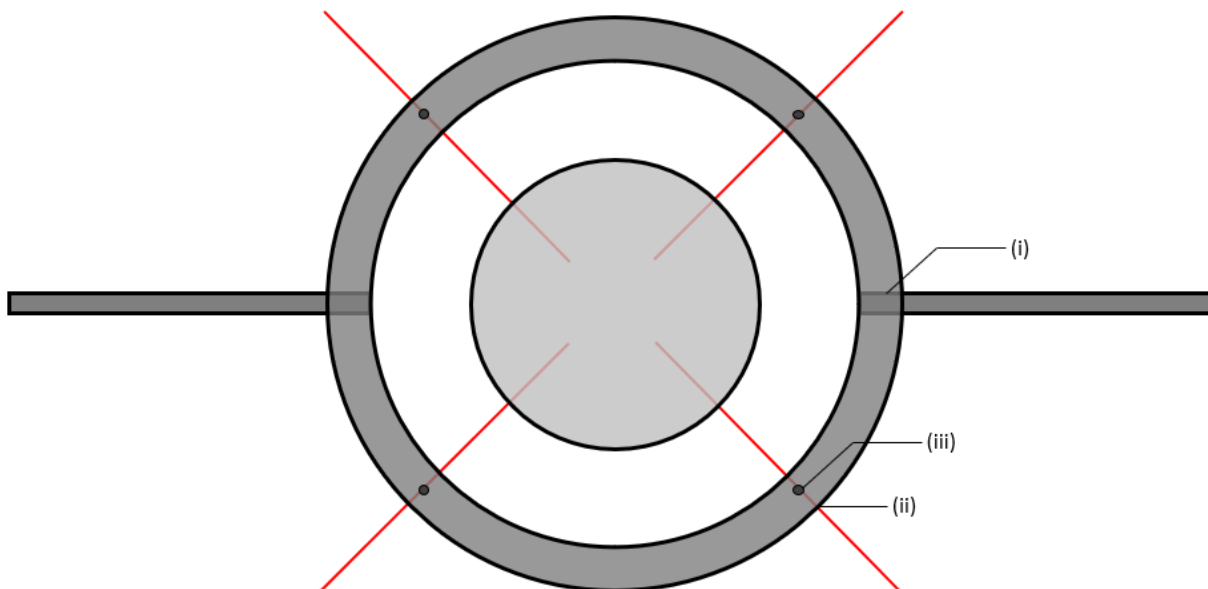
Figure 3.5 Concept sketch of the ring-holder seen from above. The four red lines indicates the thermocouples, and how they interact with the test object. Concept sketch developed by Torgrim Log.

(i) To get a practical connection between the ring and the beams, a threading solution was used. By doing this, the beams can easily be dismantled from the ring. (ii) For each 90 ° a hole was drilled, to

lead through each of the thermocouples into the disc. The disc was suspended by these four thermocouples. (iii) Threaded screws were used to carefully clamp each thermocouple and keep them fixed, thus also stabilizing the stainless steel disc.

(h) Heat supply

A Bunsen burner with propane/butane mixture was used to heat the stainless steel disc to the desired temperature before each of the experiments.

(i) Data logger

A data logger (National instruments NI cDAG-9184) was used to record and collect the temperatures of the 6 thermocouples (3.1, f) at one Hz, and transfer the data to a PC.

(j) Laptop

The laptop received and stored all the data transferred from the data logger. The output data were extracted into an Excel sheet for processing and analysis.

Additional equipment

Some additional items, not shown in Figure 3.1, are described in Table 3.4.

Table 3.4 Additional items and their function

Equipment	Function
Test cage	The test cage built of wooden laths, which forms the frames of the cage, with fine mesh screen around for visibility. Size: 1,1 m x 0,55 m x 1,55 m height. It provided to the experimental set-up partial protection from surrounding laboratory air turbulence (Log og Heskestad 1998).
Hygrometer	Hygrometer, (Extech Instruments RH390 - precision psychrometer), was used to measure the ambient temperature and relative humidity.
Balance	Balance (type AG204 DeltaRange®), used to determine the mass of the droplets (and other objects). Accuracy: 0,1-1 mg
Fine mesh screen	The fine mesh screen covered the test cage, in order to shield the experiments from external disturbances.
Acetone	Before each experiment, the stainless steel disc was cleaned with acetone.
Glass beaker	Glass beaker was used to weigh the droplets to determine the droplet mass.
Leveler	A Leveler was used to adjust the stainless steel disc to the desired inclination.

3.1.1. Methodology

In this section, the experiments will be briefly explained. The procedure consists of two parts: baseline experiment and droplet experiment. A methodology for data analysis and processing is associated to baseline and droplet experiments respectively. Combining three droplets sizes, three inclinations and three heights, a total of 27 experimental series were conducted, each individual series consisting of two baseline experiments and five droplet experiments. A more detailed experiment and data processing procedure will be presented in Appendix A.

3.1.1.1. Baseline experiment

The baseline experiments were carried out without any cooling effect from water droplets consequently meaning that the stainless steel disc is mainly affected by natural cooling due to radiation and convection. Two baseline experiments were performed during each experimental series, one before and one after the droplet-cooling experiments. A detailed step-by-step method for conducting a baseline experiment is presented in Appendix A.1.

3.1.1.1.1. Baseline data processing

Natural cooling (by heat transfer) of the stainless steel disc from approximately 400°C to approximately 85°C takes about 35 minutes. Cooling the disc with water droplets (while at the same time the natural cooling processes apply) takes about 13 minutes. It is thus not possible to plot the curves for baseline and droplet experiments against the same time-axis. Data processing is therefore based on the respective cooling rate, as a function of temperature. Plots of dT/dt vs. T allow the curves (baseline and droplet experiments) to be plotted on the same diagram. This allows for the contribution of heat transfer to be subtracted from the joint phenomenon.

The issue for baseline experiment is to get a correlation of the cooling rate $(\frac{dT}{dt})$ with respect of temperature, to use these results in the droplet experiment data. There will be a total of two baseline experiment per experiment series, which is the first and last experiment in the series, with five droplet experiments in-between. There will be an average curve of the two baseline experiments to analyze each of the droplet experiment, then the deviation between them can be addressed. In Appendix A.2, there will be a step-by-step method to address the cooling rate $(\frac{dT}{dt})$.

3.1.1.2. Droplet experiment

During the droplet experiments the disc was affected by both water cooling and natural cooling due to radiation and convection. There is a total of five droplets experiments in-between the two baseline experiments for each experiment series. A step-by-step method for conducting a droplet experiment

will be presented in Appendix A.3. It should be mentioned that the water inside the bag should be replaced once a-week, to ensure that the water is clean.

3.1.1.2.1. Droplet experiment data processing

The issue for droplet experiments will be to address the droplet cooling efficiency as a function of temperature. A total of five droplet experiments per experimental series were conducted. The baseline experiments will function as the reference experiments, which will be analyzed against the droplet experiments to address the cooling efficiency. The results from each of the droplets experiments will be compared against each other to analyze for deviations. A step-by-step method to address the droplet cooling efficiency is presented in Appendix A.4.

4. Results

This chapter will present the results obtained from the droplet impinging experiments (including respective baselines), when the chosen parameters (droplet diameter, impinging height and stainless steel disc inclination) are varied between 3 different values each. The author´s observations are also included. Diagrams and parameters will be briefly explained in this chapter and further analyzed in chapter 5.

4.1. Observations

This subsection describes the author´s observations over phenomena not directly addressed in the present study. Visual observations of the droplets` break-up (not photographed) and audible observations (not recorded). These phenomena may be studied in future research.

Around 400 ℃, the droplets bounce off the surface and disintegrate into seemingly equally sized droplets. For height 25 cm, the droplets will disintegrate into four equally sized droplets, while for height 100 cm, the droplets will disintegrate into a higher number of smaller droplets, due to increased Weber number. Since no contact between water droplets and metal surface exists, the cooling effect by water is minimal, which is verified to be less than 10 % by analyzing the results.

As the temperature decreases from 400 ℃ to 250-300 ℃ there is almost no difference in the cooling effect as the water droplets still bounces off the surface. However, as the temperature decreases below 400 ℃, the droplets will disintegrate into many smaller droplets. It can be observed that there is a vapor layer above the surface which separates the water from the hot metal surface. The disintegrated droplets will "dance" above the surface. This temperature range is called, in the literature, as the *film boiling region*.

The next region, *transition boiling*, marks the temperature range between *Leidenfrost temperature* and the temperature associated with the maximum cooling effect, called *boiling crisis*. There is a clear sizzling sound in this temperature range, which indicates that the water droplets display a higher cooling effect. By observing the disc while observing the temperature, when the sizzling sound starts, it will also be the start of a greater decline in temperature, and consequently a rise in the droplet cooling efficiency. However, this region heavily depends on the droplet size, inclination and velocity, as the curves are different for each of the parameters.

After the droplets had displayed their maximum effect, the droplets seem to be more able to attach to the surface. When the temperature is sufficiently low, the droplets will eventually form a small

puddle on the metal surface. If the stainless steel disc is in horizontal state, there will be a puddle equally distributed above the stainless steel disc, and if the stainless steel disc is inclined, there will be a puddle distributed on the lower side of the disc. This is most notable when there is a low velocity of the droplets and the stainless steel disc is in horizontal state, as the effect of bouncing is less prominent. The droplets will be more prone to be attached to the surface rather than bouncing off.

4.1.1. Errors and uncertainties

In most of the experiments, the droplet frequency/interval tends to behave relatively constant, but in some cases, there will be a drop in the interval. The valve had to be adjusted during the experiment to keep the mass rate constant, at approx. 0,023 g/s. In some cases, mainly for the smallest droplets, the droplet interval was difficult to maneuver due to its sensitivity.

The droplets could also change mass during the experiment. When there is an issue about, said interval, the user will naturally adjust the valve to the proper interval. However, in some rare cases, the droplet size could also increase, and consequently increase the mass rate by a small amount. These factors could explain small variations in the droplet mass rate.

Other difficulties, such as droplets not hitting the exact center of the stainless steel disc, could occur when the ventilation in the room influenced the experiments. The experiments, where this was an issue, (for the smallest droplets) were conducted at the times when ventilation system was shut off, such as afternoons and weekends. This uncertainty was most present for the droplets with smallest diameter, which are more easily affected by air movements.

4.2. Input parameters

In order to produce comparable results, the droplets mass flow was kept constant. The droplet interval was therefore adjusted accordingly (Small droplets falling more frequently, and larger droplets falling more seldom). However, due to the sensitivities discussed in previous subsection, there were some small deviations in droplet mass rate. Droplet characteristics of the experiments are presented in Table 4.1.

Tabell 4.1 Mass flow and droplet diameter (range and average) for the 3 different needles used.

Color of needle	Interval max-min [drop/s]	Interval average [drop/s]	Diameter max-min [mm]	Diameter average [mm]
Orange	3,08 - 2,41	2.73	2,62 – 2,49	2,53
Yellow	1,42 - 1,23	1,32	3,28 – 3,18	3,24
White	0,97 – 0,80	0,90	3,68 – 3,62	3,66

Parameter	Maximum [g/s]	Minimum [g/s]	Average [g/s]	Standard deviation [g/s]
Droplet mass rate	0,0243	0,0217	0,023	0,000619

Several other parameters were measured in each of the experimental series. This includes ambient temperature and relative humidity in the room, as well as dew point, humidity and air pressure outside. The ambient temperature had a range of approximately $18 - 23\ ℃$, while the relative humidity had a range of approximately $30 - 35\ \%$. These parameters may not be as sensitive and crucial as the parameters described in Table 4.1, nevertheless important to measure parameters that could have any impact on the experiments.

4.3. Baseline experiments

In this section, each of the results from the baseline experiments will be presented in forms of diagrams. Figure 4.1 presents the measured disc-temperature versus time for each of the three inclinations. Each of the three curves represent the average of nine baseline measurements with the same inclination. The temperature decline will be compared to identify the effect of three different inclinations on the air-cooling of the disc. The term "Baseline experiments" included both convection and radiation <u>without</u> cooling effect from water droplets.
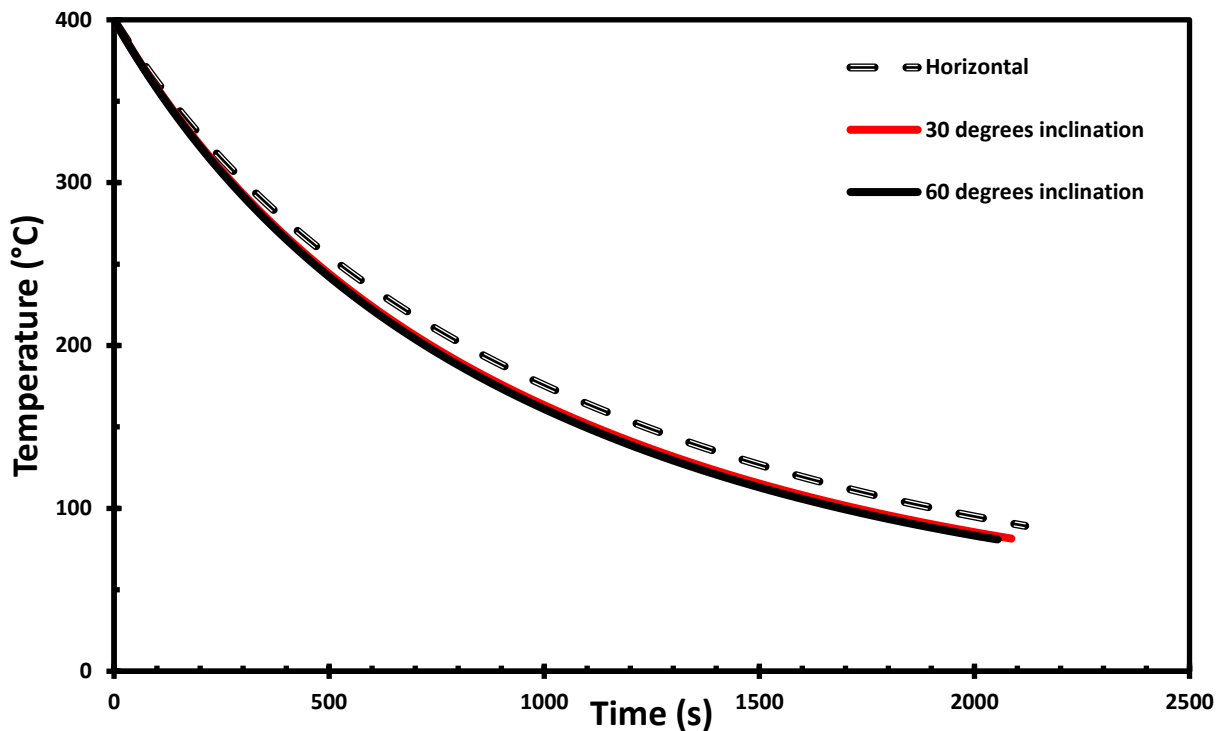
Figure 4.1 Temperature of the disc vs. time. The temperature decrease is due to merely convection and radiation, without any impact from water droplets. The temperature decrease for three different inclinations is compared.

There is more heat transfer present when the stainless steel disc is inclined instead of horizontal, probably because of stronger convective cooling. It can also be shown that the difference in natural cooling effect between 30° and 60° inclination was less compared to the difference between a horizontal and an inclined surface. This can consequently mean that effect of air cooling on an inclined surface was almost the same (irrespective of inclination), since the observed difference between 30° and 60° is so small.

4.3.1. Cooling rate

As mentioned, the baseline experiments were done by analyzing the temperature decay by mere heat transfer mechanism. Although every advanced fire calculation associated with time is numerical, there could be obtained some analytical correlations which describes complicated issues. In this case, there were obtained a 2nd degree correlation which describes the cooling rate with respect of temperature by including conduction, convection and radiation. These correlations did also verify that the cooling rate did not stay the same for each inclination, which explains why the baseline experiments were done for each experimental series.

Figure 4.2 summarizes the cooling rate (dT/dt) with respect of temperature for the three various inclinations. It can be noticed that each of the inclinations have their own 2nd degree function where x

is substituted with *T* and *y* is substituted with *dT/dt*, consequently, making it a function of $\frac{dT}{dt} = aT^2 + bT - c$. Between horizontal and 60° inclination, the c-joint of the equation had the most significant change with a deviation of approximately $4 \cdot 10^{-3}$ K/s. All around, it can be noticed that the functions with an inclined surface increased more rapidly compare to the function with a horizontal surface.

Horizontal	30° inclination	60° inclination

$y = 1{,}4211\text{E-}06x^2 + 4{,}7673\text{E-}04x - 5{,}1629\text{E-}03$
$R^2 = 9{,}9971\text{E-}01$

$y = 1{,}5509\text{E-}06x^2 + 5{,}4307\text{E-}04x - 8{,}4399\text{E-}03$
$R^2 = 9{,}9986\text{E-}01$

$y = 1{,}5082\text{E-}06x^2 + 5{,}6446\text{E-}04x - 9{,}1821\text{E-}03$
$R^2 = 9{,}9986\text{E-}01$
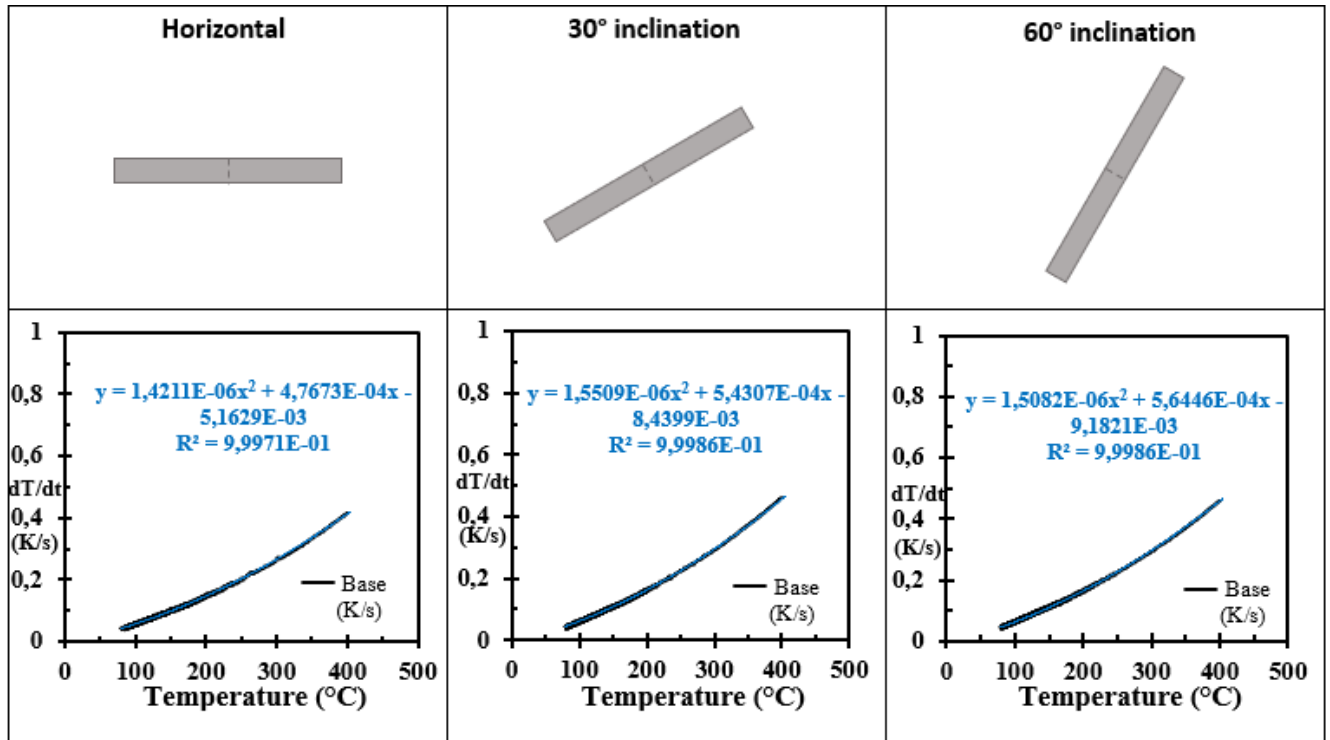
Figure 4.2 Comparison of cooling rate for three different inclinations.

4.4. Droplet cooling efficiency

In this section, each of the results from the droplet impinging experiments will be presented in form of diagrams. The droplet cooling efficiency will be presented as a function of disc temperatures between 400 ℃ and 50 ℃. The most relevant output parameters regarding the experiments and the effect of three different velocities will also be analyzed. Each of the 27 curves presented in subsection 4.4.1-4.4.3 represents an average of 5 droplet experiments. Lastly, in subsection 4.4.4, the effect of inclination will be analyzed. It is important to mention that the temperatures will be analyzed in the opposite direction, i.e. analyzing the development from 400 ℃ downwards.

4.4.1. Horizontal state

4.4.1.1. Largest droplets

The droplet cooling efficiency as a function of disc temperature for the largest droplets, are presented in Figure 4.3.

Figure 4.3 Droplet cooling efficiency vs. disc temperature for three different velocities. (Experiments conducted with the largest needle – white – and horizontal disc). The droplet sizes are displayed in the figure label.

The droplets with the highest impact velocity resulted in the highest maximum cooling efficiency (81 %). However, the droplet with the lowest velocity seems to «stick» at the surface in the nucleate boiling region due to its lower weber number (it did not bounce off to the same extent), and demonstrated higher efficiency when the temperature was lower than approximately 140 °C. It was recorded to not have that clear decline compare to the two other velocities.

The development of the cooling efficiency was observed to behave almost the same between all the velocities, with some small deviations, and the efficiency started to rise at approximately 290 °C. (i.e. the film boiling region is obtained at T > 290 °C). It can also be shown that the temperature range, where it demonstrated the highest cooling efficiency, were around 180-190 °C.

4.4.1.2. Middle-sized droplets

The droplet cooling efficiency as a function of disc temperature for the middle-sized droplets, are presented in Figure 4.4.

Figure 4.4 Droplet cooling efficiency vs. disc temperature for three different velocities. (Experiments conducted with the middle-sized needle – yellow – and horizontal disc). The droplet sizes are displayed in the figure label.

Similar behavior in droplet cooling efficiency as for the largest droplets was also observed for middle-sized droplets. Smaller differences between the highest velocity and the middle velocity for the middle-sized droplets compare to the largest droplets. Droplets with the highest velocity were recorded to have approx. the same maximum cooling efficiency as for the lowest velocity (around 73,5 %). The biggest notable difference is the temperature of the maximum efficiency, and the temperature range where the droplets have a high efficiency. The highest and middle velocity was observed to have one clear peak around the same temperature of approximately 190 °C. It is shown that the droplets with the lowest velocity gives the most overall efficiency with two peaks in a range between approximately 195 °C and 130 °C. This may be due to the lower degree of bouncing, as the Weber number is lower.

Again, the growth phase was observed to behave relatively identically for the three different velocities, and the efficiency starts to rise at approximately 295 °C. Consequently, meaning that the film boiling region was obtained at T > 295 °C.

4.4.1.3. Smallest droplets

The droplet cooling efficiency as a function of disc temperature for the smallest droplets, are presented in Figure 4.5.
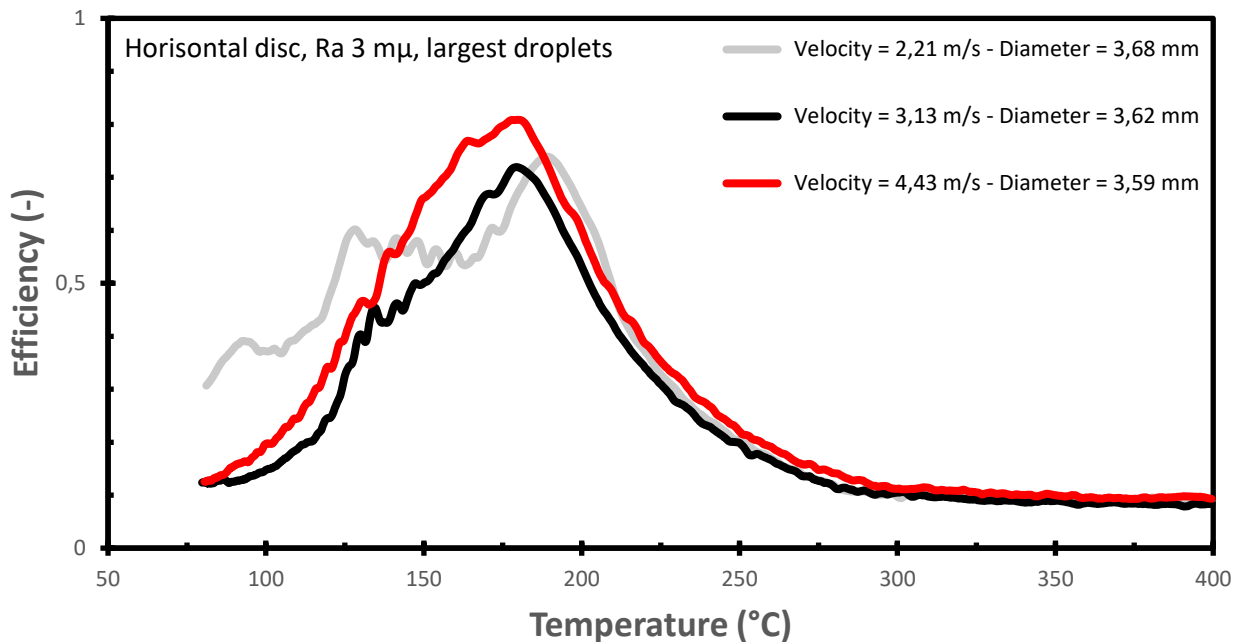

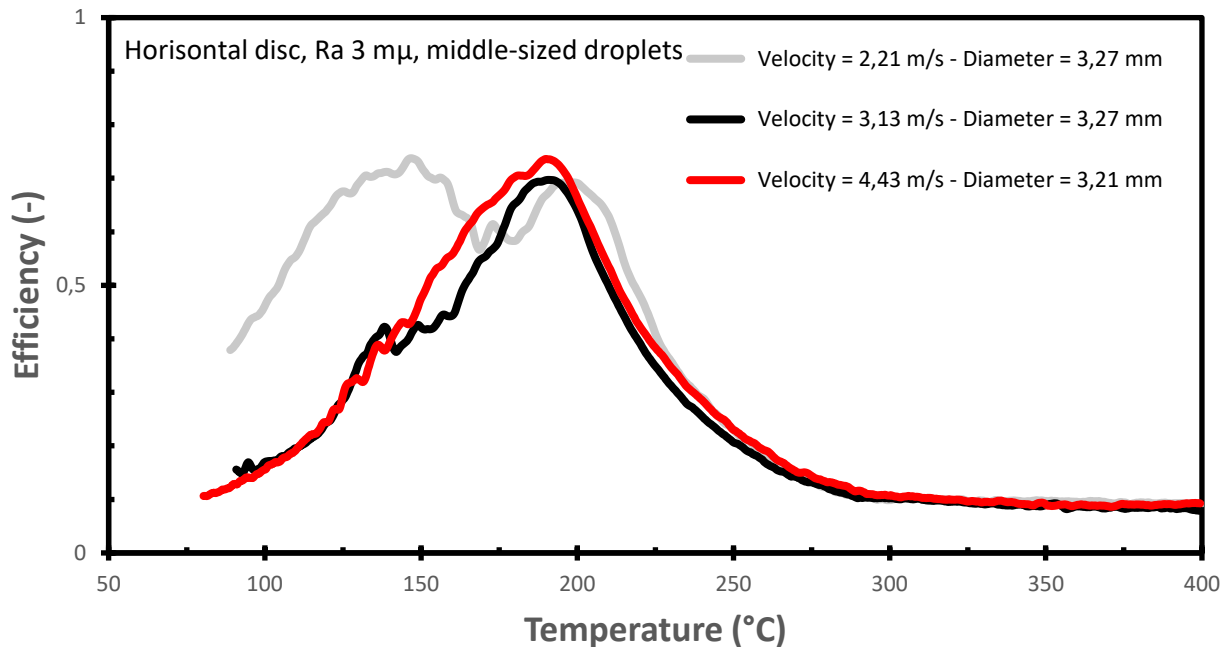**Figure 4.5** Droplet cooling efficiency vs. disc temperature for three different droplet velocities. (Experiments conducted with the smallest needle – orange – and horizontal disc). The droplet sizes are displayed in the figure label.

Almost the same trend as for the medium sized droplets. The highest and middle impact velocity droplets had approximately the same cooling efficiency, with some small deviations. The droplets with the lowest velocity will, to a higher extent stick to the surface, and therefore, displayed higher overall cooling efficiency compared to the two other velocities.

The droplets with the lowest velocity was recorded to have a seemingly continuous peak in a temperature range of approximately 140 °C - 210 °C (droplet cooling efficiency between 58,7 % and 67,4 %). The droplets with the medium velocity had a peak at temperature around 215 °C (63,5 % efficiency), while the droplets with the highest velocity had a peak at temperature around 210 °C (60 % efficiency).

The growth for efficiency behaved relatively similar for all the velocities, and the efficiency started to rise at approximately 300 °C (i.e. film boiling region observed at T > 300 °C).

4.4.1.4. Summary of horizontal setup

i) Different velocities, same droplet size (Fig. 4.3, 4.4, 4.5)

There is a clear trend when the stainless steel disc is horizontal; the droplets with the highest and middle velocity had clear «mountain peaks» with clear maximum points whereas the droplets with the lowest velocity demonstrate high efficiency over a wider temperature range. In other words, the droplets with lowest impact velocity seem more prone to stick on the surface and form a «puddle» laying on the surface.

ii) Different droplet sizes, same velocity (Figures not explicitly drawn)

For horizontal setup and the same velocity, the biggest droplets were recorded to have a higher maximum droplet cooling efficiency. The smallest droplets had its peak at around 215℃, while the biggest droplets had its peak around 190 ℃. This indicates that small droplet sizes may have higher cooling efficiency at higher temperatures compared to the bigger droplets.

4.4.2. 30º inclination

4.4.2.1. Largest droplets

Figure 4.6 presents the droplet cooling efficiency as a function of disc temperature for the largest droplets with three different heights, consequently three different impact velocities onto a fixed 30º inclined stainless steel disc.
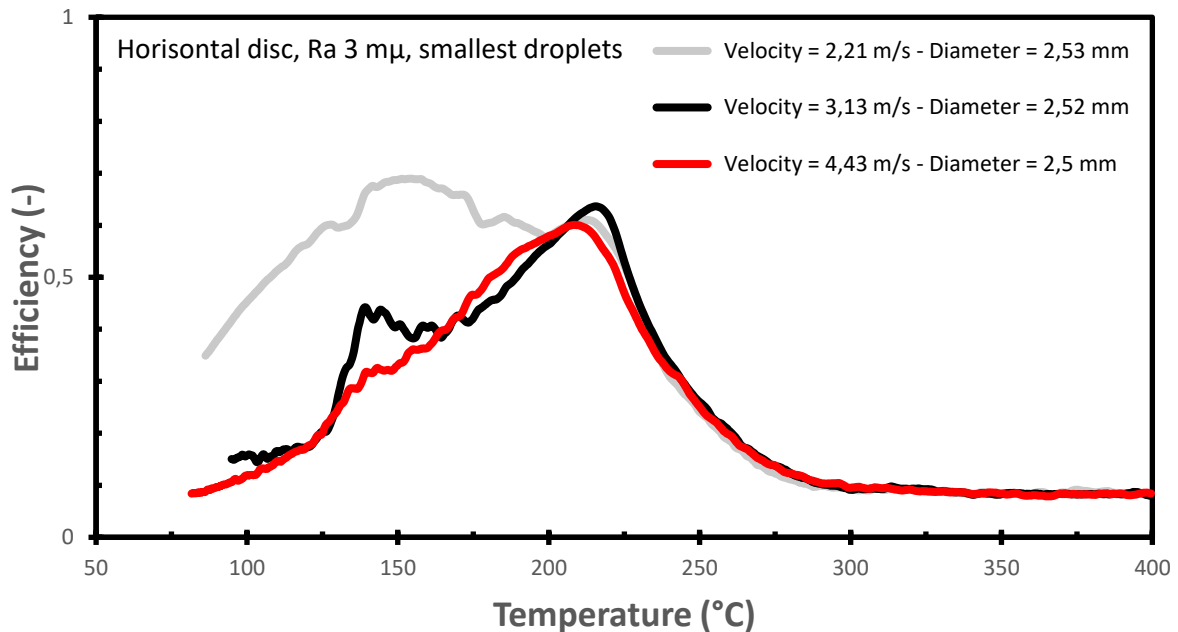
Figure 4.6 Droplet cooling efficiency vs. disc temperature for three different velocities. (Experiments conducted with the same droplet diameter - largest needle, white – and same inclination (30º) of the disc). The droplet sizes are displayed in the figure label.

The droplets with the highest velocity seemed to execute most cooling efficiency, and the droplets with the lowest velocity consequently demonstrated the lowest cooling efficiency. Droplets will naturally be less prone to attach to the surface due to the inclination.

As shown in Figure 4.6, the droplets with the highest velocity had a maximum point at a temperature of around 160 ℃ where it displayed a cooling efficiency of around 73 %. The droplets with the middle velocity had a maximum at a higher temperature of approximately 180 ℃ (around 70 % efficiency). Lastly, the droplets with the lowest velocity had a maximum cooling efficiency at temperature of approx. 170 ℃ (around 65 % efficiency).

It can also be observed that the droplets with the highest impact velocity demonstrated higher efficiency at a wider temperature range, compared to the two other velocities. The efficiency started to rise at approx. the same temperature for all the velocities, at around 290 ℃ (i.e. film boiling region observed at T > 290 °C).

4.4.2.2. Middle-sized droplets

The droplet cooling efficiency as a function of disc temperature for the middle-sized droplets, for a 30° inclined disc, is presented in Figure 4.7.
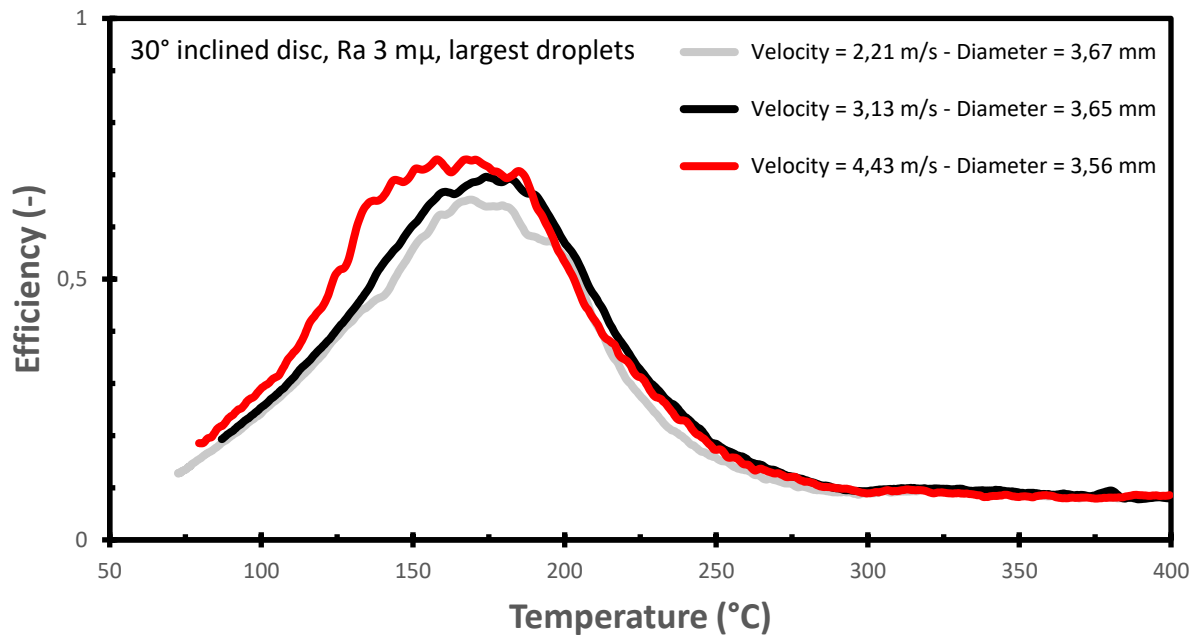

Figure 4.7 Droplet cooling efficiency vs. disc temperature for three different impingement velocities. (Experiments conducted with the same droplet diameter – middle-sized needle (yellow) – and same inclination (30°) of the disc). The droplet sizes are displayed in the figure label.

The results demonstrate very small differences in droplet cooling efficiency between droplets with the highest and middle velocity. Besides that, the efficiency was recorded to behave almost the same as for the largest droplets. It can also be observed that the peak (i.e. higher efficiency) last longer compare to the largest droplets (Between 200 ℃ and 140 ℃).

As shown in Figure 4.7, the droplets with the highest impact velocity was recorded to have a maximum efficiency at temperature of approx. 155 ℃ (73 % droplet cooling efficiency). However, it was recorded to have approximately 70 % efficiency in a temperature range of 190 ℃ - 155 ℃. The droplets with the lowest impact velocity had a maximum in droplet cooling efficiency at temperature of around 200 ℃ (around 65 % cooling efficiency). The lowest impact velocity droplets demonstrated an efficiency of around 60 % in a temperature range of approximately 200 ℃ - 150 ℃.

Again, it can be observed that the droplets with the highest impact velocity demonstrates higher efficiency at a slightly wider temperature range, compare to the two other velocity droplets. The

efficiency starts to rise at approx. the same temperature for all the velocities, at around 295 ℃ (i.e. film boiling region observed at T > 295 °C).

4.4.2.3. Smallest droplets

The droplet cooling efficiency as a function of disc temperature for the smallest droplets, for a 30° inclined disc, is be presented in Figure 4.8.
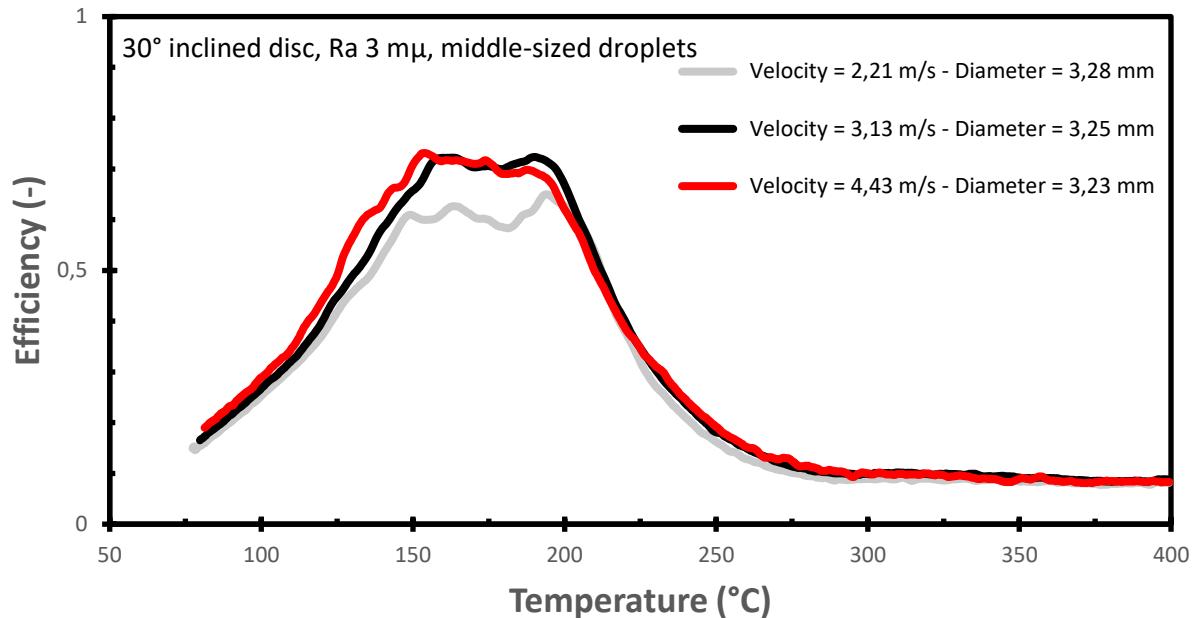

Figure 4.8 Droplet cooling efficiency vs disc temperature for three different velocities. Experiments conducted with approximately the same droplet diameter (orange needle) and the same disc inclination (30°). The droplet sizes are displayed in the figure label.

The efficiency trend behaved almost the same as for middle-sized droplets, beside from that the highest impact velocity droplets demonstrated higher efficiency at a wider temperature range compare to the middle velocity droplets. It can also be observed that the peak efficiency had a wider range compared to the largest and medium sized droplets (Between 215 ℃ and 130 ℃).

As shown in Figure 4.8, the droplets with the highest impact velocity demonstrated a higher maximum efficiency at temperature around 190 ℃, where the droplet cooling efficiency displays around 66 %. However, there was recorded to be approx. 60 % efficiency in a temperature range of 210 ℃ - 135 ℃. A notable observation is that the droplets with the middle impact velocity demonstrated higher efficiency at a higher temperature, of approx. 213 ℃ - 200 ℃. Lastly, the droplets with the lowest impact velocity had a maximum cooling efficiency at temperature around 205 ℃ (53 % efficiency). The

lowest impact velocity droplets demonstrated an efficiency of around 50 % in a temperature range of approx. 220 ℃ - 145 ℃.

Again, it can be observed that the droplets with the highest impact velocity demonstrated higher efficiency at a slightly wider temperature range, compared to the two other impact velocities. The efficiency was recorded to rise at approx. the same temperature for all the velocities, at around 295 ℃ (i.e. film boiling region observed at T > 295 ℃).

4.4.2.4. Summary of 30º inclination

i) Different velocities, same droplet size (Fig. 4.6, 4.7, 4.8)

There is an efficiency trend at 30º inclination; droplets with the highest impact velocity were recorded to have higher maximum efficiency compared to the two other impact velocities. However, there is not that much of a difference in efficiency between the droplets with highest- and middle impact velocity. It seems that the smallest droplets had higher efficiency at a wider temperature range compared to the largest droplets.

Droplets are naturally less prone to attach to the surface when there is inclination. Which can explain why the difference between the lowest and highest velocity is less notable compared to the horizontal disc setup.

ii) Different droplet sizes, same velocity (Figures not explicitly drawn)

The highest velocity corresponds to the highest cooling efficiency for the three droplet sizes studied. The two highest velocities result also in wider temperature range for efficient cooling, but the difference to the smallest droplets is rather small.

4.4.3.   60º inclination

4.4.3.1. Largest droplets

Figure 4.9 presents the droplet cooling efficiency as a function of disc temperature for the largest droplets with three different heights, consequently three different impact velocities onto a fixed 60º inclined stainless steel disc.
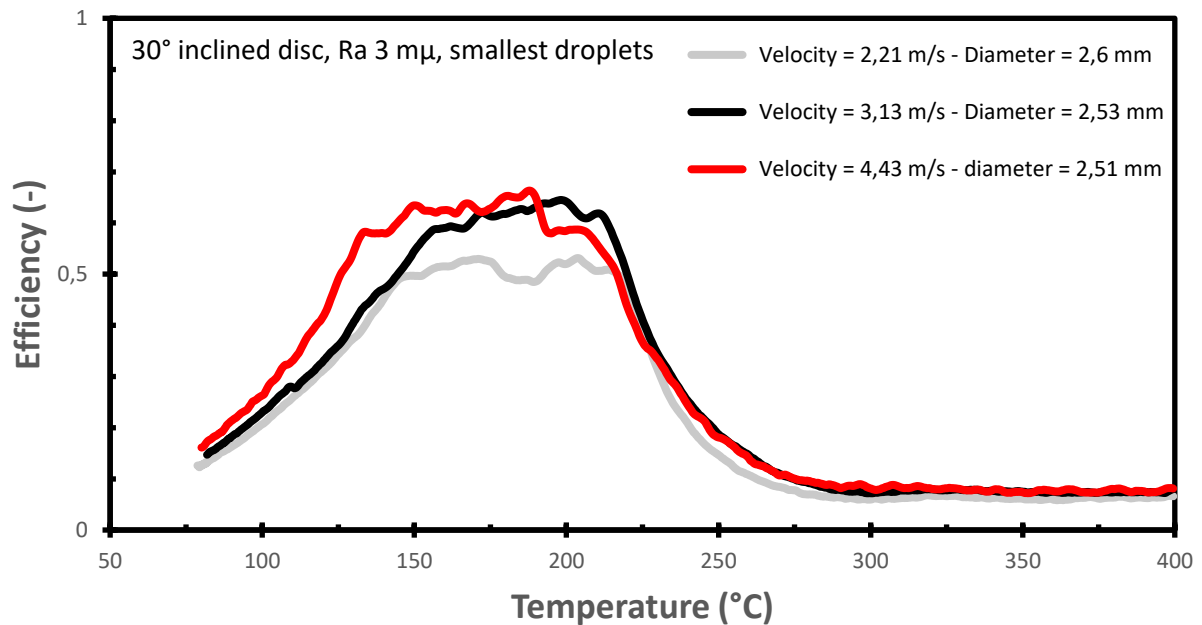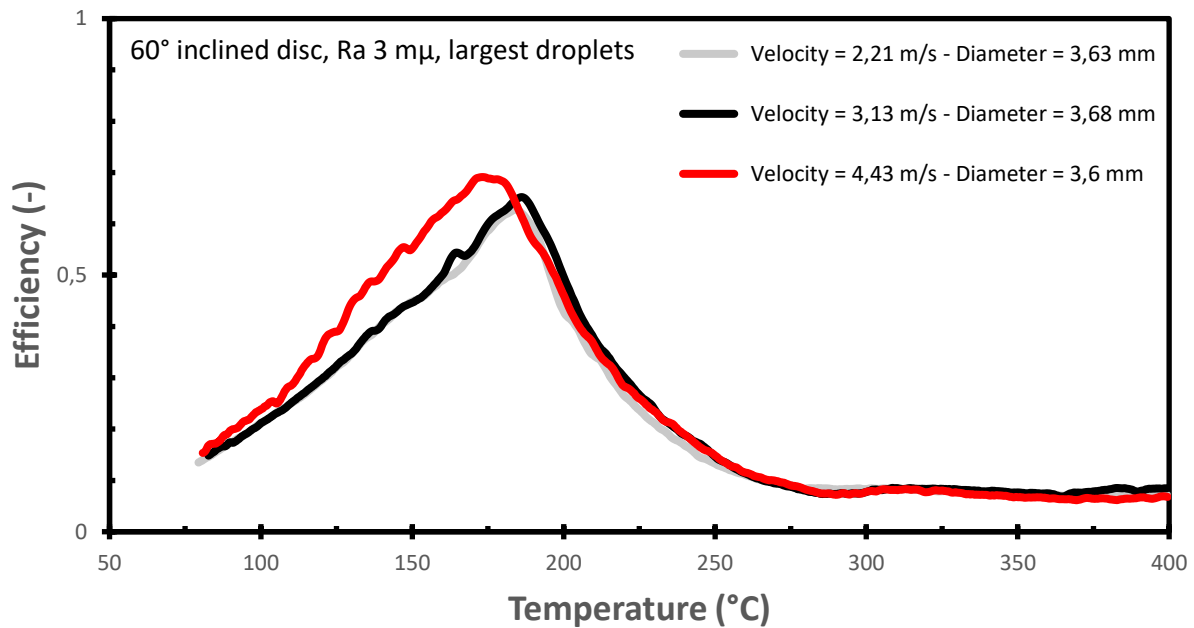
Figure 4.9 Droplet cooling efficiency vs disc temperature for three different impact velocities. Experiments conducted with approximately the same droplet diameter (white needle) and the same disc inclination (60°). The droplet sizes are displayed in the figure label.

Here, it can be shown that the curves behave more similar compared to the other inclinations, which can mean that the higher the inclination, the less the influence of velocity. However, the droplets with the highest impact velocity was recorded to give a slightly higher maximum cooling efficiency compare to the two other impact velocities.

As shown in Figure 4.9, the droplets with the highest impact velocity was recorded to have a maximum cooling efficiency at temperature around 170 ℃, where it displays an efficiency of around 69 %. The droplets with the middle impact velocity had a maximum cooling efficiency at temperature of around 185 ℃ (64 % cooling efficiency). The droplets with the lowest impact velocity displayed a maximum cooling efficiency at temperature of around 185 ℃ (63 % cooling efficiency). This indicates that the droplets with middle velocity and lowest velocity behave almost identically and demonstrated higher efficiency at a higher temperature compared to the droplets with the highest impact velocity.

It can be observed a clearer peak compare to the 30° inclination. Instead of being a range of continuous efficiency, it was observed to have one clear point which represents the maximum droplet cooling efficiency. In this case, it can also be shown a clearer Leidenfrost temperature compare to the other setups, at temperature of approx. 290 ℃, with the lowest efficiency of approx. 7 %. The efficiency

starts rising at approx. 285 ℃, to the left of the Leidenfrost temperature (i.e. film boiling region observed at T > 285 °C).

4.4.3.2. Middle-sized droplets

The droplet cooling efficiency as a function of disc temperature for the middle-sized droplets, for a 60° inclined disc, is presented in Figure 4.10.

Figure 4.10 Droplet cooling efficiency vs disc temperature for three different impact velocities. Experiments conducted with approximately the same droplet diameter (yellow needle) and the same disc inclination (60°). The droplet sizes are displayed in the figure label.

Again, it can be shown that the three velocity curves behave more similar compared to the other inclinations, which can mean that the higher the inclination, the less the influence of the velocities. However, the highest impact velocity droplets still represent a slightly higher maximum compare to the two other impact velocity droplets and demonstrates a higher overall efficiency at a wider temperature range.

As shown in Figure 4.10, the droplets with the highest impact velocity demonstrates a maximum cooling efficiency at temperature around 180 ℃ (65 % droplet cooling efficiency). The droplets with the middle impact velocity displays a maximum efficiency at temperature of around 190 ℃ (around 60 % efficiency)

Lastly, the droplets with the lowest impact velocity displayed a maximum efficiency at temperature of approx. 185 ℃ (around 60 % efficiency). Consequently, meaning that the droplets with middle- and

lowest impact velocity behave almost identical. Like the largest droplets, it is observed a clearer peak compared to the 30° inclination, in addition to a more defined Leidenfrost temperature of approximately 290 ℃ (i.e. film boiling region observed at T > 290 ℃).

4.4.3.3. Smallest droplets

The droplet cooling efficiency as a function of disc temperature for the smallest droplets, for a 60° inclined disc, is presented in Figure 4.11.
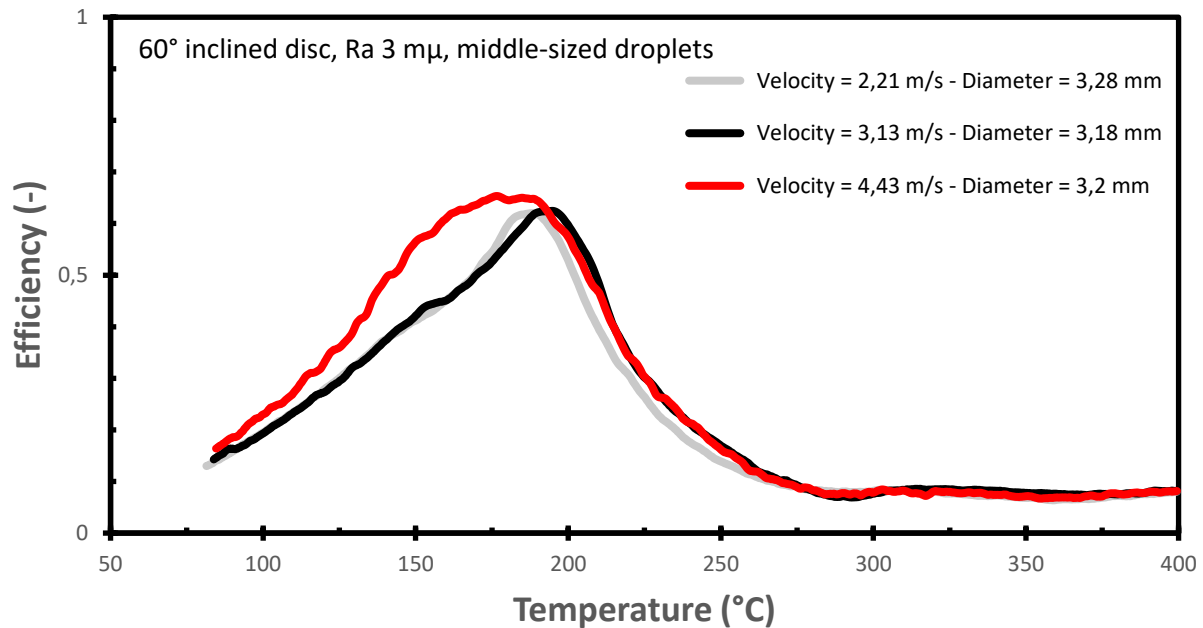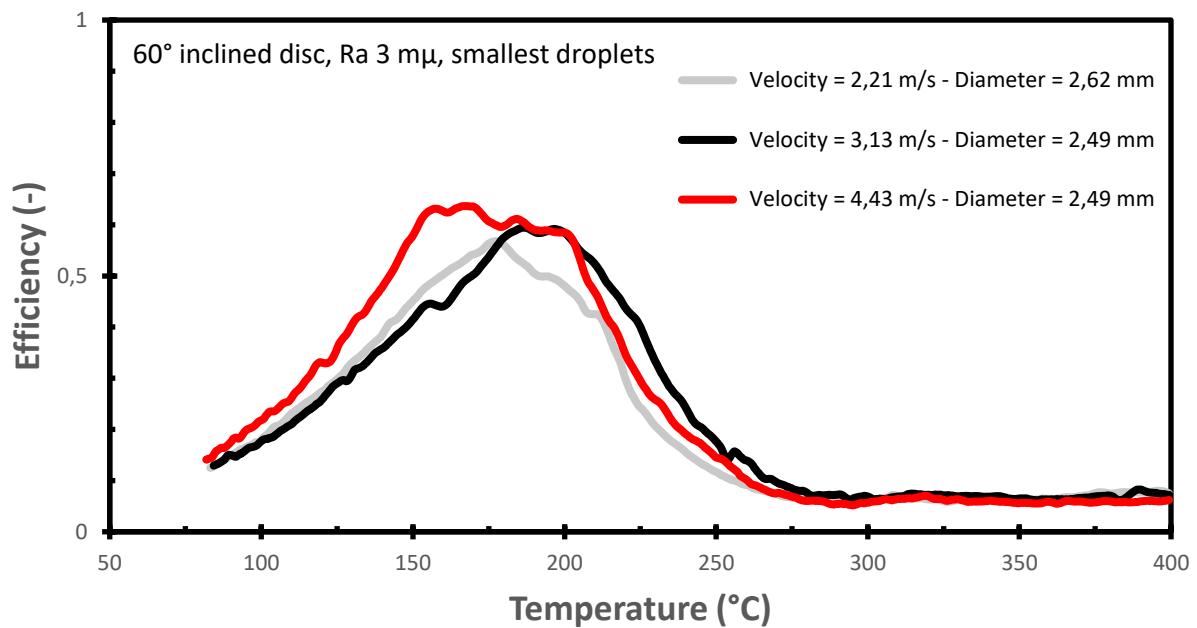

Figure 4.11 Droplet cooling efficiency vs disc temperature for three different velocities. The experiments were conducted with approximately the same droplet diameter (orange needle) and the same disc inclination (60°). The droplet sizes are displayed in the figure label.

For the smallest droplets, bigger differences can be observed depending on impingement height compared to the two other droplet sizes. Here, the middle impact velocity droplets display higher efficiency at a higher temperature (efficiency rises at higher temperature compare to the other impact velocity droplets), while the highest impact velocity droplets demonstrated the most overall efficiency in a wider temperature range. The droplets with the lowest velocity displayed the least overall efficiency.

As shown in Figure 4.11, the droplets with the highest velocity had a maximum efficiency at temperature of around 170 ℃ (64 % efficiency). There was recorded to be approx. 60 % efficiency in a temperature range of 200 ℃ - 150 ℃. As pointed out, the droplets with the middle impact velocity demonstrated higher efficiency at a higher temperature, above approx. 205 ℃. For the droplets with

the middle impact velocity, there was recorded to have a maximum cooling efficiency at approx. 190 ℃ (around 60 % efficiency). Lastly, the droplets with the lowest impact velocity had a maximum cooling efficiency at temperature of around 175 ℃ (56 % efficiency).   The lowest velocity droplets demonstrated an efficiency of around 50 % in a temperature range of approx. 200 ℃ - 160 ℃. The film boiling region is observed at approximately T > 295 ℃.

4.4.3.4. Summary of 60° inclination

i) Different velocities, same droplet size (Fig. 4.9, 4.10, 4.11)

It is a clear trend for the largest and middle-sized droplets. They were recorded to behave almost similarly with a slightly higher peak for the highest velocity. This can indicate that for these droplets sizes and this inclination, the influence of impact velocity is less compare to the other inclinations. The smallest droplet sizes were observed to have a higher cooling efficiency at a wider temperature range compare to largest droplets, whereas the largest droplets demonstrate a higher maximum efficiency. The Leidenfrost temperature was also recorded to be far more notable with the 60° disc inclination, compared to the two other disc setups.

ii) Different droplet sizes, same velocity (Figures not explicitly drawn)

Differences observed between droplet sizes for the same velocity are small, for this configuration.

4.4.3.5 Effect of droplet size and velocity for horizontal, 30-degrees and 60-degrees inclined discs

As a total, the highest observed cooling efficiency occurred for the largest droplets combined with highest velocities for the three different set-ups, horizontal disc, disc inclined 30 degrees, and disc inclined 60 degrees. These were respectively 81% (horizontal), 73% (inclined 30 degrees) and 69% (inclined 60 degrees). Smaller droplets and/or lower impingement velocities resulted in wider temperature range of efficient cooling (mainly for temperatures lower than boiling crisis).

4.4.4. Effect of inclination

This subsection analyzes the effect of inclination, at a fixed impact velocity (v = 3,13 m/s) displaying three different droplet sizes.

4.4.4.1. Largest droplets

The droplet cooling efficiency as a function of disc temperature for the largest droplets, with impact velocity v = 3,13 m/s, will be presented in Figure 4.12.

Figure 4.12 Droplet cooling efficiency vs disc temperature for three different inclinations. The experiments were conducted with approximately the same droplet diameter (Largest droplets) and the same impact velocity (v = 3,13 m/s). The droplet sizes are displayed in the figure label.

For the largest droplets, the droplet cooling efficiency was recorded to be slightly higher regarding the 30° inclination. When there is a 30° inclined disc, the cooling efficiency tends to be higher in a wider temperature range (190 – 160 ℃), compared to the horizontal and 60° inclination, where it is one clear peak at temperatures of 180 and 190 ℃ respectively. The film boiling region was also obtained at different temperatures, depending on the setup. i.e. film boiling for 60° inclined disc setup was

obtained at T > 280 ℃, and at T > 300 ℃ for 30º inclined disc and horizontal disc. The droplets impinging on a 60º inclined disc was recorded to give the least overall droplet cooling efficiency.

4.4.4.2.   Middle-sized droplets

The droplet cooling efficiency as a function of disc temperature for the middle-sized droplets, with impact velocity v = 3,13 m/s, is presented in Figure 4.13.
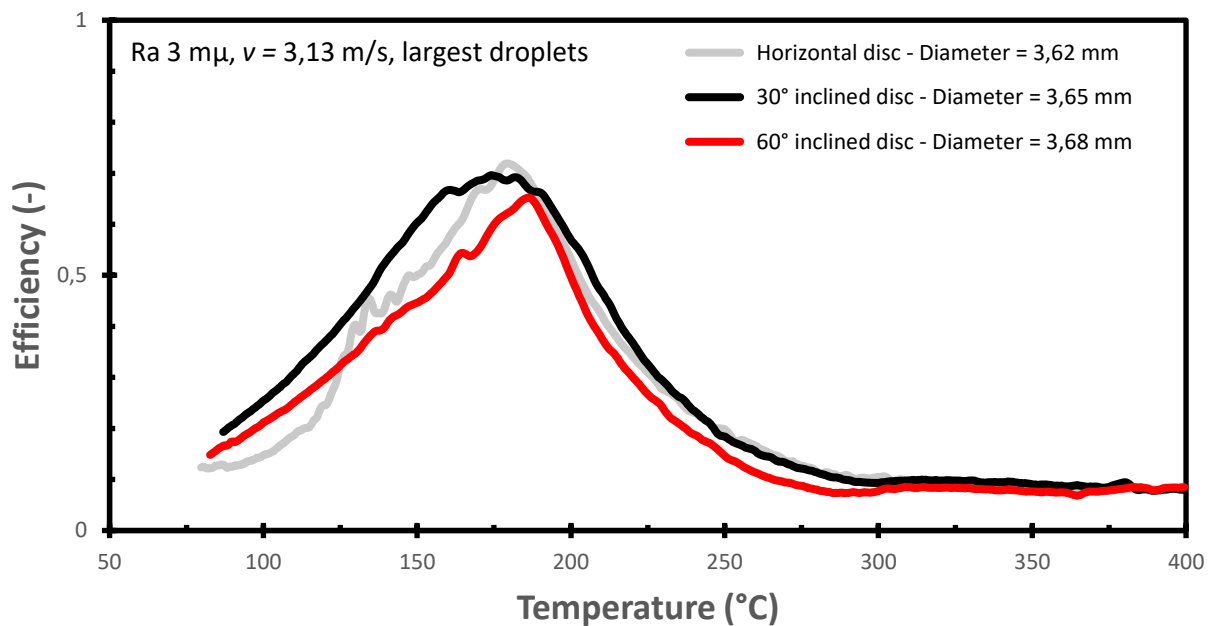

Figure 4.13 Droplet cooling efficiency vs disc temperature for three different inclinations. The experiments were conducted with approximately the same droplet diameter (middle-sized droplets) and the same impact velocity (v = 3,13 m/s). The droplet sizes are displayed in the figure label.

For the middle-sized droplets, the droplet cooling efficiency was recorded to be significantly higher regarding the 30º inclination. When there is a 30º inclined disc, the cooling efficiency tends to be higher in a wider temperature range (200 – 160 ℃) compared to the horizontal and 60º inclination, where it is one clear peak at temperatures of 195 ℃. The film boiling region was obtained at approximately the same temperatures for all the disc setups (T > 290 ℃). Again, the droplets impinging on a 60º inclined disc was recorded to give the least overall droplet cooling efficiency.

4.4.4.3.   Smallest droplets

The droplet cooling efficiency as a function of disc temperature for the smallest droplets, with impact velocity v = 3,13 m/s, is presented in Figure 4.14.
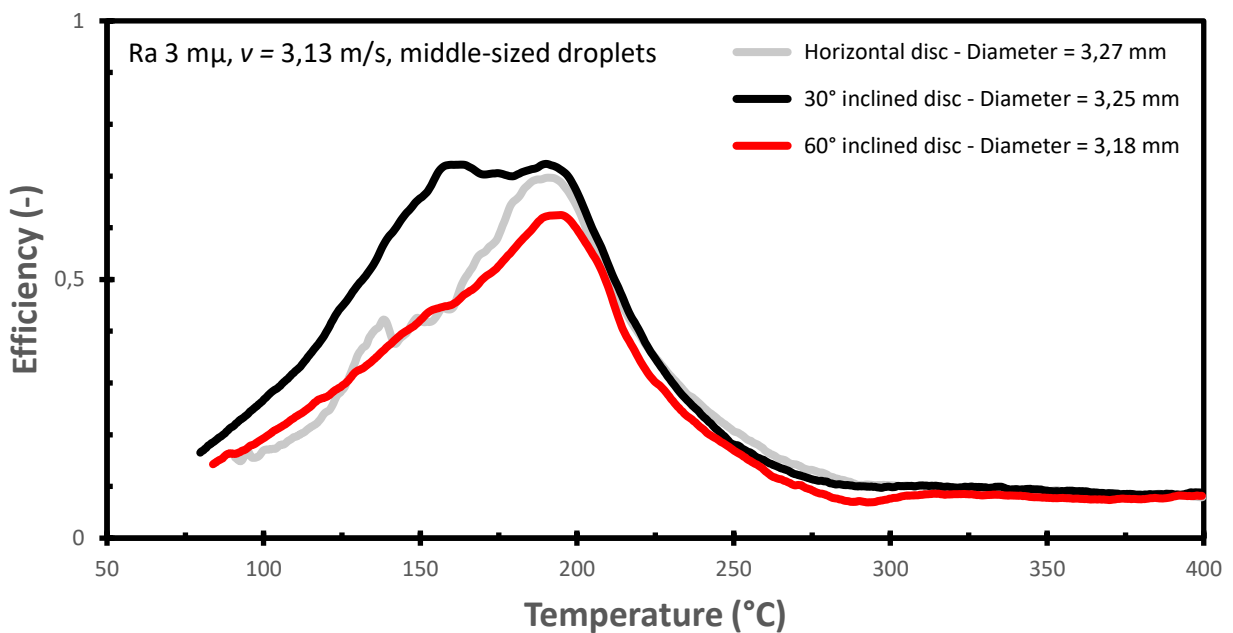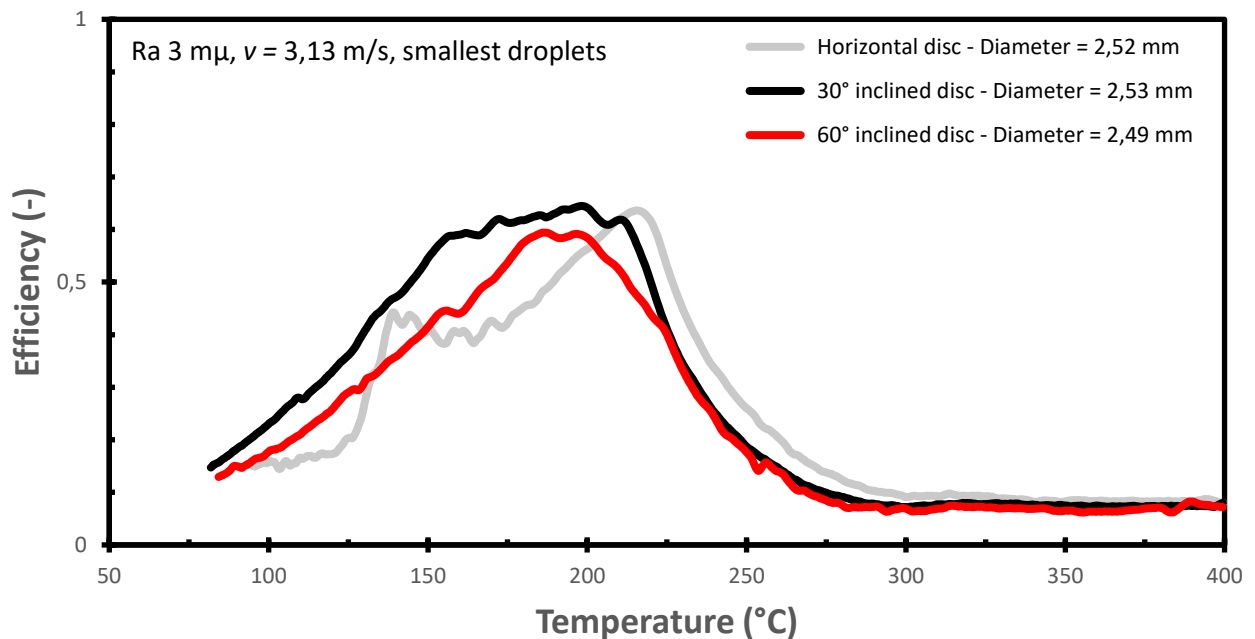
Figure 4.14 Droplet cooling efficiency vs disc temperature for three different inclinations. The experiments were conducted with approximately the same droplet diameter (smallest droplets) and the same impact velocity (v = 3,13 m/s). The droplet sizes are displayed in the figure label.

For the smallest droplets, the overall droplet cooling efficiency was recorded to be significantly higher regarding the 30° inclination. When there is a 30° inclined disc setup, the cooling efficiency tends to be higher in a wider temperature range (210 – 150 ℃) compared to the horizontal and 60° inclination. However, when the disc is horizontal, the droplet cooling efficiency was recorded to be higher in the transition zone region, and consequently a higher temperature of the observed film boiling region, at T > 300 ℃. The film boiling region was obtained at approximately the same temperature for both inclined disc setups (T > 290 ℃).

4.4.4.4. Summary

Evenly across the results, the droplets impinging on a 30° inclined disc was recorded to give the highest overall droplet cooling efficiency, and the least overall efficiency for the 60° inclined disc setup, for an impinging velocity of 3,13m/s.

Chapter 5

5. Discussion

In this chapter, strengths and limitations of the present work will be discussed. Obtained results are compared with literature, when relevant values are available. The values of water-cooling as a safety measure in the process industry will also be addressed.

5.1. Experimental

There was some trial and error to determine the best possible experimental setup and procedure. The procedure was changed from three baselines and two droplet experiments to two baselines and five droplet experiments. Based on analysis and processing, the baseline experiments are far more reproducible compared to the droplet experiments, which in return are far more sensitive to both external and internal influence. This explains why those five droplet experiments are more prone to be slightly deviated from each other due to the sensitivities discussed in Section 4.1. and 4.2.

Five droplet experiments gave a fair average on a statistic analysis, which consequently determined that five experiments were an "optimal" number of experiments. Of course, 100 droplet experiments would be more accurate. However, it was a matter of time by conducting the experiments. Conducting five droplet experiments took about three to four hours, consequently meaning that it would take time to conduct more than five experiments. In most of the experimental series, the five droplet experiments agree well to each other, which raises the question if it is necessary to conduct more experiments. Also, the probability of error would also increase with increasing number of experiments, i.e. external influences due to for example an opened door etc.

In the previously mentioned trial and error period, the needle position and water supply system were optimized to get reproducible results. The repeatability of the experiments was optimized with an aluminum shielding around the injection needle. This will minimize the external impact from beneath and from the sides. The water supply (water bag) was finally placed at elevation 2 m above the needle, which made the water run more adequately. This phenomenon is explained in fluid dynamics as an increase in pressure difference in water due to elevation of heights. Figure 5.1 summarizes the changes of the experimental setup. The figure on the left-hand side presents the appearance of the setup before, while the figure on the right-hand side presents the appearance of the setup after the changes. These changes were gradually developed throughout the thesis period.
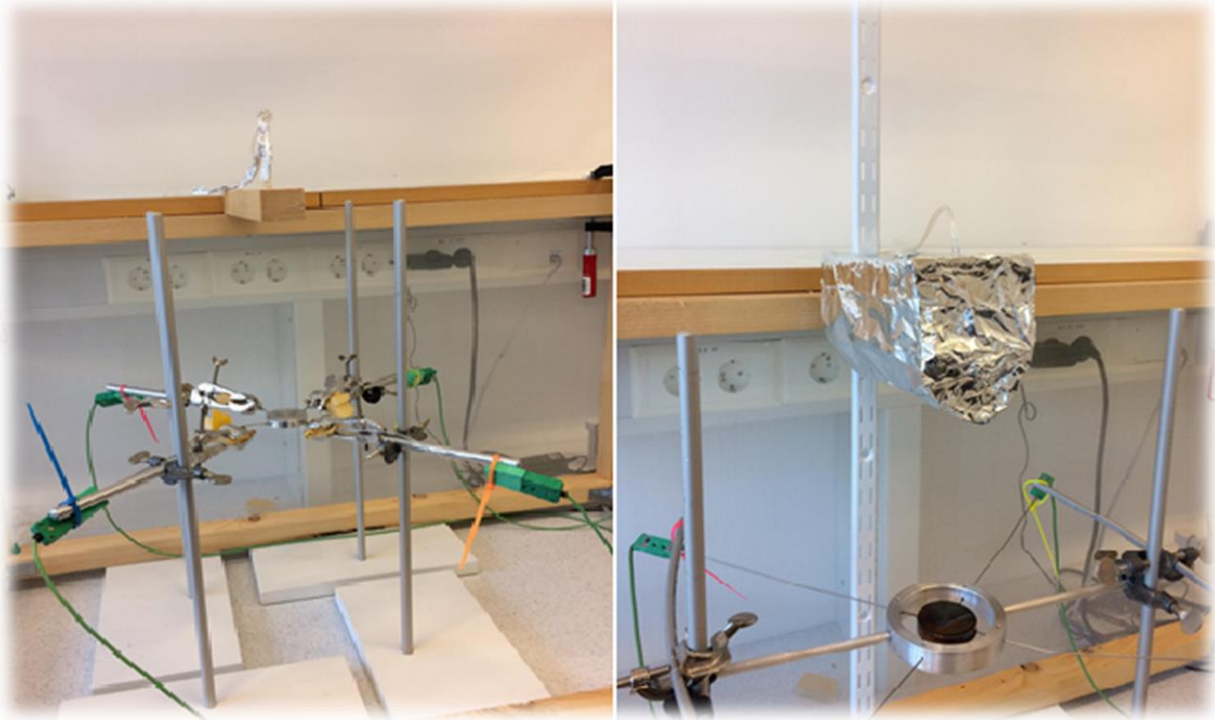
Figure 5.1 Comparison of how the experimental setup appear before (left) and after (right) the development.

Despite being an improved setup, there was still a small risk of air drafts and impacts (i.e. doors open etc.) would affect the experiments. This was verified when some experiments were destroyed due to opened doors and were redone at times when the conditions were more favorable (i.e. evenings and weekends). The issue with air drafts is illustrated in Fig. 5.2. When a droplet has a mass of 8-9 mg and it falls from a height of 1 m will naturally be exposed to air conditions more effortlessly compare to larger droplets and a lower drop. This issue was mainly present for the smallest droplets at 100 cm and 50 cm height, where it sometimes struggles hitting the exact center of the disc and could have a rapid change in the droplet interval. The most sensitive experimental series had ten droplet experiments instead of five. Thanks to observations during these experiments, the five to six most presentable results could be gathered, and consequently made an average of these five or six.
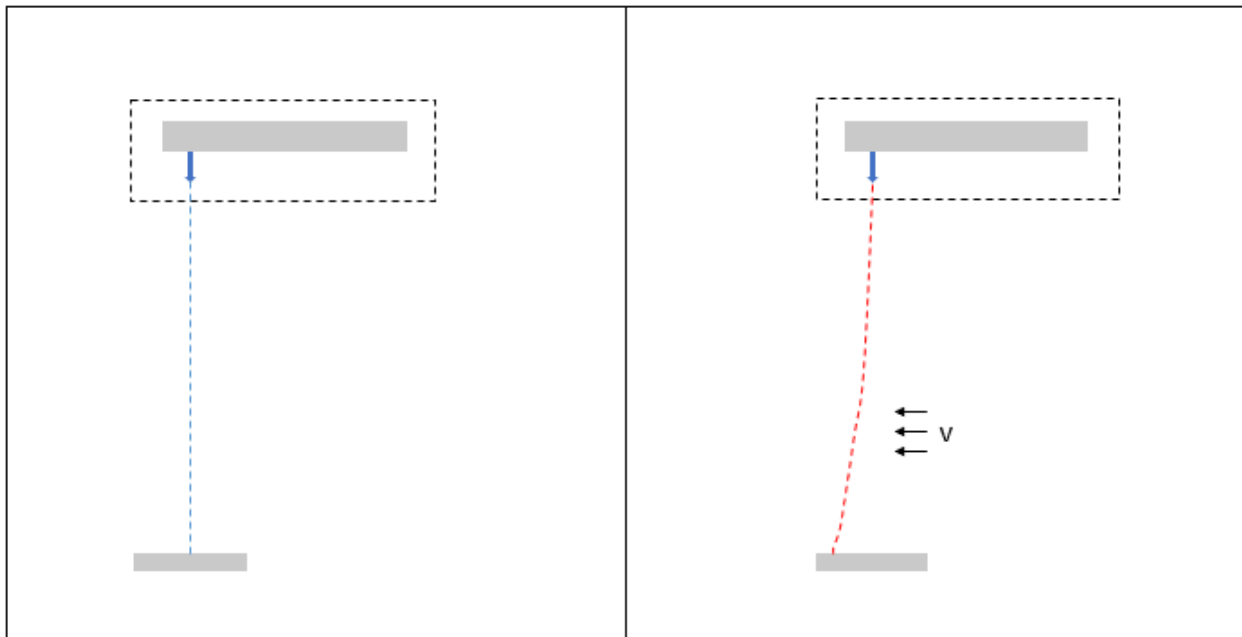
Figure 5.2 Principle sketch of droplet trajectory without and with disturbing draft.

Prior to the experiments, relative humidity inside the room, air temperature, dew point, outdoor relative humidity and air pressure outside were recorded. These parameters were logged on separate lab reports/protocols conducted for each of the experimental series (example of a lab protocol in Appendix C). It is currently unknown how much impact these parameters have on the experiments, as the temperature-time curve for the baseline experiments, on a given fixed inclination, behaved almost identical.

5.2.   Disc heat losses

Heat transfer includes aspects such as heat conduction, convection and radiation. All these forms of heat transfer will influence the cooling. This section will focus on the cooling effect without the effect of water droplets. Figure 5.3 shows how the different forms of heat transfer influence the stainless steel disc.
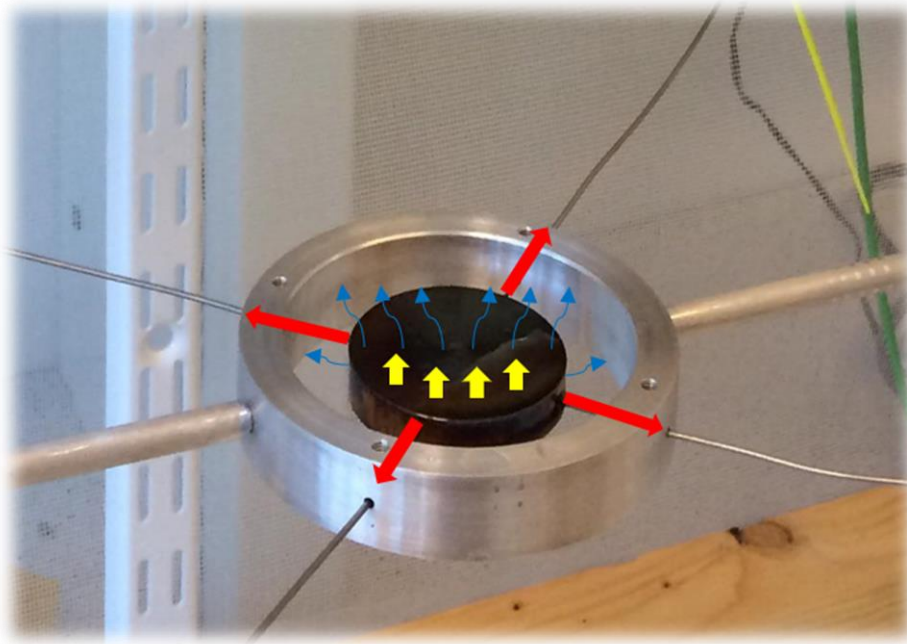
Figure 5.3 Representation of the heat losses of the disc, during baseline recordings. Conduction through thermocouples (red), convection to the air (yellow) and radiation emitted to the surroundings (blue).

Heat conduction will lead limited amount of the heat from the stainless steel disc to surrounding solid objects, such as the four thermocouples attached to the disc, and will further spread to the ring-holder mechanism. Overall, convection will arguably be the most dominant form of heat transfer, as the heat from the disc transports to the surrounding air due to temperature differences between the air and the disc. The natural convective heat will be transported upwards due to buoyancy (Drysdale 2011). Radiation will emit heat from the entire surface in every direction, due to electromagnetic waves.

Radiation will in this case arguably be more dominant than convection at temperatures around 400 ℃. While convection eventually will be more and more dominant as the temperature decreases below 400 ℃. It can be found in literature that radiation will be dominant at temperatures above 400 ℃ due to the temperature in power of four, while convection will be dominant at temperatures up to 150-200 ℃ (Drysdale 2011). This will of course depend on the heat transfer coefficient, and the chosen emissivity. Figure B.1 in Appendix B demonstrates an example of convection heat transfer (h = 10 W/m^{2}K and h = 25 W/m^{2}K) versus radiation heat transfer (ε = 0,6). It can clearly be seen that whether heat radiation is higher than convection strongly depends on the heat transfer coefficient h. Nevertheless, it can be assumed that radiation was highest at the beginning of the experiment (i.e. around 400 ℃).

All these heat transfer mechanisms, however, will decrease gradually as the temperature difference between the disc itself and the surroundings decreases. This can be verified by analyzing Figure 4.1

from Section 4.3. It can be seen from all the curves that there will be a steeper temperature decrease at the beginning and will eventually flat out as the temperature decreases (i.e. exponentially). The literature states that steel is a material that distribute heat quite easily within the material. This can be observed during the experiments while detecting the temperature of each of the thermocouples. After heating the disc, the temperatures of the four thermocouples will quickly be equalized, indicating the heat is uniformly distributed inside the stainless steel disc. This was ensured by allowing the temperature increase to 430 ℃. The temperatures equalized at approximately 410 ℃.

As pointed out in Section 4.3; the heat transfer will be more extensive when the stainless steel disc is inclined compare to horizontal. The inclined surface can create more organized airflow pattern from the sides, as well as from above and underneath, due to a more efficient flow of surrounding air. This may increase the total airflow around the disc. When the disc is horizontal, there will be more chaotic flow pattern, as the airflow above and underneath the disc is restricted.

5.3.   Droplet cooling efficiency and boiling regimes

By processing and analyzing Figure 2.2, the pattern will conform well with most of the results obtained in this master`s thesis. It must be mentioned that Figure 2.2 is just a theoretical presentation of how water droplets will interfere on a heated surface but will still be an accurate demonstration of the droplet heat transfer. A common trend between each of the efficiency curves presented in Section 4.4, is the transition between transition zone and film boiling region (i.e. Leidenfrost temperature), which occurs at temperatures between 290 ℃ - 300 ℃. Beyond this temperature point, 10 % efficiency from water droplets was recorded.

However, the theoretical transition zone regime and the transition zones showcased in this thesis did not conform for each of the setups. Transition zone is the transition between the minimum (Leidenfrost) and the maximum (Boiling crisis). The boiling crisis marks the temperature point where the droplets demonstrated their maximum efficiency, and this temperature point turns out to be a very sensitive output. By analyzing the results in Section 4.4, the transition zone for the same droplet size (with different velocity) could either traverse from 300 ℃ to 220 ℃, or from 300 ℃ to 160 ℃. The growth from Leidenfrost temperature to the first peak efficiency, however, behaved relatively similar for the same droplet size and same inclination. This indicates that the transition between the transition zone regime and nucleate boiling regime had some sensitive outputs regarding droplet cooling efficiency, which makes it difficult to decide where the exact transition zone will be located for each droplet size. Liang and Mudawar (2016) also concluded in their review that the transition zone regime is not yet accurately determined. The results may also indicate that boiling crisis can preferably be defined as a broad temperature range with high cooling efficiency, rather than one narrow peak.

5.3.1. Effect of impact velocity

The impinging velocity was governed by the gravitational acceleration g and the droplet height. There are some assumptions and simplifications involved however, where the velocity was assumed to be equal to the theoretical impinging velocity. Due to the extremely low impinging time (around 0,1 s – 0,5), it was impossible to get an accurate overview of the real velocity which was affected by drag forces. Nevertheless, it can be assumed that the droplets never fully reached terminal velocity due to the limited alteration of heights. According to Pasandideh-Fard et.al (2001), the calculated impinging velocities (i.e. affected merely by gravity g and height) corresponds to the real impinging velocity, when the alteration of heights is between 0 and 1 m.

By analyzing and processing the results, the effect of impact velocity will in most cases adapt to the effect of inclinations. By increasing the inclination of the stainless steel disc to 30º and 60º, the effect of velocity will seemingly be less significant, with a slightly higher boiling crisis as the velocity increases – and consequently the most overall efficiency. This phenomenon will be further discussed in Subsection 5.3.3. The effect of velocity will also be less significant considering the growth phase in the transition zone regime, as each of the diagrams showcased in Section 4.4 displays that the pattern will almost be same from Leidenfrost to the first peak effect.

Shinya Fukuda et al. (2014) studied the effect of impinging velocity, droplet diameter and surface roughness. Although, their input parameters were different from the parameters showcased in this study (with exception from Ra 3 µm), they concluded that the cooling efficiency increased with an increase in the impinging velocity. This corresponds to the fact that if the momentum and pressure of the droplets increases, the droplet will spread more extensively above the surface, consequently increasing the droplet contact area. Their conclusion can be argued to be representative for most of the results showcased in this thesis, with an exception to the horizontal stainless steel disc setup - for smallest and middle-sized diameter.

At this setup and for these two diameters, the effect of impinging velocity will be less significant between velocity 3,13 m/s and 4,43 m/s, while the effect of velocity 2,21 m/s will deviate from the two other velocities. The efficiency was recorded to almost follow the same pattern for all the velocities until it reaches the first peak efficiency (i.e. same pattern in transition zone), and while the efficiency for the two highest velocities droplets tends to decrease after the maximum, the lowest velocity droplets tends to "stick" more to the surface and execute higher efficiency at a continuous range of temperature, consequently a higher total efficiency. This can be related to the Weber number, where increased impinging velocity means increased Weber number.

If the Weber number increased, bouncing droplets was more prominent, and the disintegrated droplets were more prone to bounce further away from the surface. For the droplets with the lowest velocity; instead of bouncing off the surface, the disintegrated droplets were more prone to be attached to the surface. Imagine a 1 m³ water cube impinging on a surface (i.e. 1 m² contact area), dividing into 1000 water cubes of 1 l with a contact area of 1 dm² each, resulting in 10 m² total contact area. If majority of these 1000 droplets bounces away from the surface, it will naturally demonstrate less droplet cooling efficiency compare to a case where those 1000 droplets would stay on the surface (i.e. not bounce away). This phenomenon could be observed during the experiments, especially in the nucleate boiling regime, when there was less violent sizzling and boiling.

5.3.2. Effect of droplet size

It is natural to think that smaller droplets require less energy to be transformed into water vapor. This phenomenon will probably make it easier for the smallest droplets to reach transition zone sooner compared to bigger droplets. This statement can be verified based on the results (Section 4.4); for a horizontal stainless steel disc, the transition zone for the smallest droplets would start at approximately 300 °C, while for the biggest droplets, the transition zone will start at approximately 290 °C. The biggest droplets, however, would execute a higher maximum effect (i.e. higher boiling crisis) and will in general have a clearer peak.

As mentioned earlier, the impingement interval for the droplets was adjusted accordingly to the droplet size, which means that smaller droplets fall more frequent compared to bigger droplets. The smallest droplets with the highest interval will execute effect at a wider temperature range compared to the biggest droplets and the less frequent interval, in addition to a higher temperature of transition zone for the smallest droplets. This can also be seen for the middle-sized droplet, which will be balanced on a temperature range somewhere between smallest and biggest droplet.

Based on these statement, there will be a balance when deciding the optimal droplet size as there is some pros and cons. The more frequent interval with smaller droplet size would demonstrate more continuous effect at a wider range of temperature, and a higher Leidenfrost temperature (i.e. start of transition zone), while the less frequent interval with bigger droplet size had a higher boiling crisis. The explanation for these phenomena can be the different nature of the impingement. By altering the three different droplet sizes (from 2,53 mm to 3,66 mm), the Weber number will be significantly changed (20-50 %), thus explaining why the results were so different from each other. Also, when there is a more frequent interval with smaller droplets, the evaporation time between each droplet impingement will be shorter, consequently meaning that there will be a lower possibility of the stainless steel disc being cooled down by mere natural heat transfer after it reached the boiling crisis

(nucleate boiling regime). This will explain why there is a wider temperature range of continuous effect by droplet impinging. This will also probably explain why the less frequent interval with the biggest droplets had a clearer peak maximum effect, where the evaporation time is higher and there will be one clear temperature point where droplets had more extensive efficiency.

Shinya Fukuda et al. (2014) concluded that the cooling efficiency increases with a decrease in the droplet diameter, which also can be mostly representative compared to the results obtained in this thesis. As described in the section above, smaller droplet diameters demonstrated higher efficiency at a wider range of temperature. However, this statement is debatable for the horizontal stainless steel disc setup, as the efficiency will seemingly be higher regarding the biggest diameter. This phenomenon must be further researched to be verified.

5.3.3. Combined effect of velocity and inclination

The effect of inclination is difficult to measure exactly, due to the variating results. It can still be seen that the effect of velocity become less significant when droplets hit an inclined surface compared to the horizontal disc setup. As the surface is inclined, the droplets are less capable to be attached to the surface regardless of impinging velocity. Consequently, meaning that the droplets are more prone to "slide" off the surface instead of forming an equally distributed puddle above the surface, especially below the boiling crisis and into the nucleate boiling region.

For the lowest droplet impinging velocity (2,21 m/s), the droplet cooling efficiency will increase as the inclination decreases. This can again be argued to be because of bouncing; low velocity droplets tend to attach themselves to the horizontal surface more effectively compare to an inclined surface. For an inclined surface, the droplets will only have limited options of directions to bounce off to, in addition to sliding off the surface when the temperature is low enough. Figure 5.5 represents a rough estimate of all the possibilities the droplets could bounce off the disc, for horizontal and 60° respectively. It shows that for a horizontal surface the droplets can spread out in every direction around the disc (180°). The inclined surface, in the other hand, could have a bouncing range at approximately 90-120°. The observed combined effects can be summarized as follows: For horizontal setup the lowest impingement velocity (2,21 m/s) provides better cooling. While at 30° inclination the two other velocities (3,13 m/s and 4,43 m/s) show better, and very similar, cooling efficiency.
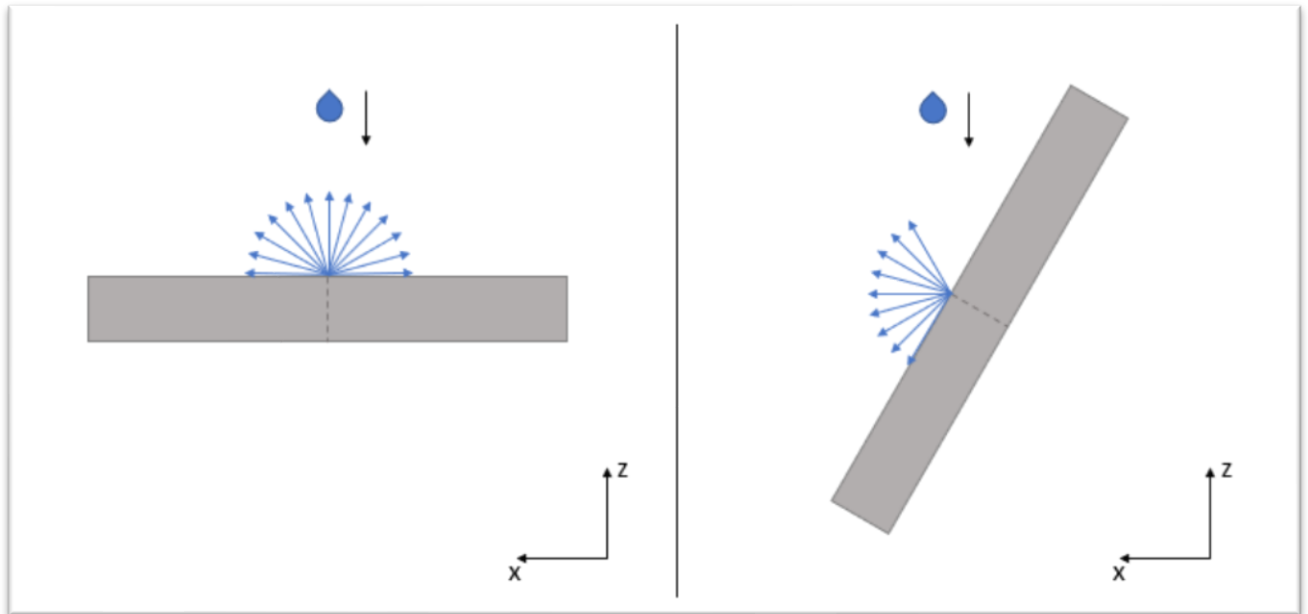
Figure 5.4 Graphic representation of the possible directions the disintegrated droplets could bounce off to after landing. This is just a rough estimate based on observations during the experiments.

However, evenly across for the 30° stainless steel disc setup, the droplets tended to exercise higher efficiency in a wider temperature range compare to the other setups. It can be argued that for 3,13 m/s and 4,43 m/s impinging velocity, the overall droplet cooling efficiency will be highest when there is a 30° stainless steel disc setup. The explanation for this could be that the water does not slide down the surface the same pace compared to the 60° inclination, especially in the nucleate boiling regime. The lowest position of the stainless steel disc in the 30° inclination will be cooled down more efficient compare to the two other setups.

By processing the result in Section 4.4; when the stainless steel disc becomes more inclined, a clearer Leidenfrost temperature was revealed. Leidenfrost (1756) performed his experiments with an iron spoon heated by a coal-fire. A spoon has a curved surface, meaning that there are different inclinations dependent on orientation on the spoon. Considering these factors, makes it reasonable to believe that the Leidenfrost temperature becomes clearer when a metal surface is inclined, and it will become less revealing when a metal surface is horizontal. However, there must be further research on several other metallic materials to be able to verify this for sure.

5.4. Practical applications in the industry

There exists numerous of steel alloys used for constructions. The present work is limited to the use of stainless steel AISI 316, which is a common material for constructions in industrial facilities utilized for storing and transporting liquid materials. This thesis also studies the effect of inclination, which substantially targets various orientations of a curved surface, i.e. pipe constructions, fluid containers

and load beams etc. To get a better insight of the practical aspects of the thesis, will Figure 5.5 demonstrates the various experimental stainless steel disc setups versus an example of a common steel pipe used for transporting fluids.
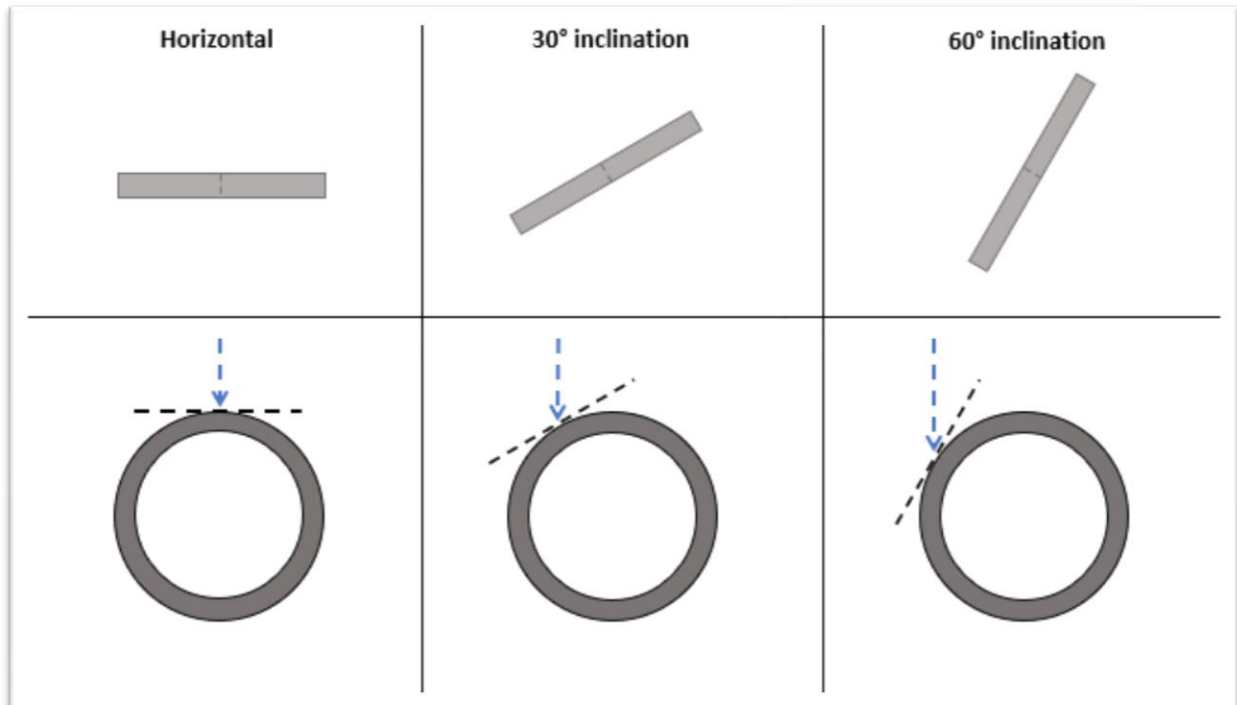

Figure 5.5 Sketch of the stainless steel disc vs. a common steel pipe exposed to water droplets at different orientations.

The thesis examines droplet cooling efficiency on a small-scale and may therefore not be applicable for large-scale fire or explosion scenarios. For instance, it is currently unknown how these small-scale results would compare to the mitigating effect on a massive jet fire incident in the petroleum industry. Nevertheless, it will still give an insight of how water droplets will interact with a heated steel surface, by using a cooling efficiency from 0 – 100 %. %. If the droplet cooling efficiency is 10 % means that the water will have limited cooling effect, and perhaps not perform its intended cooling function. However, this does not necessarily mean that all the water goes to waste. Even though the effect is limited, the water can make an inert atmosphere in the enclosure made of vaporized water to suppress the oxygen level, eventually putting the fire out. In addition, water evaporation will create an atmosphere which operates as a radiation shield. This will reduce the amount of radiation emitted from the fire to other objects, which will make evacuation more efficient and effectively reduces the fire development. The water will also assumingly limit the global heat load from a jet fire incident, by fairly reducing the pressure profile in the enclosure. It can be summarized that the secondary effects of water droplets are more prominent compare to the primary cooling effect, when the temperature surpasses Leidenfrost temperature (i.e. film boiling region).

5.4.1. Jet fire vs. water droplet impact

The most critical droplet regime regarding firewater application, is the film boiling region associated with temperatures above approximately 300 ℃. Above this temperature, less than 10 % droplet cooling efficiency by the droplets may be expected. Consequently, meaning that above the Leidenfrost temperature, there is a lack of cooling, and it will be difficult to maintain control of the situation. This subsection will focus on an unwanted jet fire incident, and how the fire will affect the steel temperature. The analysis will be quantified with time (minutes) for several target events, and will be based upon literature, experience and results obtained in this master`s study. Figure 5.6 represents temperature vs. time for a steel tubular exposed to a jet fire incident.
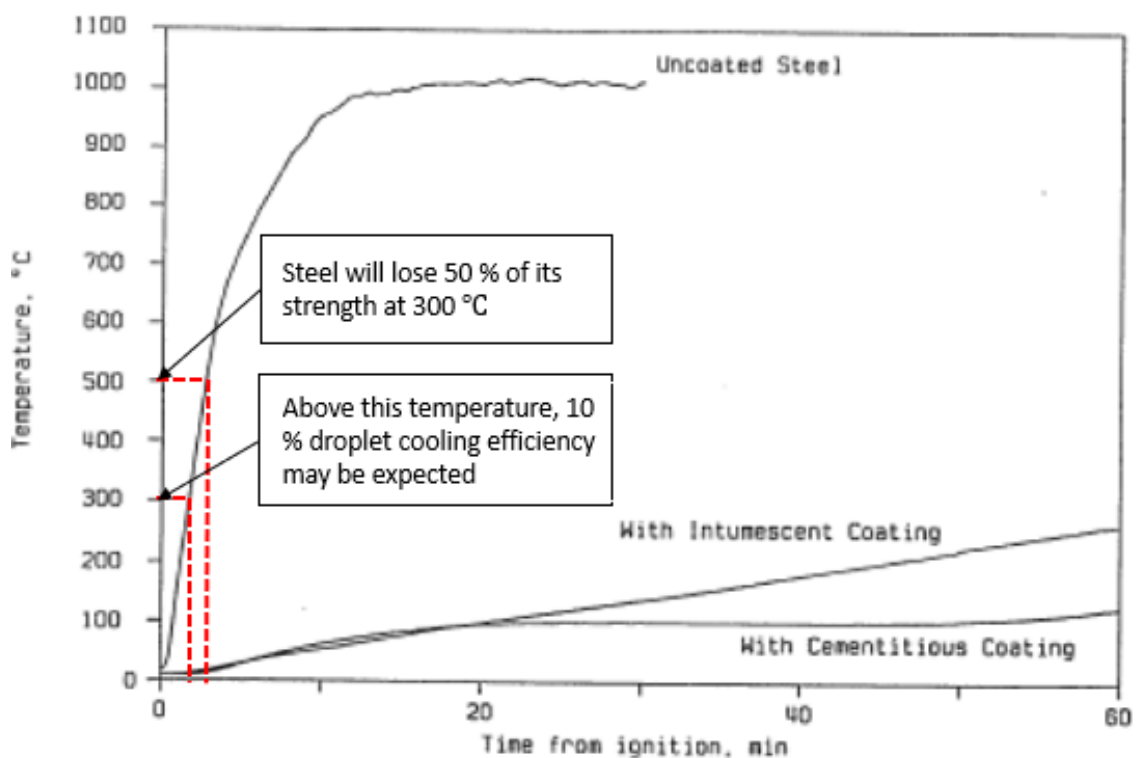
Figure 5.6 The temperature response of fire protected and unprotected steel tubulars in a jet fire. Figure obtained and adapted from (Shirvill 1992).

It can be demonstrated from Figure 5.6 that the steel temperature will reach 300 ℃ at approximately 2 minutes and will reach 500 ℃ at approximately 3 minutes, when exposed to a jet fire. As mentioned earlier, 10 % droplet cooling efficiency from water droplets may be expected, at steel temperature above 300 ℃ (i.e. above Leidenfrost and in film boiling region). The steel will lose half of its strength and integrity at approximately 500 ℃. However, this will depend on the steel quality. Thermal breakage (rupture) will occur due to a local heat peak load of 250 – 350 kW/m^2 exposed onto a local area in the steel construction (The Norwegian Oil Industry Association (OLF) 2008). Statistically,

thermal rupture of a 2" – 4" steel pipe will occur around 2 – 4 minutes[1], which will mean that steel could rupture around the same temperature where it loses half of its strength. Detection and activation of the firewater monitors will occur around 3 – 5 minutes[2] after ignition. Considering the challenges associated with monitors precision, water may not hit where it is most needed. Adjustment of the monitors will further increase the time before the cooling process really starts. To simplify, time to rupture is assumed to be 4 minutes (optimistic) and time to activation is assumed to be 5 minutes (conservative).

Figure 5.7 summarizes the target events in their respective timestep, by using a timeline for easy representation. There are some uncertainties involved in the timeline, however, as the various target events and their respective timesteps heavily depend on type of steel, geometric characteristics, jet fire characteristics, amount of fuel available, interfaces with other fire safety measures etc. The 3 - 5 minutes range of activating the firewater mechanism, as pointed out above, will depend on human awareness, and how quickly the person can verify the fire incident. Then again, it is not certain that the firewater will hit where it is desired. ,
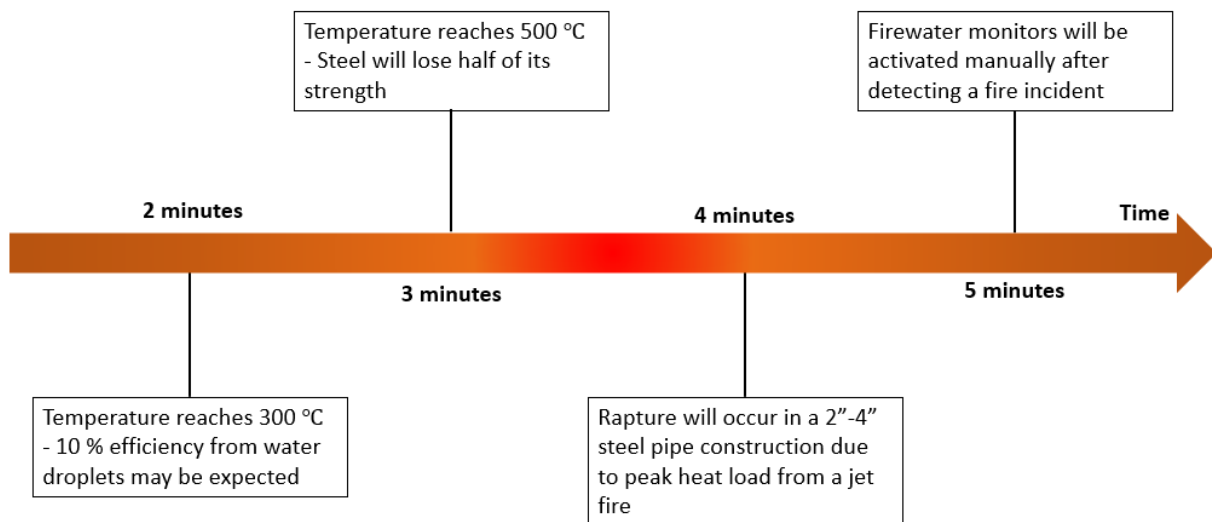
Figure 5.7 Overview of the various target events in a timeline format. The timesteps showcased is time from jet fire ignition.

Considering the timeline above, while analyzing the various uncertainties targeting a jet fire incident versus droplet impact, it can be safe to assume that firewater alone cannot function as a consequence

---

[1] According to interviews with experienced people from the petroleum industry
[2] According to interviews with experienced people from the petroleum industry

57

reducing measure in case of a jet fire. Other fire safety measures combined with firewater (e.g. passive fire protection and blowdown). Safety measures will be further discussed in the next subsection.

5.4.2. Industrial fire safety

As mentioned earlier, jet fire peak heat load will directly affect a small area on the structure, which can lead to rupture. On the other hand, jet fire global heat load ($0 - 100$ kW/m^2) will represent the average heat load exposed to a part of the structure. Consequently, the global heat load will affect the pressure build-up in the segment (The Norwegian Oil Industry Association (OLF) 2008). This can lead to an inadequate situation where the pressure and temperature could increase to the point where thermal expansion can occur inside the segment (i.e. explosion pressure increases).

According to NORSOK S-001, the requirement for mass flow/flux is 10 (l/min)/m^2, i.e. 0,1667 (kg/s)/m^2, for process areas, which is significantly higher compare to the mass flow obtained in this study (i.e. approximately 60 times higher). However, the 10 % droplet cooling efficiency, which was recorded in the film boiling region could be used to analyze the cooling effect per unit area (kW/m^2) when the temperature surpasses $290 - 300\ ℃$. Equation 2.9 considers the cooling effect per unit area for which the droplets are being evaporated completely.

$$\dot{Q}''_{evap} = \dot{m}''_{rate} \cdot \Delta H_{evap} \tag{2.9}$$

Inserting the evaporation energy of $\Delta H_{evap} = 2570,75$ kJ/kg and mass flux of $\dot{m}''_{rate} = 0{,}1667$ (kg/s)/m2:

$$\dot{Q}''_{evap} = 0{,}1667\ (\text{kg/s})/\text{m}^2 \cdot 2570{,}75\ \text{kJ/kg} \tag{2.9}$$

Which results in a heat flux of $\dot{Q}''_{evap} = 429$ kW/m^2. This is higher than a jet fire and pool fire peak heat load of 350 kW/m^2 and 150 kW/m^2 respectively. However, by including the 10 % droplet cooling efficiency in the film boiling region, results in a droplet cooling effect per unit area of $\dot{Q}''_{evap} = 42{,}9$ kW/m^2. This could verify that cooling by water droplet interaction is not sufficient in the film boiling region, and water droplets must be applied earliest stages possible to have the best possible effect on the heated segment.

All safety measures in interface with firewater, will be sufficient according to NORSOK S-001. If the temperature surpasses 290 - 300 ℃, the segment will be extremely sensitive based on the analysis conducted in Subsection 5.4.1 and 5.4.2. Many of the safety measures heavily depend on humans' awareness, and their ability to react effectively in case of a fire incident. It can be suggested to add an automatic blowdown function into the interfaces, which will effectively lead the fluid from a dangerous

zone into an associated flare for depressurization. It can also be suggested to add a water curtain feature, which will divide the enclosure in several "sections" and subsequently reduces the radiation. It will provide a more efficient evacuation, in addition to neglecting the heat to transport to surrounding materials. Another suggestion, if feasible, is to substitute firewater with passive fire protection, which will not depend on human maneuvers, but will still have a fire resistance for a longer period. Mitigating measures must be considered in an ALARP analysis, meaning that the costs of the safety measures are not significantly disproportionate to the risk reduction.

6. Conclusion

The thesis covers droplet cooling efficiency on a small-scale and may therefore not represent cooling at large-scale fire or explosion scenarios. Due to the sensitive nature of the experiments, there were several errors and uncertainties which must be considered. Difficulties were detected regarding the use of the smallest droplet diameter, due to external impact, i.e. opened door etc.

In the film boiling region (i.e. temperatures above 290 - 300 ℃) 10 % droplet cooling efficiency may be expected, which means that mitigating actions by using firewater must be considered in earliest stages as possible, to perform its primary effect. By analyzing a standardized jet-fire curve, it will take 2 minutes to reach 300 ℃, statistically it takes 2 – 4 minutes to get a rupture in a 2" – 4" pipe segment, and consequently 3 – 5 minutes to activate the firewater application. It should be considered adding a blowdown function and water curtain or substituting firewater with passive fire protection, provided that the costs of mitigating measures are not significantly disproportionate to the risk reduction.

The results may indicate that boiling crisis can preferably be defined as a broad temperature range with high cooling efficiency, rather than one narrow peak.

Evenly across the results, smallest droplets were observed to have a higher cooling efficiency in a wider temperature range, while the largest droplets demonstrated a higher peak efficiency (i.e. higher boiling crisis). Based on most of the results, the droplet cooling efficiency increased with increasing impact velocity, due to higher momentum impact and a larger contact area. However, regarding the horizontal stainless steel disc setup – middle-sized and smallest droplets, the effect of bouncing was less prominent, and droplets had a higher ability to be attached to the surface (i.e. lower weber number). The droplet cooling efficiency will decrease with increased inclination regarding the lowest impact velocity, due to a lower amount of possible directions for reflected disintegrated droplets. As the impinging velocity increases, the droplets demonstrated higher efficiency when there is a 30° inclined disc setup.

7. Further work

- Experiment with other metallic materials, consequently different roughness's.

- Further investigate the effect of inclination vs. Leidenfrost

- Do full-scale experiments (Either in CFD or real-scale)

- Further investigate this topic with extended input parameters (i.e. impact velocity, droplet sizes etc.)

- Investigate the validation of this topic in CFD. Will the results conform to the results obtained in this thesis?

- Do a full-scale analysis of firewater and its respective interfaces in a major accident and test the resilience/robustness of the system. Include sensitivity analysis.

- The results obtained in this thesis is based on small-scale experimenting. The 0,33 g/s – 0,66 g/s mass rate requirement from NORSOK S-001 was not obtained, due to the limited options of droplet diameters. However, this can be investigated in further research.

- Investigate the effect of using saltwater instead of fresh water.

8. Bibliography

Bernardin, J.D, and I. Mudawar. "The Leidenfrost point: Experimental Study and Assessment of Existing Models." *Journal of Heat Transfer*, 1999: 894-903.

Bjørge, Joachim, Torgrim Log, Monika Metallinou, and Øyvind Frette. "Apparatus for studying water droplet cooling of hot metal disks (Still in progress)." 2018.

British Stainless Steel Association. *Elevated temperature physical properties of stainless steels.* n.d. https://www.bssa.org.uk/topics.php?article=139 (accessed April 27, 2018).

Casal, Joaquim. *Evaluation of the Effects and Consequences of Major Accidents in Industrial plants.* 2. Amsterdam: Elsevier, 2017.

Dembele, S., V.H.Y. Tam, S. Ferraris, A.F Rosario, and J.X. Wen. "Effectiveness of water deluge in fire suppression and mitigation." *12th International Symposium on Loss Prevention and Safety Promotion in the Process Industries*, May 2007, 153 ed.: 22-24.

Drange, Leiv Anfin. *A study of selected problems related to accidental process fires.* Doctor thesis, Faculty of Mathematics and Natural Sciences - Department of Physics and Technology - Process Technology Section, Universitet i Bergen, Bergen: University of Bergen, 2011.

Drysdale, Dougal. *An introduction to fire dynamics.* Third. Edinburgh: A John Wiley & Sons, Ltd. publication, 2011.

Engineers edge, LCC. *Properties for metal.* August 28, 2017. http://www.engineersedge.com/properties_of_metals.htm.

Faghri, Amir, Yuwen Zhang, and John Howell. *Advanced heat and mass transfer.* Columbia: Global Digital Press, 2010.

Frohn, Arnold, and Norbert Roth. *Dynamics of Droplets.* London: Springer, 2000.

Fukuda, Shinya, Masamichi Kohno, Keisuke Tagashira, Nobuya Ishahara, Sumitomi Hidaka, and Yasuyuki Takata. "Behavior of small droplet impinging on a hot surface." *Heat transfer Engineering*, 2014: 204-211.

Gottfried, B.S., C.J. Lee, and K.J. Bell. "The leidenfrost phenomenon: film boiling of liquid droplets on a flat plate." *International journal of heat and mass transfer*, November 1966: 1167-1188.

Hall, NASA Official: Nancy. *Terminal Velocity (gravity and drag).* Mai 5, 2015. https://www.grc.nasa.gov/WWW/K-12/airplane/termv.html (accessed Mars 26, 2018).

Hewitt, Paul G. *Conceptual Physics.* 12. Pearson Education, 2014.

Kadocsa, Andràs, Reinhard Tacschl, and Gergely Kristòf. "Analysis of spray evolution in internal combustion engines using numerical simulation." *Journal of Computational and Applied Mechanics*, January 29, 2007: 85-100.

Kandlikar, Satish G., and Mark E. Steinke. "Contact angles and interface behavior during rapid evaporation of liquid on a heated surface." *International Journal of Heat and Mass Transfer*, August 2002: 3771-3780.

Kazemi, Zia. *Droplet impaction on Solid Surfaces Exposed to impinging jet fires.* Doktoravhandling , Fakultet for ingeniørvitenskap og teknologi, Institutt for energi- og prosessteknikk, Trondheim: Norges teknisk-naturvitenskapelige universitet (NTNU), 2005.

KBT. *Fagutrykk.* n.d. www.kbt.no/faguttrykk.asp (accessed Mai 8, 2018).

Kodur, V.K.R., and T.Z. Harmathy. "Properties of Building Materials." Chap. 9 in *SFPE handbook of fire protection engineering*, by Morgan J. Hurley, et al., edited by Morgan J. Hurley, et al., 277-324. London: Springer, 2016.

Lautenberger, C., C.L. Tien, K.Y. Lee, and A.J. Stretton. "Radiation Heat Transfer." Chap. 4 in *SFPE handbook of fire protection engineering*, by Morgan J. Hurley, et al., edited by Morgan J. Hurley, et al., 102-137. London: Springer, 2016.

Liang, Gangtao, and Issam Mudawar. "Review of drop impact on heated walls." *International Journal of heat and mass transfer*, Oktober 21, 2016: 103-126.

Log, Torgrim. "Water droplets evaporating on horizontal semi-infinite solids." *Applied Thermal Engineering*, 2016: 214-222.

Log, Torgrim, and Gunnar Heskestad. "Temperatures of restricted turbulent fire plumes." *Fire Safety Journal 31*, 1998: 101-115.

Misyura, S.Y. "The effect of Weber number, droplet sizes and wall roughness on crisis of droplet boiling." *Experimental thermal and fluid science*, Februar 16, 2017: 190-198.

Pasandideh-Fard, M, S.D Aziz, S Chandra, and J Mostaghimi. "Cooling effectiveness of a water drop impinging on a hot surface." *International Journal of Heat and Fluid Flow*, 2001: 201-210.

Petroleumstilsynet. *Forskrift om tekniske og operasjonelle forhold på landanlegg i petroleumsvirksomheten med mer .* Forskrift, Petroleumstilsynet, helsedirektoratet, Petroleumstilsynet, 2016.

Petroleumstilsynet. *HELSE, MILJØ OG SIKKERHET I PETROLEUMSVIRKSOMHETEN OG PÅ ENKELTE LANDANLEGG.* Forskrift, Petroleumstilsynet, Miljødirektoratet, Helsedirektoratet, Mattilsynet, Petroleumstilsynet, 2016.

Pilch, M., and C. A. Erdmann. "Use of breakup time data and velocity history data to predict the maximum size of stable fragments." *International Journal of Multiphase flow*, 1987: 741-757.

Shirvill, L. C. "PERFORMANCE OF PASSIVE FIRE PROTECTION IN JET FIRES." *IChemE Symposium series no. 130: Major Hazards I*, October 1992: 111-122.

Standard norge. *NS-EN 1993-1-1:2005+A1:2014+NA:2015 - Eurocode 3: prosjektering av stålkonstruksjoner.* EU: Standard Norge, Revidert 2015.

Storulykkeforskriften. *Forskrift om tiltak for å forebygge og begrense konsekvensene av storulykker i virksomheter der farlige kjemikalier forekommer (storulykkeforskriften).* Lov, Justis- og beredskapsdepartementet, Hele Norge: Justis- og beredskapsdepartementet, 2016.

The Norwegian Oil Industry Association (OLF). *NORSOK STANDARD S-001 Technical safety.* Standards - Regulations, The Federation of Norwegian Industry , Lysaker: Standards Norway, 2008.

9. Appendix

Appendix A – Procedures

This section will give a step-by-step method of conducting both the experiments and data processing in Excel.

A.1. Baseline experiment procedure

STEP #	ACTION
(1)	Measure the ambient temperature and relative humidity. Eliminate sources of air turbulence as far as possible. (Turn off air supply devices placed around the room, including closing doors and windows.)
(2)	Everything around the test object, and the stainless steel disc itself must be cleaned, and dry. The stainless steel disc must be cleaned with Acetone. While using Acetone, it is important to wear gloves for personal safety.
(3)	The stainless steel disc must be in the desired inclination. Therefore, a leveler was used to adjust the disc.
(4)	Make sure that no droplets are falling during the entire baseline experiment.
(5)	Place the gas burner under the stainless steel disc, turn on the gas and then use a spark to get a sustainable flame. Turn off the gas burner when the temperature exceeds approximately 430 ℃.
(6)	Start the datalogging when the temperature is around 410 ℃.
(7)	Stop the datalogging when the temperature is around 80 – 85 ℃.

A.2. Baseline data processing

STEP #	DATA PROCESSING
(1)	First, plot all temperature-time data from the experiment into an Excel sheet.
(2)	Calculate the average temperature from the four thermocouples and let the temperature $T = 400\ ℃$ be start of the time ($t = 0$). Also, allow the temperatures from $t = -10\ s$ till $t = 0$ include in the Excel sheet.
(3)	In the next column, calculate the cooling rate ($\frac{dT}{dt}$) by using the slope of temperatures and time.
(4)	In the next column, calculate the baseline heat transfer by using Equation 3.2.

$$Q_{Base} = \rho c_p V \left(\frac{dT}{dt} \right) \qquad (3.2)$$

ρ [kg/m³] is the density of the stainless steel disc, which is a constant.

V [m³] is the volume of the stainless steel disc

c_p [J/kgK] is the specific heat capacity, which will depend on temperature. However, in this case, it will be considered as a constant value.

(5) In the next column, calculate the cooling rate based on a 2nd degree correlation of the cooling rate determined in step 3. This correlation will be further used when the droplet experiments is being analyzed.

(6) The results will be presented in diagrams.

A.3. Droplet experiment procedure

STEP #	ACTION
(1)	Measure the ambient temperature and relative humidity in the room. Eliminate sources of air turbulence as far as possible. (Turn off air supply devices placed around the room, including closing doors and windows.)
(2)	Everything around the test object, and the stainless steel disc itself must be clean, and dry. The stainless steel disc must be cleaned with Acetone. While using Acetone, it is important to wear gloves for personal safety.
(3)	If necessary, adjust to the desired height of injection needle above the stainless steel disc.
(4)	Adjust the valve to the desired droplet interval. This is conducted by using a timer and investigate how many seconds it takes for 20 droplets impinging. The frequency will be adjusted so each of the needles from every experiment shares approximately the same droplet mass rate. The reason for this is to get comparable results. This will consequently mean that the smallest needle will have a higher droplet interval compare to the largest needle. \ This step must be conducted both <u>before</u> and <u>after</u> the droplet experiment to verify the frequency, and possibly discover any experimental errors.
(5)	Find the mass of each droplet; Use a glass beaker and collect 20 droplets and remember to extract the mass of the glass beaker, use the mass of 20 droplets and divide by 20. This

step must be conducted both <u>before</u> and <u>after</u> the droplet experiment to find an average value.

(6) Again, ensure that everything around the stainless steel disc, and the stainless steel disc itself is cleaned with paper, to get a dry environment.

(7) Place the gas burner under the stainless steel disc, activate it by turn on the gas and then use a spark to get a sustainable flame. Turn off the gas burner when the temperature exceeds approximately 430 ℃.

(8) During the heating process: Ensure that there are no droplets impinging.

(9) Start the datalogging when the temperature is around 410 ℃, and then allow the droplets impinging.

(10) Stop the datalogging when the temperature is around 80 – 85 ℃.

A.4. Droplet experiment data processing

STEP #	DATA PROCESSING
(1)	First, transfer all temperature-time data from the experiment into an Excel sheet (Baseline 1, Droplet experiments 1-5, and Baseline 2).
(2)	Calculate the average temperature from the four thermocouples and let the temperature $T = 400$ ℃ be start of the time ($t = 0$). Also, allow the temperatures from $t = -10\ s$ to $t = 0$ include in the Excel sheet. Also represent the average temperature between baseline 1 and baseline 2 experiment in the next column.
(3)	Calculate c_p based on the 3rd degree correlations presented in Figure 2.1 in section 2.1.4. *X* will be replaced with average temperature from the droplet experiment. To get J/K, it must be multiplied with the mass of the stainless steel disc.
(5)	Calculate the cooling rate ($\frac{dT}{dt}$) of the droplet experiment by using the Excel slope function of temperatures and time.
(6)	In the next column, find the average cooling rate from the 2nd degree correlation given from baseline experiment 1 and 2.
(7)	In the next column, find the percentile difference/deviations between the 2nd degree correlations of cooling rate given from baseline experiment 1 and 2.
(8)	In the next column, calculate the total rate of heat transfer (Q_{tot}) for the droplet experiment. This will naturally include both cooling from droplets and convective

cooling. This is being done by multiplying the heat capacity (c_p) in that timestep with the cooling rate determined in step 5.

(9) In the next column, calculate the rate of heat transfer from convective and radiant cooling (Q_{base}), based on heat capacity and the average cooling rate. This is being done by multiplying the heat capacity (c_p) in that timestep with the cooling rate determined in step 6.

(10) In the next column, calculate the heat transfer from mere droplet cooling (Q_{drops}). This is addressed by the difference between the total heat transfer determined in step 8 and the convective heat transfer determined in step 9.

(11) The final step is to calculate the droplet cooling efficiency. In the next column, calculate the droplet cooling efficiency by using Equation 2.8 below.

$$\chi_{drop} = \frac{Q_{drops}}{Q_{evap}} \qquad (2.8)$$

χ_{drop} [-] is the droplet cooling efficiency, and a dimensionless parameter.
Q_{drops} [W] is the heat transfer from mere droplet cooling, calculated in step 10.
Q_{evap} [W] is the amount of heat required to evaporate the droplets completely.
The formula can be further rearranged to:

$$\chi_{drop} = \frac{Q_{drops}}{\Delta H_{vap} \cdot W_{rate}} \qquad (2.8)$$

ΔH_{vap} [J/g] is the energy required to evaporate 1 gram of water. This will be a constant value of 2570,75 J/g.
W_{rate} [g/s] is the droplet mass rate, or the average mass of droplets impinging per second. By using the average droplet frequency and mass of both before and after the experiment, the mass rate of droplets can be adjusted.

(12) The results will be presented in diagrams.

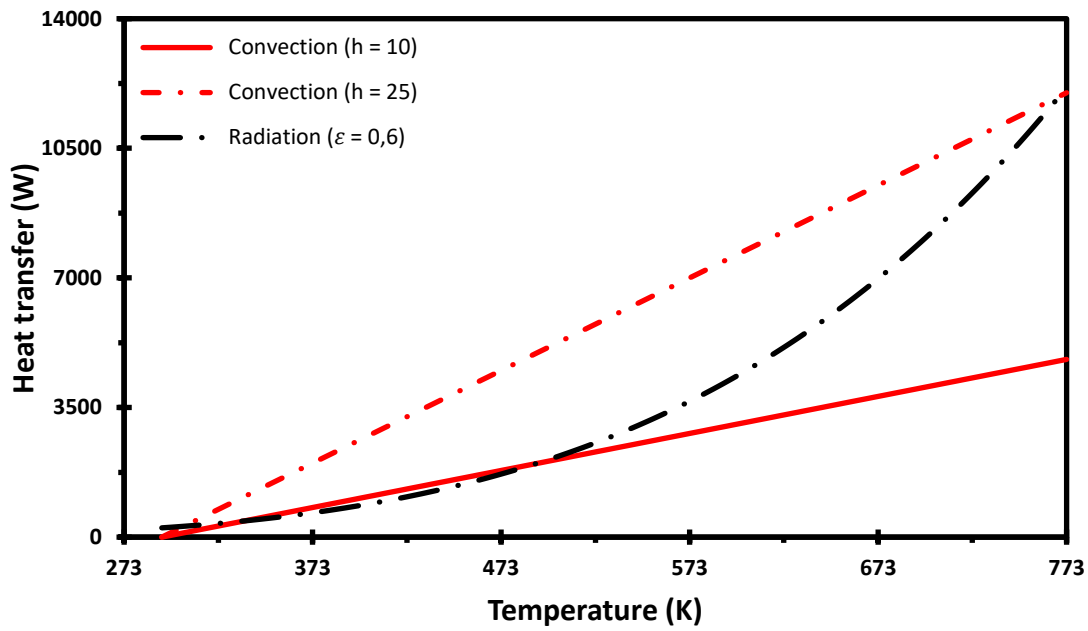# Appendix B – Heat loss analysis

Figure B.1 Presentation of the effect of heat transfer vs temperature for radiation and convection heat transfer.

Appendix C – Lab protocol

This section will give an example of how each of the lab protocols were conducted for each of the experiments. This report particularly regards the largest droplets, lowest impact velocity and horizontal disc setup.

Experiment report – 15.01.2018

Purpose

This experiment's intension was to get results for the master's thesis.

Baseline 1

Input parameters

PARAMETER	INPUT VALUE
CASE FILE	20180115Base1WhiteSSHRa3T186RH335Height25
DATE AND TIME	15.01.2018, 08.30
AMBIENT HUMIDITY	33,5 %
AMBIENT TEMPERATURE	18,6 ℃
HEIGHT OVER TEST OBJECT (STAINLESS STEEL DISC)	25 cm
MATERIAL	Stainless steel
ROUGHNESS	Ra 3
AIR PRESSURE (OUTSIDE)	993 hPa (source: yr.no)
AIR DENSITY (OUTSIDE)	93 % (source: yr.no)
DEWPOINT (OUTSIDE)	3 degrees (source: yr.no)

Test results analysis

The figure down below represents the cooling rate (dT/dt) of the stainless steel disc with respect of temperature, when the stainless steel disc is affected by mere convective cooling. It can be shown that

the cooling rate will follow a 2nd degree correlation as indicated below.

$$y = 1{,}3993E\text{-}06x^2 + 4{,}6588E\text{-}04x - 4{,}8749E\text{-}03$$
$$R^2 = 9{,}9988E\text{-}01$$
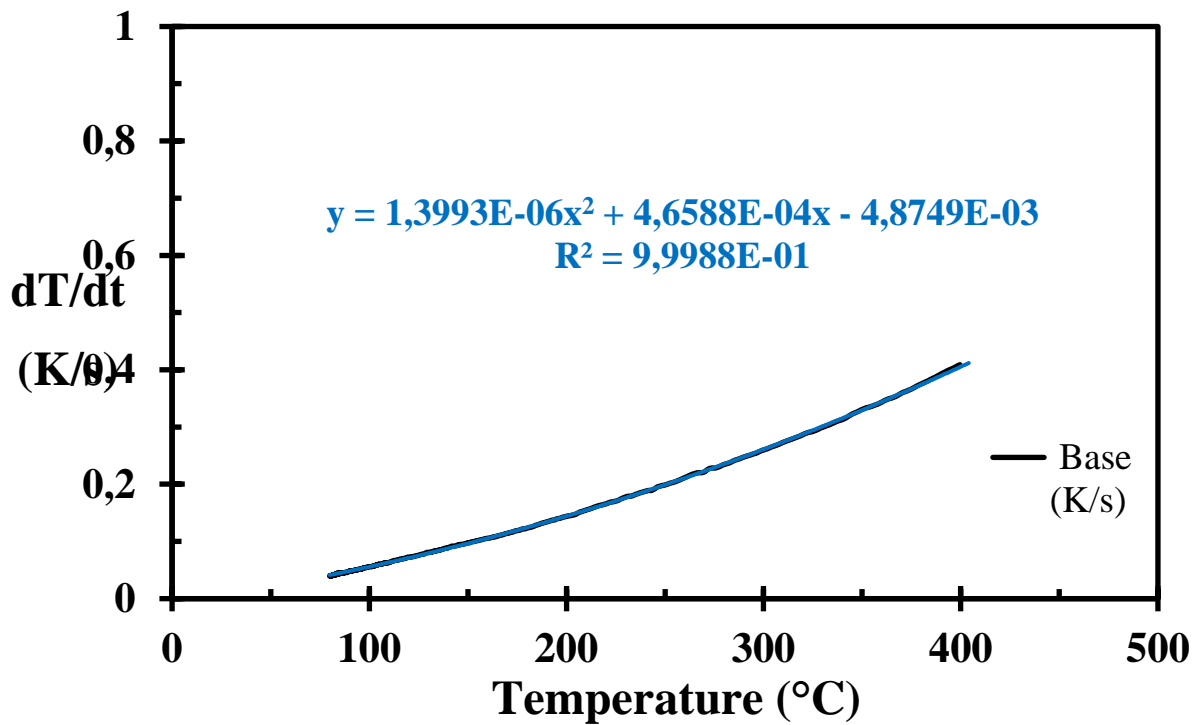
Observations

Errors

- Extreme wind outside

- Some activity in the room

- Door open several times

Droplet 1

Input parameters

PARAMETER	INPUT VALUE
CASE FILE	20180115Drop1WhiteSSHRa3T191RH335Height25
DATE AND TIME	15.01.2018
AMBIENT HUMIDITY	33,5 %
AMBIENT TEMPERATURE	19,1 °C
HEIGHT OVER TEST OBJECT (STAINLESS STEEL DISC)	25 cm
DROPLET FREQUENCY BEFORE	20 drops in 21,3 seconds
NEEDLE DIAMETER	1,6 mm
MASS OF GOBLET BEFORE	45,082 g

X

TOTAL MASS BEFORE	45,6 g
MASS PER DROPLET BEFORE	0,0259 g
MATERIAL	Stainless steel
ROUGHNESS	Ra 3
INJECTION NEEDLE	White 1.6x25mm 16Gx 1"

Test results analysis

The figure down below represents the temperature decrease with respect of time, for both the droplet experiment and baseline experiment. After approx. 210 ℃ and 500 seconds it can be shown that temperature curve of the droplet experiment will be steeper, consequently means that the effect of cooling will be higher at this timestep.
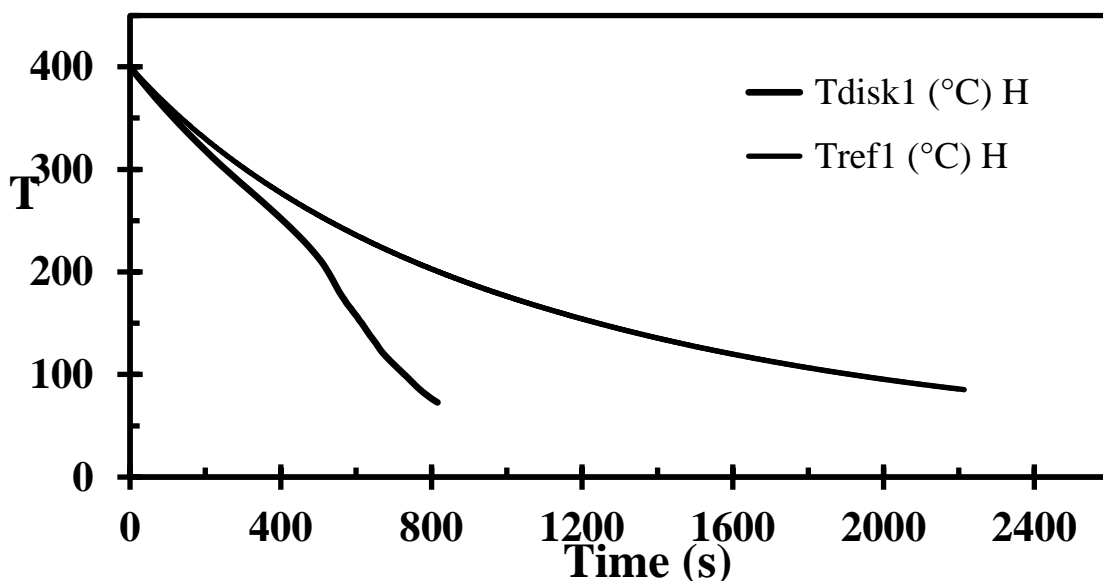

Figure down below represents the cooling rate with respect of temperature. It can be shown from the figure that in temperature range of 130-210 ℃, the rate of cooling will be higher, consequently means that the effect of cooling will be at its highest in this range. The cooling rate for baseline is an average curve of baseline experiment 1 and 2.
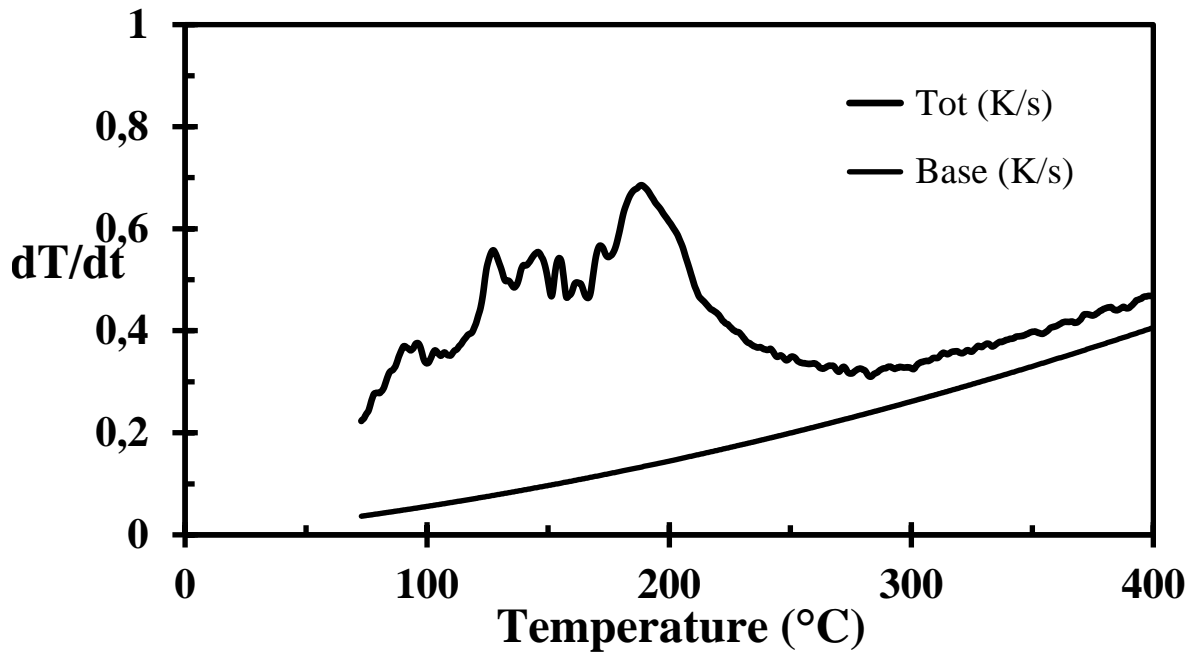
Figure down below summarizes the rate of heat transfer with respect of temperature. Again, it can be shown that in-between temperatures 130-210 ℃ the rate of heat transfer will be higher, and at its highest at temperature 188,1 ℃. The rate of heat transfer at this temperature will be 44,42 W. The stippled line indicates the total heat required to evaporate the entire droplet.
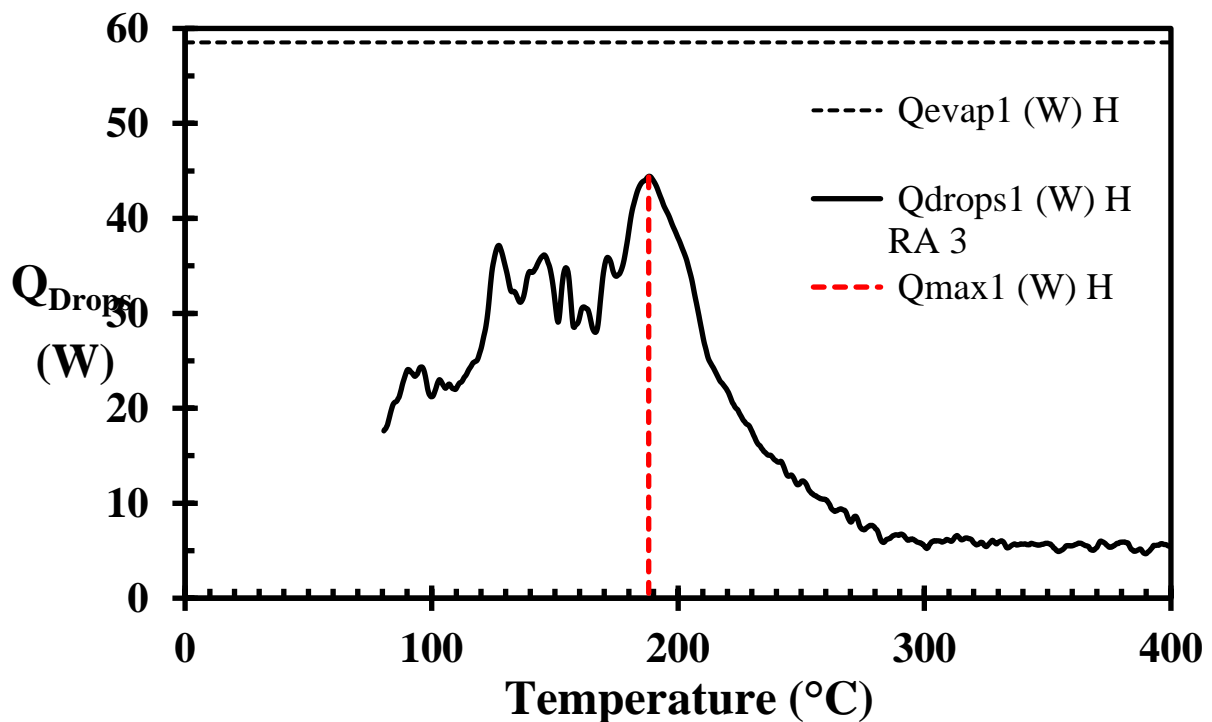
Observations

- Frequency relatively stable (20 drops/22,7 seconds)

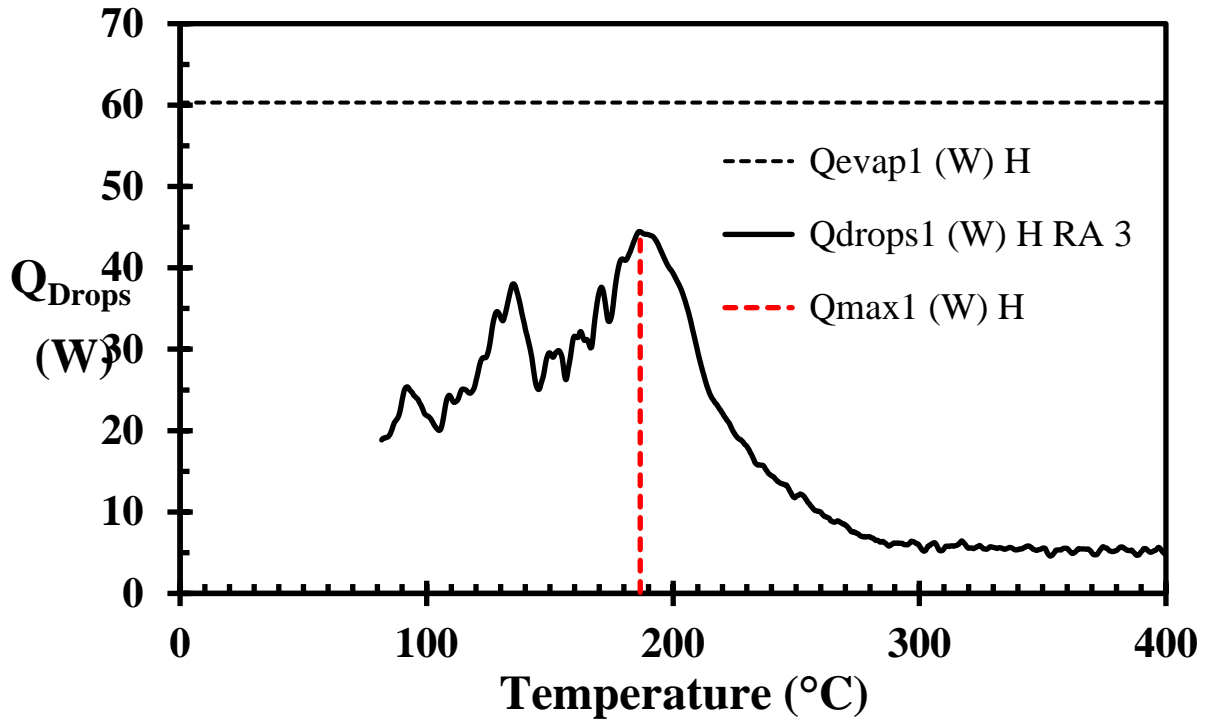**Errors**

- Some activity in the room. Some students were working.

Droplet 2

Input parameters

PARAMETER	INPUT VALUE
CASE FILE	20180115Drop2WhiteSSHRa3T195RH334Height25
DATE AND TIME	15.01.2018
AMBIENT HUMIDITY	33,4 %
AMBIENT TEMPERATURE	19,5 ℃
HEIGHT OVER TEST OBJECT (STAINLESS STEEL DISC)	25 cm
DROPLET FREQUENCY BEFORE	20 drops in 23 seconds
NEEDLE DIAMETER	1,6 mm
MASS OF GOBLET BEFORE	45,1022 g
TOTAL MASS BEFORE	45,62 g
MASS PER DROPLET BEFORE	0,0259 g
MATERIAL	Stainless steel
ROUGHNESS	Ra 3
NEEDLE	White 1.6x25mm 16Gx 1”

Test results analysis

Figure down below summarizes the rate of heat transfer with respect of temperature. It can be shown that in-between temperatures 130-220 ℃ the rate of heat transfer will be higher, and at its highest at temperature 186,7 ℃. The rate of heat transfer at this temperature will be 44,44 W. The stippled line indicates the total heat required to evaporate the entire droplet.

Observations

Errors

- Droplet frequency tends to be a little unstable. However, it varies around 20 drops/23 seconds. Was adjusted a little bit to 20 drops/22,6 seconds
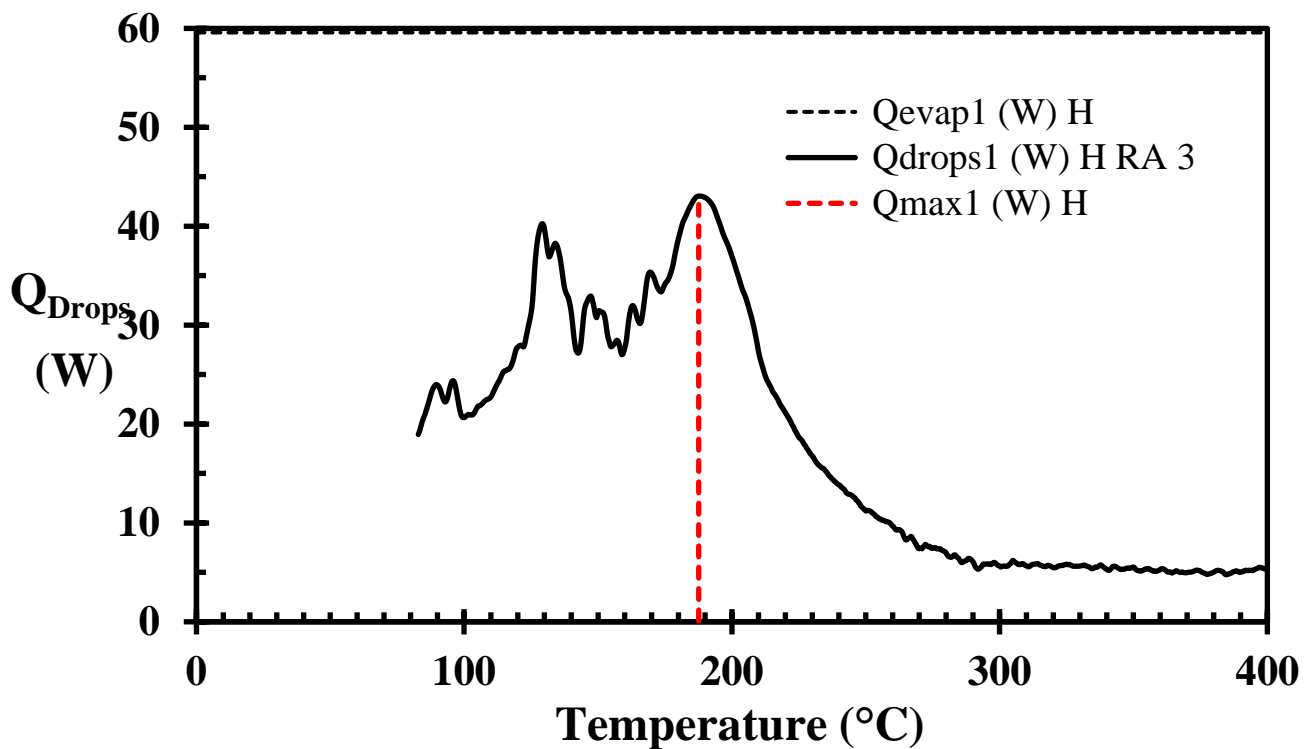
Droplet 3

Input parameters

PARAMETER	INPUT VALUE
CASE FILE	20180115Drop3WhiteSSHRa3T197RH335Height25
DATE AND TIME	15.01.2018
AMBIENT HUMIDITY	33,5 %
AMBIENT TEMPERATURE	19,7 ℃
HEIGHT OVER TEST OBJECT (STAINLESS STEEL DISC)	25 cm
DROPLET FREQUENCY BEFORE	20 drops in 23 seconds
NEEDLE DIAMETER	1,6 mm
MASS OF GOBLET BEFORE	45,106 g
TOTAL MASS BEFORE	45,66 g
MASS PER DROPLET BEFORE	0,0277 g
MATERIAL	Stainless steel

ROUGHNESS	Ra 3
NEEDLE	White
	1.6x25mm
	16Gx 1"

Test results analysis

Figure down below summarizes the rate of heat transfer with respect of temperature. It can be shown that in-between temperatures 130-220 ℃ the rate of heat transfer will be higher, and at its highest at temperature 187,6 ℃. The rate of heat transfer at this temperature will be 43,05 W. The stippled line indicates the total heat required to evaporate the entire droplet.

Observations

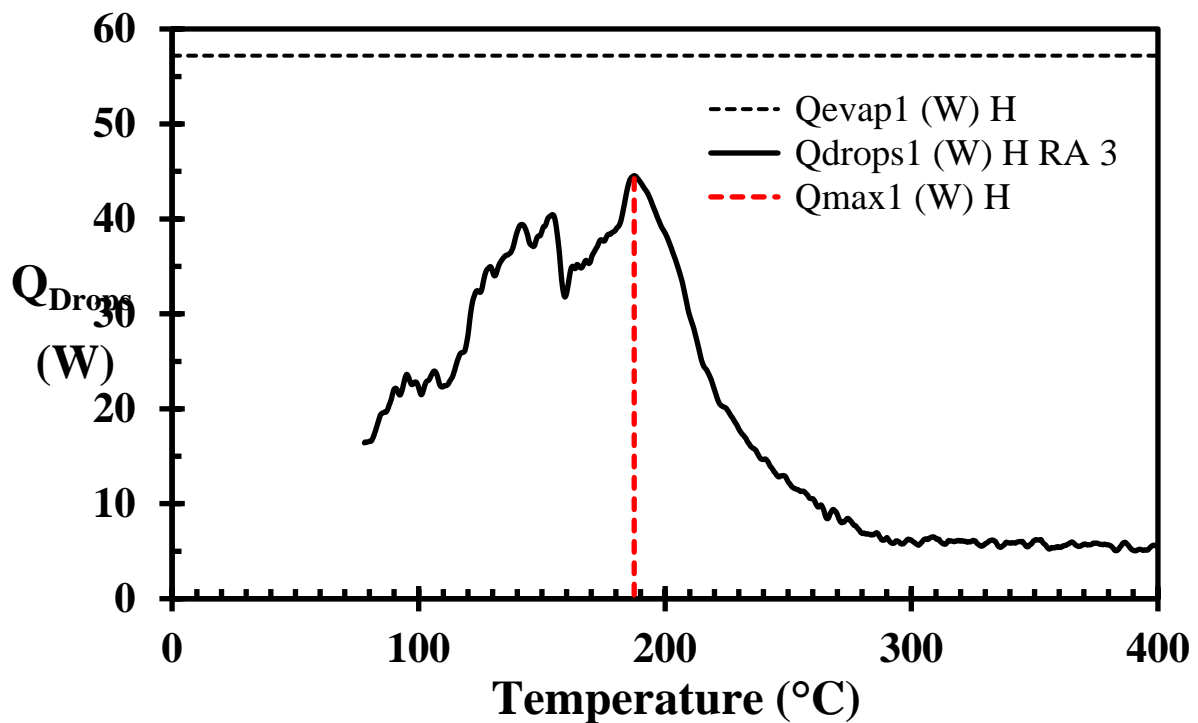Droplet frequency tends to be stable.

Droplet 4

Input parameters

PARAMETER	INPUT VALUE
CASE FILE	20180115Drop4WhiteSSHRa3T200RH335Height25
DATE AND TIME	15.01.2018
AMBIENT HUMIDITY	33,5 %

AMBIENT TEMPERATURE	20,0 ℃
HEIGHT OVER TEST OBJECT (STAINLESS STEEL DISC)	25 cm
DROPLET FREQUENCY BEFORE	20 drops in 22,6 seconds
NEEDLE DIAMETER	1,6 mm
MASS OF GOBLET BEFORE	45,109 g
TOTAL MASS BEFORE	45,61 g
MASS PER DROPLET BEFORE	0,0250 g
MATERIAL	Stainless steel
ROUGHNESS	Ra 3
NEEDLE	White 1.6x25mm 16Gx 1"

Test results analysis

Figure down below summarizes the rate of heat transfer with respect of temperature. It can be shown that in-between temperatures 130-220 ℃ the rate of heat transfer will be higher, and at its highest at temperature 187,5 ℃. The rate of heat transfer at this temperature will be 44,55 W. The stippled line indicates the total heat required to evaporate the entire droplet.

Observations

Droplet frequency tends to be stable
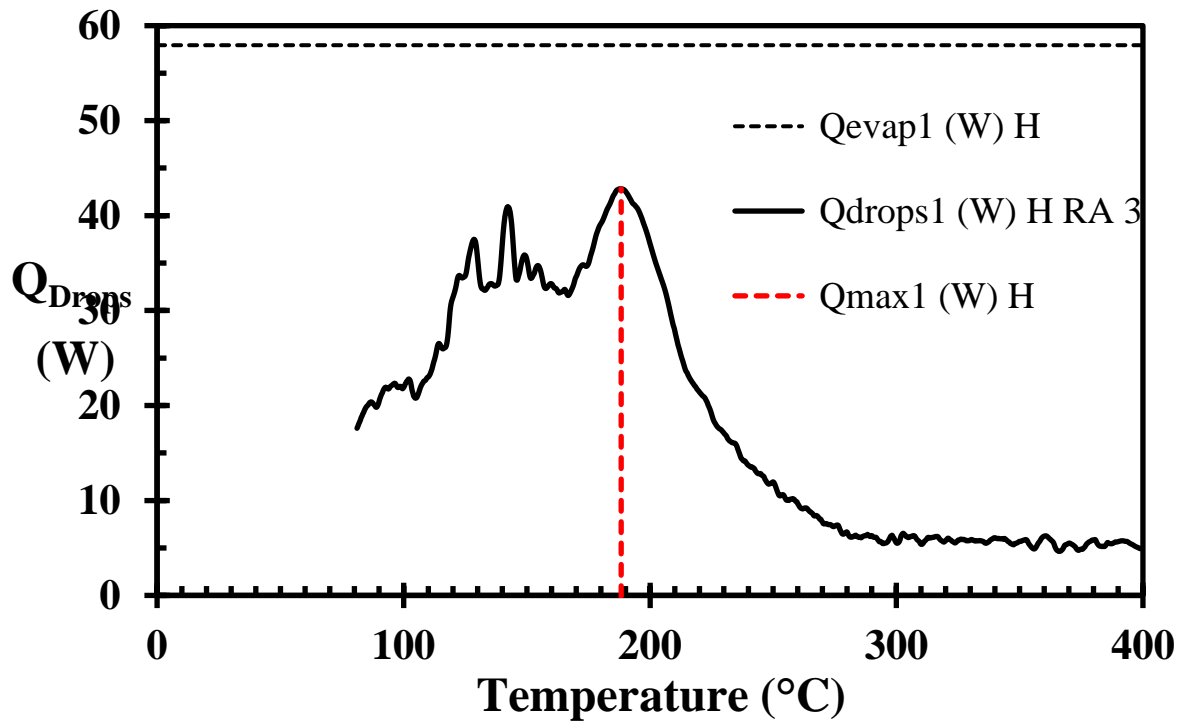
Errors

- Door were open several times

Droplet 5

Input parameters

PARAMETER	INPUT VALUE
CASE FILE	20180115Drop5WhiteSSHRa3T202RH334Height25
DATE AND TIME	15.01.2018
AMBIENT HUMIDITY	33,4 %
AMBIENT TEMPERATURE	20,2 ℃
HEIGHT OVER TEST OBJECT (STAINLESS STEEL DISC)	25 cm
DROPLET FREQUENCY BEFORE	20 drops in 23 seconds
NEEDLE DIAMETER	1,6 mm
MASS OF GOBLET BEFORE	45,103 g
TOTAL MASS BEFORE	45,612 g
MASS PER DROPLET BEFORE	0,0255 g
MATERIAL	Stainless steel
ROUGHNESS	Ra 3
NEEDLE	White
	1.6x25mm
	16Gx 1"

Test results analysis

Figure down below summarizes the rate of heat transfer with respect of temperature. It can be shown that in-between temperatures 120-220 ℃ the rate of heat transfer will be higher, and at its highest at temperature 188,3 ℃. The rate of heat transfer at this temperature will be 42,82 W. The stippled line indicates the total heat required to evaporate the entire droplet.

Observations

Droplet frequency tends to be stable, despite being unstable in beginning

Errors

- Frequency tends to vary in the beginning, was adjusted.

Baseline 2

Input parameters

PARAMETER	INPUT VALUE
CASE FILE	20180115Base2WhiteSSHRa3T203RH333Height25
DATE AND TIME	15.01.2018, 11.30
AMBIENT HUMIDITY	33,3 %
AMBIENT TEMPERATURE	20,3 ℃
HEIGHT OVER TEST OBJECT (STAINLESS STEEL DISC)	25 cm
MATERIAL	Stainless steel
ROUGHNESS	Ra 3

Test results analysis

The figure down below represents the cooling rate (dT/dt) of the stainless steel disc with respect of temperature, when the stainless steel disc is affected by mere convective cooling. It can be shown that the cooling rate will follow a 2nd degree correlation as indicated below.

$$y = 1{,}3960E\text{-}06x^2 + 4{,}7196E\text{-}04x - 5{,}3224E\text{-}03$$
$$R^2 = 9{,}9978E\text{-}01$$
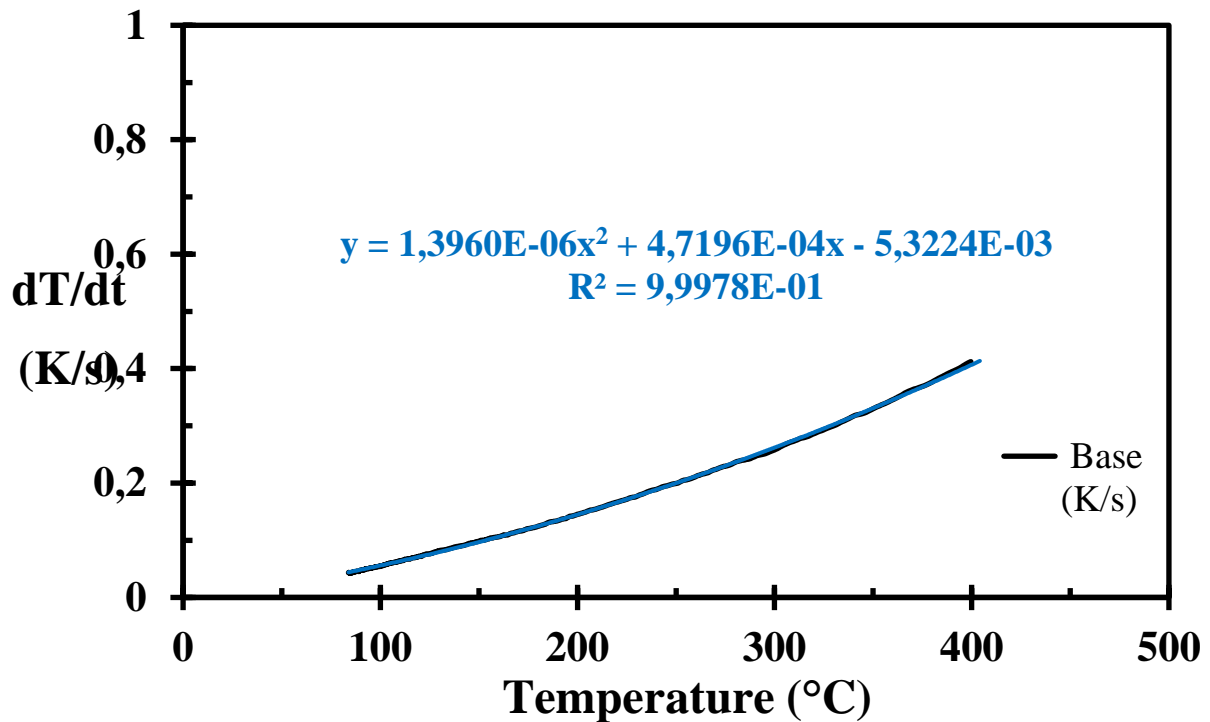
Observations

Errors

Door were open a few times

Compilation of results

As shown in the figure below, there are some differences in the efficiency between the 5 droplet experiments. However, the pattern in transition zone (between the two extrema's), will behave relatively equivalent. In the nucleate boiling regime, the efficiency for the 5 experiments will be different due to various reasons, such as small difference in droplet diameter, or whether the disc was completely horizontal or not etc. When the results from this experiment series will be prepared and compared to other series, there will be an average curve of the 5 experiments.